Administration transdermique par ionophorèse des agents thérapeutiques

Cazares Delgadillo, Jennyfer

UNIVERSITÉ DE GENÈVE
Section des sciences pharmaceutiques
Laboratoire de Chimie Thérapeutique

FACULTÉ DES SCIENCES
Professeur Pierre-Alain Carrupt
Dr. Yogeshvar N. Kalia

Administration transdermique par ionophorèse des agents thérapeutiques

THÈSE

Présentée à la Faculté des Sciences de l'Université de Genève pour obtenir le grade de Docteur ès sciences, mention sciences pharmaceutiques

Par

Jennyfer CAZARES DELGADILLO
de Mexico (Mexique)

Thèse N°4198

GENÈVE
Atelier d'impression ReproMail

2009

REMERCIEMENTS

Merci d'abord au professeur Pierre-Alain Carrupt pour m'avoir donné l'occasion d'effectuer une thèse sous sa direction.
Je remercie tout particulièrement Dr. Yogeshvar Kalia qui m'a accueilli au sein de son équipe de recherche et qui a dirigé et supervisé mon travaille avec beaucoup d'intérêt et de pertinence.
Je remercie très chaleureusement Dr. Adriana Ganem-Rondero pour son soutien, sa disponibilité et pour m'avoir accompagnée, tant scientifiquement que moralement, sur le chemin qui m'a conduit à cette thèse.
Un grand merci à tous les membres du jury ayant évalué ce travail: le professeur Pierre-Alain Carrupt, le Dr.Yogeshvar N. Kalia, le professeur Eric Allémann et le professeur Jouni Hirvonen qui est venu de si loin pour l'occasion.
Je remercie également Dr. Virginia Merino pour m'avoir donné l'occasion de réaliser les études *in vivo* à la Faculté de Pharmacologie à l'Université de Valencia et Dr. Alicia López-Castellano, Cristina Balaguer-Fernández et Araceli Calatayud-Pascual de l'Université Cardenal Herrera (CEU) pour sa collaboration dans le projet.
Merci à CONACYT pour son soutien pendant le doctorat.
Merci à tous mes collègues de Sciences II et du Pavillon Ansermet, ainsi que mes collaborateurs de Pharmapeptides.
Merci à David Quintanar-Guerrero et à mes collègues de la FES-C (UNAM) pour ses encouragements.
Je souhaite remercier immensément mes parents pour avoir cru en moi et pour tout l'amour qu'ils me donnent, ma sœur et mon frère pour leurs encouragements et leur incomparable affection et mes amis pour leur précieux soutien dans les moments difficiles.

TABLE DE MATIERES

RESUME

L'ionophorèse utilise un faible courant électrique afin de faciliter le passage transdermique des principes actifs hydrophiles et ionisés avec plusieurs applications thérapeutiques possibles: par exemple, le FDA aux Etats-Unis a récemment donné les autorisations de mise sur le marché pour deux systèmes ionophorétiques contre la douleur. Le premier système, qui contient le lidocaïne (LidoSite™), a été développé pour effectuer une anesthésie locale avant une injection. Le deuxième produit, qui contient le fentanyl (Ionsys™), vise une action centrale et il a été développé pour traiter la douleur postopératoire.

Le but de cette thèse a été d'étudier la possibilité d'utiliser l'ionophorèse pour l'administration des molécules thérapeutiques – principalement des médicaments pour le traitement des nausées et vomissements induits par chimiothérapie (NVIC) – et aussi de montrer qu'elle permettrait l'administration non-invasive des molécules de plus haut poids moléculaire, p.ex., les protéines, par voie transdermique. Les chapitres 1, 2 et 3 présentent les études de l'administration transdermique par ionophorèse des agents antiémétiques sélectionnés parmi les différentes classes thérapeutiques utilisées pour traiter des vomissements retardés (par ex., les antagonistes des récepteurs D_2 et 5-HT_3 et les corticostéroïdes). L'influence de différents paramètres sont évalués, tels que la concentration du principe actif, la densité du courant appliqué, la présence d'ions compétiteurs, le métabolisme cutané, ainsi que la faisabilité d'administrer des quantités thérapeutiques de ces médicaments par ionophorèse transdermique *in vivo*.

L'étude portant sur le granisétron, décrite dans le premier chapitre, a confirmé que ce principe actif est un candidat idéal pour l'administration transdermique par ionophorèse. Son transport, dont le mécanisme principal est l'électromigration, varie linéairement en fonction de la concentration. Les flux maximaux, obtenus à 0,3 $mA.cm^{-2}$ en l'absence de chlorure de sodium sont supérieurs à ceux obtenus avec d'autres techniques déjà essayées afin d'améliorer son passage transdermique. Bien que le flux *in vivo* ait été inférieur à celui *in vitro*, les résultats de l'étude chez le rat ont démontré qu'il serait possible d'administrer des quantités thérapeutiques du granisétron en quelques heures avec un patch de dimension tolérable (4 - 6 cm^2).

La métoclopramide, lors de son passage à travers la peau, subit des dégradations enzymatiques (~20%). Des expériences conduites *in vitro* ont montré que le transport du principe actif à travers la peau est favorisé par l'absence d'ions compétitifs, augmentant le flux total d'un facteur de 1,5. Bien que l'administration du métoclopramide *in vivo* ait été plus

faible que celle prédite à partir des données *in vitro*, comme pour le granisétron, les flux mesurés pourraient être suffisants pour atteindre des concentrations thérapeutiques chez l'homme.

En ce qui concerne la dexaméthasone, il a été établi que le transport ionophorétique de sa prodrogue, la dexaméthasone phosphate sodique, augmente linéairement en fonction de la concentration et de la densité du courant, permettant ainsi de contrôler la cinétique d'administration. Compte tenu de la posologie quotidienne de la dexaméthasone de 4 - 20 mg (par voie parentérale) et de 12 mg *per os*, il pourrait être possible d'atteindre des taux thérapeutiques du médicament à des densités de courant acceptables en utilisant des patches de taille moyenne avec une zone d'application de 10 - 20 cm^2.

Le traitement des (NVIC) représente un défi considérable en raison de la complexité de son étiologie. Bien que la première génération d'antagonistes sérotoninergiques (5-HT_3) soit efficace, près de 50% des patients continuent à souffrir de vomissements aigus et retardés, malgré le traitement prophylactique de ces agents. Un certain nombre d'essais cliniques ont démontré la supériorité de la combinaison de dexaméthasone par rapport à la monothérapie avec des antagonistes des récepteurs 5-HT_3 et D_2 administrés individuellement. Dans ce contexte, le chapitre 4 présente l'effet de l'ionophorèse simultanée de granisétron, de métoclopramide et de dexaméthasone phosphate sodique administrés *in vitro* et *in vivo*. L'étude a permis de mettre en évidence l'impact de l'administration concomitante de deux molécules avec la même charge et l'effet sur leur transport ionophorétique. Il serait par ailleurs intéressant de relier le transport ionophorétique avec les propriétés physicochimiques (et leur distribution sur la surface moléculaire). Les résultats *in vivo* indiquent qu'il serait possible d'obtenir des concentrations thérapeutiques des antagonistes D_2 et 5-HT_3 (porteurs de charge positive) et d'un corticostéroïde (porteur de charge négative) administrés simultanément par ionophorèse, tout en gardant une intensité de courant bien tolérée par la peau (0.5 $mA.cm^{-2}$).

Les concentrations plasmatiques des trois médicaments sont restées importantes après la fin de l'application ionophorétique, indiquant que des taux significatifs de médicaments pourraient être maintenus pendant des durées plus longues que ce qui est possible avec des formulations injectables. Ceci offre une bonne alternative aux modes d'administration actuellement disponibles pour traiter des NV retardés induits par chimiothérapie. Néanmoins, ces résultats doivent être confirmés chez l'humain.

Le potentiel de l'ionophorèse comme moyen non-invasif d'administrer des protéines à travers la peau est démontré en chapitre 5 par l'étude du passage transdermique du Cytochrome c, une protéine du poids moléculaire de 12.4 kDa. Les résultats ont confirmé l'administration des quantités importantes de Cytochrome c (~ 0.9 $mg.cm^{-2}$ sur 8 heures) à

travers la peau intact. L'étude a aussi mis en évidence l'effet de la structure et des propriétés moléculaires (p. ex., la distribution de charges sur la surface moléculaire) de la protéine sur son passage transdermique par ionophorèse.

Finalement, l'intérêt pharmacologique de différentes voies d'administration et des nouvelles technologies permettant l'administration de l'hormone de croissance font l'objet du chapitre 6. Leurs applications potentielles, ainsi que leurs limitations sont passées en revue.

INTRODUCTION

Administration de médicaments à travers la peau

L'administration transdermique est de plus en plus courante, la commodité et la facilité d'utilisation de dispositifs transdermiques comme les patches a fait de cette voie d'administration l'une des mieux acceptées. La peau permet d'éviter la dégradation chimique dans le tractus gastro-intestinal et l'effet du premier passage hépatique. Elle est utile pour l'administration des agents thérapeutiques qui ont une faible biodisponibilité ou une courte demi-vie.

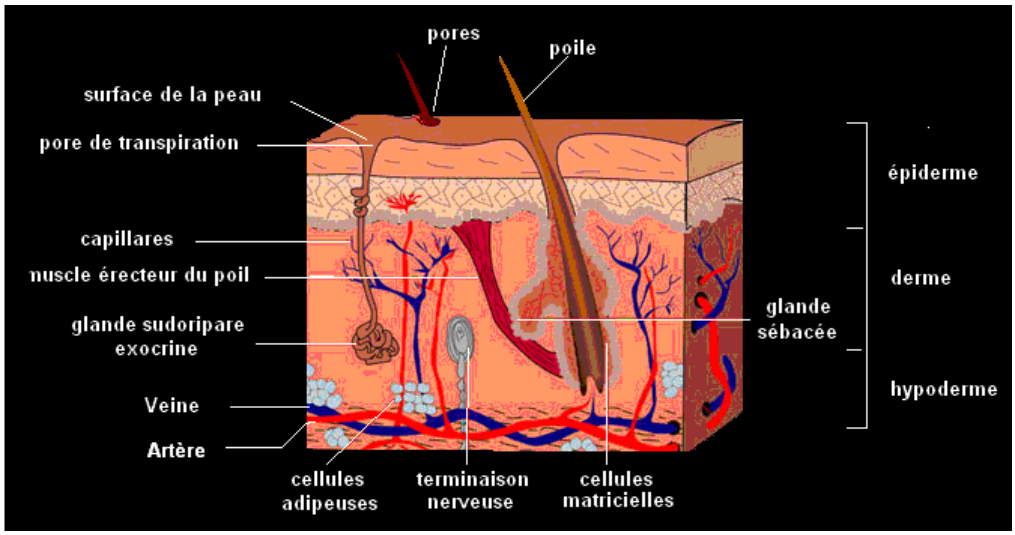

Figure 1. Structure de la peau.

La peau est composée de deux parties, à l'extérieur l'épiderme et en dessous une couche plus épaisse, le derme. Une troisième couche plus profonde est parfois assimilée à la peau: l'hypoderme. Plusieurs fonctions physiologiques de la peau résident essentiellement dans la couche cornée qui contrôle notamment l'entrée de substances exogènes et la perte d'eau. La structure lipidique de la couche cornée limite la pénétration dans l'organisme et restreint la perméabilité de nombreux médicaments qui peuvent être administrés à travers la peau, à des molécules possédant une lipophilie adéquate**.** En général, la diffusion passive des molécules polaires est insuffisante pour obtenir un effet thérapeutique. Afin d'élargir le champ d'application médical de la voie transdermique à des molécules polaires, des efforts considérables dans le développement de techniques impliquant un transport actif à travers la peau ont été faits.

Parmi les nouvelles techniques, l'ionophorèse se caractérise par son degré de contrôle qu'elle offre sur la cinétique de médicaments, son confort d'utilisation et son innocuité.

L'ionophorèse et ses avantages

L'ionophorèse emploie un potentiel électrique à faible intensité pour faciliter la mobilité des molécules à travers la peau. Cette technique augmente de plusieurs ordres de grandeur la pénétration de médicaments dans ou à travers la peau, induisant très peu de dommages [1]. Ses deux mécanismes de transport, l'électromigration et l'électroosmose, permettent le transport de molécules hydrophiles et neutres à travers la couche cornée lipidique. Il a été constaté que l'électromigration domine le transport de molécules chargées de faible poids moléculaire, alors que la présence d'électroosmose facilite la libération de molécules neutres. L'avantage le plus significatif est que l'ionophorèse offre la possibilité de moduler l'intensité et la durée du courant appliqué, permettant ainsi un contrôle stricte du profil d'administration de médicaments à travers la peau [2] :

Flux à travers la peau (mol/cm^2/s): $$J_{tot} = J_{EM} + J_{EO} = \left(\frac{t_i I}{z_i F} \right) + V_W c_i \quad (1)$$

Où: t = la fraction du charge transporté à travers la peau par l'ion), I = densité de courant, z_i = charge de l'ion, F = constante de Faraday, c_i = concentration du principe actif et V_w = flux de solvant qui résulte de la charge négative de la peau à pH physiologique.

Ainsi, l'efficacité de l'administration thérapeutique par ionophorèse peut être améliorée soit par l'augmentation de la densité de courant, soit par la modification de la formulation. La modulation de ces deux facteurs peut offrir une libération continue ou de type pulsée, particulièrement profitable pour les médicaments exerçant des effets pharmacologiques différents en fonction du profil d'administration.

L'importance et la prévalence des nausées et vomissements induits par la chimiothérapie (NVIC)

Le risque de nausées et les vomissements chez les patients recevant une chimiothérapie a été estimée entre 60% et 80% [3, 4]. Néanmoins, l'incidence des symptômes dépend de la substance utilisée (classe, dose, schéma d'administration), mais également des facteurs propres à l'individu. En effet, les facteurs associés à un risque plus élevé des NVIC comprennent la population féminine de moins de 50 ans, la consommation chronique

d'alcool et l'absence d'émèse durant des cycles de chimiothérapie antérieurs [5-7]. Le risque des NVIC est également affecté par le type et le nombre de médicaments utilisés dans un régime de chimiothérapie, ainsi que la dose et la durée du traitement. Des doses élevées par voie intraveineuse injectées rapidement et fréquemment augmentent le risque de NVIC [3, 8]. Le taux de prévalence des NVIC aigu est très variable, en fonction du régime de la chimiothérapie. Il a été estimé que 20% à 30% des patients recevant une chimiothérapie modérément émétisante ont des NVIC. L'incidence des nausées et des vomissements anticipatoires chez les patients recevant une chimiothérapie peut varier entre 14% et 63% [9]. Les mécanismes des NV chimio-induits ont été graduellement élucidés depuis les 25 dernières années.

Ces nausées et vomissements peuvent avoir de graves conséquences qui comprennent la détérioration de la qualité de vie et éventuellement la suspension du traitement médical [10]. Les désordres hydroélectrolytiques sont parmi les conséquences les plus importantes des NVIC puisqu'ils peuvent précipiter des événements cardiovasculaires (de l'hypotension et des arythmies ventriculaires), rénaux (l'augmentation de la sensibilité à la néphrotoxicité), pulmonaires (de l'hypoventilation), musculaires (des spasmes et des crampes) et neurologiques (des paresthésies, de l'agitation) [11]. Les nausées et vomissements prolongés peuvent également conduire à la malnutrition, pouvant aboutir à la dégradation musculaire et la perte de poids affectant la survie des patients. Les NVIC peuvent être difficiles à supporter émotionnellement et avoir un impact négatif sur tous les aspects de la qualité de vie (physique, cognitif, affectif et social). La fatigue, l'étourdissement, la confusion et l'anorexie sont parmi les effets psychosociaux des NVIC. Les patients ayant une expérience incontrôlée des NVIC doivent parfois différer leur traitement ou même réduire les doses, ce qui peut compromettre l'efficacité finale du traitement anticancéreux [11].

En outre, les patients mal contrôlés avec des NVIC sont plus à risque pour le développement de nausées et vomissements anticipatoires pendant les traitements futurs avec pour conséquence de devenir plus sensible à d'autres effets indésirables de la chimiothérapie [12].

Physiologie des NVIC

Les vomissements sont produits lors de la stimulation du centre du vomissement par les neurotransmetteurs libérés au niveau de la zone de déclenchement de chimiorécepteurs (qui est située sur la surface dorsale du myélencéphale) et le tractus gastro-intestinal [13]. Les cinq principales voies afférentes mises en cause dans la stimulation du centre du vomissement sont:

a) la zone de déclenchement des chimiorécepteurs qui contient de nombreux récepteurs dopaminergiques (D_2), sérotoninergiques (5-HT_3), opioïdes, et des récepteurs à l'acétylcholine et à la substance P;
b) la voie muqueuse vagale du système gastro-intestinal qui transmet les informations sur l'état du système gastro-intestinal ;
c) les voies neuronales du système vestibulaire qui envoient les informations au cerveau via le nerf crânien VIII;
d) les voies afférentes du réflexe issues du cortex cérébral C2, C3;
e) les voies afférentes mésencéphales.

Types de nausées et vomissements

Il existe trois types de NVIC:
a) les nausées et vomissements (NV) aigus qui surviennent dans les 24 premières heures suivant le début de l'administration de la chimiothérapie [13, 14] ;
b) les NV retardés qui surviennent 24 heures après le début de la chimiothérapie; ce type de nausées et vomissements peut persister jusqu'à une semaine environ (5 à 7 jours) après le début du traitement [15] ;
c) le troisième type de NVIC sont les NV anticipatoires qui se produisent avant le début du traitement. Ils sont directement reliés au mauvais contrôle des nausées et vomissements lors des cycles précédents de chimiothérapie [16]. Les NV réfractaires peuvent être observés dans la phase aiguë, retard ou anticipatoire. Ils sont considérés cliniquement par deux vomissements ou 4 heures de nausées modérées à importantes par 24 heures.

Traitement des NVIC

Les antagonistes des récepteurs sérotoninergiques 5-HT_3 sont devenues la pierre angulaire du traitement des NVIC en raison de leur efficacité et de leur innocuité. Ces molécules bloquent l'effet de la sérotonine libérée par les cellules entérochromaffines du tube gastro-intestinal et bloquent aussi la stimulation sérotoninergique directement au centre du vomissement. Les molécules les plus utilisées sont l'ondansétron, le dolasétron, le granisétron et plus récemment le palanosétron. Les corticostéroïdes font aussi partie intégrante de l'arsenal thérapeutique du traitement des nausées et vomissements. Ils sont généralement associés aux antagonistes 5-HT_3 dans le traitement des NVIC à haut potentiel émétisant [17]. Le mécanisme d'action des corticostéroïdes comme agents anti-nauséeux n'est pas clairement élucidé. Leur action pourrait venir d'une inhibition des voies afférentes vers le cortex cérébral où se retrouve le centre du vomissement. Les corticostéroïdes

recommandés sont la dexaméthasone et la prednisone ou la methylprednisolone [15]. Le métoclopramide et la dompéridone sont deux antagonistes dopaminergiques couramment employés dans le traitement des NVIC. Le métoclopramide bloque les récepteurs D_2 centraux et diminue donc la stimulation CTZ par la dopamine. Employée à haute dose, le métoclopramide bloquerait aussi les récepteurs 5-HT_3, procurant donc une couverture plus complète. Les bloquants dopaminergiques de types phénothiazines ou butyrophénones peuvent aussi être utilisés mais leur profils d'effets secondaires limitent souvent leur utilisation. Les benzodiazépines sont des substances habituellement réservées à la prévention des nausées anticipatoires. Le lorazépam, clonazépam, le midazolam ou l'alprazolam peuvent être utilisés d'emblée lors du premier cycle de chimiothérapie afin de diminuer le plus possible le risque de nausée d'anticipation lors des cycles subséquents. Les cannabinoïdes, comme la nabilone et le dronabinol, peuvent aussi être utilisés dans le traitement des NVIC. L'aprépitant, un antagoniste des récepteurs de la neurokinine-1 (NK-1), est un nouveau médicament qui a démontré une certaine efficacité dans la prévention des nausées retardées, comparativement aux antagonistes sérotoninergiques qui ne sont pas très efficaces à ce niveau.

Les inconvénients des traitements existants

Les médicaments antiémétiques sont administrés par voie intraveineuse au cours de perfusions. Généralement, les injections répétées ont tendance à irriter et à abîmer les veines. En plus, la réalisation des perfusions s'accompagne d'un certain nombre de difficultés: la présence indispensable de personnel médical qualifié, la prise en charge des dispositifs d'injection (p. ex., cathéters) et le risque d'infection, ce qui rend cette voie d'administration moins pratique pour traiter des NV retardés. L'administration orale diminue les risques liés aux perfusions mais elle n'est pas la mieux adaptée au traitement des patients atteints du cancer et qui sont justement sujettes à des vomissements. La diarrhée et l'ulcération gastro-intestinale peuvent gravement réduire la biodisponibilité orale. En outre, les effets toxiques de la chimiothérapie et des radiations sur la muqueuse buccale peuvent provoquer une inflammation de la muqueuse localisée au niveau de la bouche et du tube digestif, survenant chez ~40% des patients. Cela provoque la douleur et la détresse mais aussi la possibilité de diminuer la tolérance de la chimiothérapie ainsi que l'efficacité d'autres thérapies. Vu l'importance de la thérapie dans le maintien de la qualité de vie des patients recevant un traitement de chimiothérapie, il faut développer une alternative qui permette l'administration simple et efficace des médicaments antiémétiques.

Les études sur l'ionophorèse transdermiques d'antiémétiques ont commencé à la fin des années quatre-vingt-dix. L'administration des antagonistes dopaminergiques (D_2) et

sérotoninergiques (5-HT_3) comme la domperidone [18], la metoclopramide [19] et le granisétron [20] par cette voie ont été évalués. La déxamethasone a aussi été étudiée et administrée avec succès *in vivo* et *in vitro* – mais dans le contexte d'une application locale comme anti-inflammatoire [21-24]. Compte tenu des propriétés physicochimiques, l'administration parallèle des agents antiémétiques sélectionnés parmi les différentes classes thérapeutiques par ionophorèse semble être faisable.

Références

1. Jadoul A., Bouwstra J., Préat V. Effects of iontophoresis and electroporation on the stratum corneum. Review of the biophysical studies. Adv. Drug. Deliv. Rev. 35 (1999) 89-105.
2. Kalia Y. N., Naik A., Garrison J., Guy R. H. Iontophoretic drug delivery. Adv. Drug. Deliv. Rev. 56 (2004) 619-658.
3. Gunmerg, S. M., Hesketh, P. J. Control of chemotherapy-induced emesis. N. Engl. J. Med. 329 (1993) 1790-1796.
4. Cohen L., de Moor C. A., Eisenberg P., Ming E. E., Hu H. Chemotherapy-induced nausea and vomiting: incidence and impact on patient quality of life at community oncology settings. Support Care Cancer. 15 (2007) 497-503.
5. Roila F., Boschetti E., Tonato M., Basurto C., Bracarda S. Picciafuoco M., Patoia L., Santi E., Penza O., Ballatori E., et al. Predictive factors of delayed emesis in cisplatin-treated patients and antiemetic activity and tolerability of metoclopramide or dexamethasone. A randomized single-blind study. Am. J. Clin. Oncol. 14 (1991) 238-242.
6. Morrow G.R. Clinical characteristics associated with the development of anticipatory nausea and vomiting in cancer patients undergoing chemotherapy treatment. J. Clin. Oncol. 2 (1984)1170-1176.
7. Sullivan J. R., Leyden M. J., Bell R. Decreased cisplatin-induced nausea and vomiting with chronic alcohol ingestion. N. Engl. J. Med. 309 (1983) 796.
8. Hesketh P.J. Defining the emetogenicity of cancer chemotherapy regimens: relevance to clinical practice. The Oncologist 4 (1999) 191-196.
9. Gralla R. Antiemetic Therapy In: Bast R., Kufe D., Pollock R., et al., eds. Cancer Medicine (online version). Hamilton, Ontario: BC Decker, 2000.
10. Griffin A. M., Butow P. N., Coates A. S., Childs A. M., Ellis P. M, Dunn S. M., Tattersall M. H. On the receiving end. V: Patient perceptions of the side effects of cancer chemotherapy in 1993. Ann. Oncol. 7 (1996)189-195.

11. Bender C. M., McDaniel R. W., Murphy-Ende K., Pickett M., Rittenberg M., Rogers M. P., Schneider S. M., Schwartz R. N. Chemotherapy-induced nausea and vomiting. Clin. J. Oncol. Nurs. 6 (2002) 94-102.
12. Dobkin P., Zeichner A., Dickson-Parnell B. Concomitants of anticipatory nausea and emesis in cancer patients in chemotherapy. Psychol. Rep. 56 (1985) 671-676.
13. Veyrat-Follet C., Farinotti R., Palmer J. L. Physiology of chemotherapy-induced emesis and antiemetic therapy. Predictive models for evaluation of new compounds. Drugs 53 (1997) 206-234.
14. Hesketh P.J. Defining the emetogenicity of cancer chemotherapy regimens: relevance to clinical practice. Oncologist 4 (1999)191-196.
15. Tavorath R., Hesketh P. J. Drug treatment of chemotherapy-induced delayed emesis. Drugs. 52 (1996) 639-648.
16. Eckert R. M. Understanding anticipatory nausea. Oncol. Nurs. Forum. 28(2001) 1553-1558.
17. American Society of Clinical Oncology, Kris M. G. Hesketh P. J., Somerfield M. R., Feyer P., Clark-Snow R., Koeller J. M., Morrow G. R., Chinnery L. W., Chesney M. J., Gralla R. J., Grunberg S. M. American Society of Clinical Oncology guideline for antiemetics in oncology: update 2006. J. Clin. Oncol. 24 (2006) 2932-2947.
18. Jadoul A., Preat V. Electrically enhanced transdermal delivery of domperidone. Int. J. Pharm. 154 (1997) 229-234.
19. Cormier M., Chao S. T., Gupta S. K., Haak R. Effect of transdermal iontophoresis codelivery of hydrocortisone on metoclopramide pharmacokinetics and skin-induced reactions in human subjects. J. Pharm. Sci. 88 (1999) 1030-1035.
20. Chaturvedula, A., Joshi, D. P., Anderson, C., Morris, R., Sembrowich, W. L., Banga, A. K. Dermal, subdermal, and systemic concentrations of granisetron by iontophoretic delivery. Pharm. Res. 22 (2005) 1313-1319.
21. Glass J. M., Stephen R. L., Jacobson S. C. The quantity and distribution of radiolabeled dexamethasone delivered to tissue by iontophoresis. Int. J. Pharm. 19 (1998) 519-525.
22. Petelenz T. J., Buttke J. A., Bonds C., Lloyd L. B, Beck J. E., Stephen R. L., Jacobsen S. C., Rodriguez P. Iontophoresis of dexamethasone: laboratory studies. J. Control. Rel. 20 (1992) 55-66.
23. Sylvestre J.-P., Guy R. H., Delgado-Charro M. B. In vitro optimization of dexamethasone phosphate delivery by iontophoresis. Phys. Ther. 88 (2008) 1177-1185.

24. Sylvestre J.-P., Díaz-Martín C., Delgado-Charro M. B., Guy R. H. Iotophoresis of dexamethasone phosphate: competition with chloride ions. J. Control. Rel. 131 (2008) 41-46.

Using transdermal iontophoresis to increase granisetron delivery across skin *in vitro* and *in vivo*: effect of experimental conditions and a comparison with other enhancement strategies

Jennyfer Cázares-Delgadillo[1], Adriana Ganem-Rondero[2], David Quintanar-Guerrero[2], Alicia C. López Castellano[3], Virginia Merino[4], Yogeshvar N. Kalia[1]

[1] School of Pharmaceutical Sciences, University of Geneva & University of Lausanne, 30 Quai Ernest Ansermet, 1211 Geneva, Switzerland.

[2] División de Estudios de Posgrado (Tecnología Farmacéutica), Facultad de Estudios Superiores Cuautitlán, Universidad Nacional Autónoma de México, Av. 1° de Mayo S/N Cuautitlán Izcalli, Estado de México 54704, Mexico.

[3] Departamento de Fisiología, Farmacologia y Toxicología, University Cardenal Herrera (CEU), Edificio Seminario s/n, 46113 Moncada, Valencia, Spain.

[4] Departamento de Farmacia y Tecnología Farmacéutica, Faculty of Pharmacy, University of Valencia, Avda. Vicente Andrés Estellés s/n, 46100 Burjassot, Valencia, Spain.

European Journal of Pharmaceutical Sciences, Vol. 39, No. 5 (2010): 387- 393

ABSTRACT

The objectives of the study were (i) to investigate the effect of experimental parameters on the iontophoretic transport of granisetron, (ii) to identify the relative contributions of electromigration (EM) and electroosmosis (EO), (iii) to determine the feasibility of delivering therapeutic amounts of drug for the treatment of chemotherapy-induced nausea and vomiting and (iv) to test the *in vitro* results in a simple animal model *in vivo*. Preliminary *in vitro* studies using aqueous granisetron formulations investigating the effect of drug concentration (5, 10, 20 and 40 mM) and current density (0.1, 0.2, 0.3 $mA.cm^{-2}$) were performed using porcine ear skin. As expected, cumulative delivery *in vitro* at the 20 and 40 mM concentrations was significantly greater than that at 5 and 10 mM, which were not statistically different ($p<0.05$). Increasing the applied current density from 0.1 to 0.3 $mA.cm^{-2}$

resulted in a ~4.2-fold increase in iontophoretic flux. Furthermore, in the absence of Na^+ in the formulation, no dependence of iontophoretic flux on drug concentration was reported (at a granisetron concentration of 40 mM, the transport rate was 2.93 ± 0.62 $\mu g.cm^{-2}.min^{-1}$). Co-iontophoresis of acetaminophen was used to show that EM was the predominant transport mechanism accounting for 71-86% of total granisetron delivery. *In vivo* studies in Wistar rats (40 mM granisetron; application of 0.3 $mA.cm^{-2}$ for 5 h with Ag/AgCl electrodes and salt bridges) showed an average iontophoretic input rate (k_{input}) of 0.83 ± 0.26 $\mu g.min^{-1}$ and a maximum plasma concentration (C_{max}) of 0.092 ± 0.004 $\mu g.ml^{-1}$. Based on these results and given the known pharmacokinetics, transdermal iontophoresis could achieve therapeutic drug levels for the management of chemotherapy-induced emesis using a reasonably sized (4-6 cm^2) patch.

Key words: granisetron, iontophoresis, electromigration, electroosmosis, transdermal.

INTRODUCTION

Prevention and control of nausea and vomiting is vital for the effective treatment of cancer patients. The administration of 5-hydroxytryptamine type 3 (5-HT_3) receptor antagonists has transformed the therapeutic approach to acute and delayed emesis. Granisetron (GST; MW: 348.9, pKa 9.4 (Figure 1)), has demonstrated efficacy in preventing and controlling chemotherapy induced nausea and vomiting. However, effective control depends not only on the dose, but also on the duration of treatment and the route of administration. Both the oral and intravenous (IV) routes, which are routinely used, present disadvantages; for example, IV administration requires qualified medical personnel and it is not practical for chronic treatment on an outpatient basis (for example, in the treatment of delayed emesis) whereas the oral route can be associated with erratic drug absorption, especially in patients suffering from nausea and prone to vomiting. Transdermal iontophoresis provides a non-invasive alternative for controlled drug delivery (Kalia *et al.*, 2004); the application of a small electric potential enables the transport of polar and charged drug molecules into the skin. In addition to expanding the range of drugs that can be delivered by this route, iontophoresis provides a tight control over drug input kinetics and reduces intra- and inter-individual variability. The transdermal iontophoretic delivery of GST has been achieved across hairless rat skin (Chaturvedula *et al*., 2005). This study showed that drug could be delivered by iontophoresis and microdialysis was used to show that the drug penetrated a few millimeters within the skin leading to the formation of a depot in the subcutaneous and dermal tissues. The objectives of the present study were: (i) to examine the effect of experimental conditions on GST transport *in vitro*, (ii) to investigate the transport

mechanism, including the identification of the relative contributions of electromigration (EM) and electroosmosis (EO), which can impact upon formulation conditions, (iii) to study the pharmacokinetic drug profile *in vivo* and hence (iv) to evaluate the feasibility of delivering therapeutic amounts of granisetron for the teatment of chemotherapy-induced nausea and vomiting using a novel transdermal iontophoretic system.

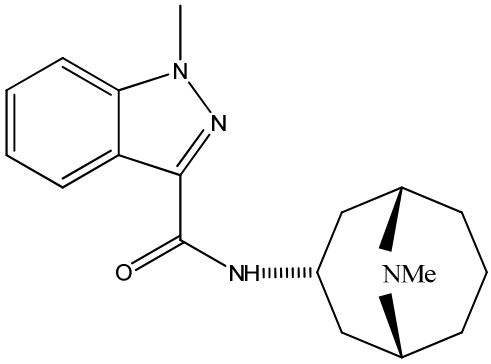

Figure 1. Chemical structure of granisetron (GST; MW: 348.9, pKa 9.4).

MATERIALS AND METHODS

Materials

Porcine ear skin was obtained from two abattoirs (STAC, Chambery, France and Carre Coopérative des Abattoirs de Rolle, Switzerland). The skin was excised (thickness 750 µm) with an electro-dermatome (Zimmer, Etupes, France), wrapped in Parafilm® and stored at -20℃ for a maximum period of 2 months.

Granisetron hydrochloride was a gift from Roche Diagnostics GmbH (Mannheim, Germany). HEPES buffer and sodium chloride were obtained from Fluka (Buchs, Switzerland). Acetaminophen (ACE), agarose, sodium heptanesulfonate, silver wire and silver chloride used for the fabrication of electrodes were purchased from Sigma-Aldrich (Steinheim, Germany). Silicon tubing (1.6 mm ID, 3.2 mm OD, 0.8 mm wall thickness) for collecting samples and PVC tubing (3 mm ID, 5 mm OD, 1 mm wall thickness) used to prepare the salt bridge assemblies were obtained from Fisher Bioblock Scientific S.A. (Illkirch, France). Chromatographic reagents were obtained from VWR (Dietikon, Switzerland). All solutions were prepared using deionised water (resistivity > 18 MΩ.cm). All other chemicals were at least of analytical grade.

***In vitro* protocol**

Electrical stability

The stability of GST solutions was evaluated in contact with current prior to the iontophoretic permeation studies. Briefly, 5 ml of GST solution (10 mM GST in 100 mM NaCl, pH 6.8) was subjected to a current density of 0.3 $mA.cm^{-2}$. Samples were collected and analyzed every hour for a period of 7 h. Experiments were performed in triplicate.

Stability in the presence of skin

The influence of porcine ear skin on GST stability in solution was assessed by preparing (a) 200 µM GST in 25 mM HEPES / 133 mM NaCl (pH 7.4) and (b) 10 mM GST in 100 mM NaCl (pH 6.8). The dermal and epidermal surfaces of dermatomed skin samples were placed in contact with solutions (a) and (b), respectively during 7 h. Aliquots from the medium in contact with the dermal surface were collected after 15, 30, 45, 60, 90, 120, 180, 240, 300, 360, 420 min. Samples of the solution in contact with the epidermal surface were withdrawn hourly. Experiments were performed in triplicate.

Iontophoretic permeation studies

1) Effect of drug concentration: Dermatomed porcine ear skin (thickness 750 µm) was clamped in three-compartment vertical flow-through diffusion cells (area 0.95 cm^2). After a 40 min. equilibration period with 25 mM HEPES / 133 mM NaCl (pH 7.4), 1 ml of aqueous GST solution (5, 10, 20 or 40 mM) containing 100 mM NaCl was placed in the anodal compartment (pH 6.6 - 6.8). Co-iontophoresis of acetaminophen (ACE) was used to report on convective solvent flow. The cathodal and receptor compartments were filled with 1 and 6 ml of 25 mM HEPES/133 mM NaCl (pH 7.4), respectively. Samples were collected hourly using a syringe pump (SP220IZ, WPI, Sarasota, FL), which ensured a continuous flow of buffer solution (1 $ml.h^{-1}$). A constant current density of 0.3 $mA.cm^{-2}$ was applied for 7h via Ag/AgCl electrodes connected to a power supply (APH 1000M, Kepco, Flushing, NY).

2) Effect of competing ions: GST formulations (20 and 40 mM; pH 6.8) were prepared in the absence of NaCl in order to study the effect of competing cations. Salt bridges (SB) were included to separate the electrode and formulation compartments; transport experiments were conducted at a current density of 0.3 $mA.cm^{-2}$.

3) Effect of current density: GST transport at different current densities (0.1, 0.2 and 0.3 $mA.cm^{-2}$) was also investigated. A 20 mM GST unbuffered solution and SB were used in these experiments (pH 6.8).

All experiments were performed in at least triplicate.

The total flux (J_{tot}) of GST during iontophoresis, assuming negligible passive diffusion, is given by the following equation (Kalia *et al.*, 2004):

$$J_{tot} = J_{EM} + J_{EO} = \left(\frac{i_d}{F} \bullet \frac{u_{GST}}{\sum_{1}^{i} z_i u_i c_i} + V_W \right) c_{GST}$$

where J_{EM} and J_{EO} represent the contributions of EM and EO to the total flux. J_{EM} is related to the current density (i_d), by Faraday's constant (F) and is proportional to the mobility (u_{GST}) and concentration (c_{GST}) of the molecule in the membrane; z_i, u_i, and c_i refer to the corresponding values for the other charge carriers in the system. J_{EO} is the product of the solvent permeability coefficient (V_w) and drug concentration, c_{GST}.

Inhibition Factor

For each experiment, co-iontophoresis of ACE also enabled the calculation of an inhibition factor (IF) to report on the effect of GST transport on skin permselectivity:

$$IF = \frac{Q_{ACE,\ control}}{Q_{ACE}}$$

where $Q_{ACE,control}$ is the cumulative amount of ACE delivered calculated during 7 h of iontophoresis, and Q_{ACE} is the corresponding value when GST was simultaneously iontophoresed.

***In vivo* protocol**

Surgical procedure

The clinical protocol was approved by the Ethics Committee for Animal Experimentation at the University of Valencia, Spain. Male Wistar rats weighing 260-300 g were used for the experiments. Twenty four hours before iontophoresis, the rats were anesthetized by intraperitoneal administration of pentobarbital sodium (Dolethal solution, 40 $mg.kg^{-1}$; Vetoquinol, Madrid, Spain). The jugular vein was cannulated using medical grade silicon tubing (Silastic, Dow Corning Co.; inner diameter 0.5 mm; outer diameter, 0.94 mm). The surgical site was cleaned carefully using povidone iodine before and after the surgical procedure. Under anesthesia, 3.4 cm of the cannula was introduced into the jugular vein

toward the heart and the free end was subcutaneously conducted to the dorsal base of the neck, where it emerged. The cannula was permanently filled with heparinized saline solution (20 $IU.ml^{-1}$) and closed with a polyethylene plug. An incandescent lamp (placed ~35 cm from the animal) was used to maintain rat body temperature during the surgical procedure and recovery. Water intake was allowed during the postoperative period and until drug administration.

Iontophoretic delivery experiments

The studies were performed with 3 rats. Animals were anesthetized using pentobarbital sodium (40 $mg.kg^{-1}$) and mounted on a plastic support. Two glass chambers (area 1.33 cm^2) were then placed 2.5 cm apart on the animal's abdomen (shaved beforehand) and fixed with glue (Figure 2). The cathodal and anodal compartments were filled with 25 mM HEPES buffer / 133 mM NaCl (pH 7.0). The donor formulation consisted of 0.7 ml of unbuffered 40 mM GST solution (pH 6.6), which was separated from the anodal compartment by means of a salt bridge. Ag/AgCl electrodes were introduced in the respective solutions; the cathode was maintained at least 5 mm from the skin. A power supply (APH 1000M, Kepco, Flushing, NY) delivered a constant, direct current of 0.4 mA (0.3 $mA.cm^{-2}$) for 5 h. In order to facilitate blood sampling, a 15 cm long silicon tube (bridge-tubing) was connected to the free end of the cannula.

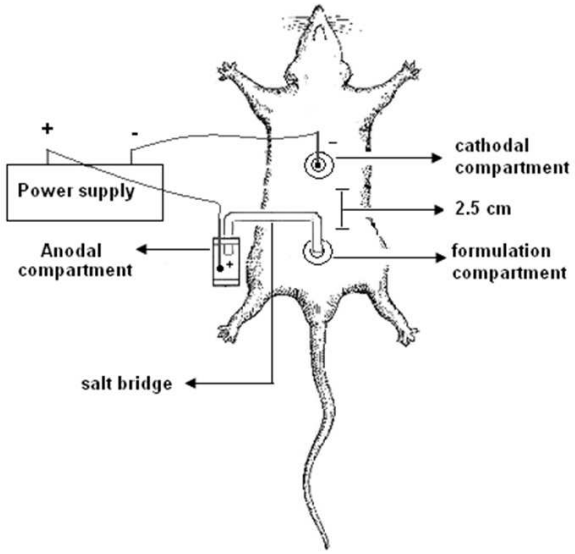

Figure 2. Schematic representation of the experimental set-up for the *in vivo* studies.

Blood samples (0.7 ml) were withdrawn into heparinzed syringes from the jugular vein cannula at intervals of one hour. After each sampling, the blood volume was replaced with the same volume of saline solution. After collection, blood samples were immediately centrifuged at 10,000 rpm and plasma separated and stored at -20℃ until analysis by HPLC

(no longer than 2 months). Repeat doses of the anesthetic (20 mg.kg^{-1}) were administered to maintain anesthesia throughout the experiment. At the end of each experiment, the animal was sacrificed by intraperitoneal administration of a lethal dose of pentobarbital sodium (200 mg.kg^{-1}).

HPLC analysis

A P680A LPG-4 pump equipped with an ASI-100 autosampler and a RF-2000 fluorescence detector (Dionex, Voisins LeBretonneux, France) were used to quantify GST using a method adapted from a published protocol (Boppana, 1995). Resolution was achieved using a Sunfire^{TM} 100 C-18 4.6 µm column. The flow-rate was 2.0 ml.min^{-1} and the column temperature was kept at 50°C using a thermostat (TC C-100, Dionex GmbH, Germany). For the *in vitro* experiments, the mobile phase consisted of acetate buffer 0.1 M at pH 4.7 with 2 g sodium heptanesulfonate and 0.2 g EDTA and acetonitrile (ACN) (73:27 v/v) and the injection volume was 1-100 µl. The optimal fluorescence response for granisetron was observed at excitation and emission wavelengths of 305 and 360 nm, respectively; the gain of the detector was set at unity. The limits of detection (LOD) quantification (LOQ) were 11 and 34 ng, respectively. *In vivo* samples were eluted in a mobile phase similar to that described above, except for the addition of deionised water (30%). The overall composition buffer: ACN: water was 51:19:30 (v/v) and the injection volume was 10 µl. All solvents were filtered (0.45 µm pore size nylon membrane filter) and degassed prior to use and the column was equilibrated for at least 1 h.

Plasma samples were extracted using a method adapted from literature (Hussain *et al.,* 2000). A volume of 0.2 ml of ACN was added to plasma (0.1 ml) and the mixture was vortex-mixed for 5 min and centrifuged at 10000 rpm for 2 minutes at 5°C. An aliquot of the supernatant was injected directly into the HPLC column. Calibration curves (n = 5) spanning the range of GST concentrations in plasma samples were prepared in triplicate in order to validate the analytical method. A linear correlation was obtained and the intercept was not significantly different from zero (r^2 = 0.9998). The relative error and coefficient of variation were the parameters evaluated for accuracy and precision. These values (Food and Drug Administration, 2001) are shown in Table 1. The mean recovery of GST averaged 102.20 ± 4.40 % (n=7); the LOQ was 36.33 ng.ml^{-1}.

The stability of GST in plasma stored at -20°C was also evaluated. Results showed that the drug was stable for 6 weeks; the relative error was ~ 4 % over a concentration range from 88 to 795 ng.ml^{-1}.

Table 1. Accuracy and precision of the HPLC method to quantify GST in plasma samples

Theoretical concentration ($\mu g.ml^{-1}$)	Experimental concentration (Mean ± S.D.) ($\mu g.ml^{-1}$)	C.V. (%)	Deviation from theoretical value (%)	Recovery (%)
Within-day (n=3)				
0.07	0.08 ± 0.00	3.38	6.36	106.36
0.29	0.29 ± 0.02	6.20	0.24	99.76
0.73	0.81 ± 0.04	4.54	10.30	110.30
Between-day (n=3)				
0.07	0.07 ± 0.00	2.59	1.92	101.92
0.29	0.28 ± 0.02	8.91	4.97	95.03
0.73	0.74 ± 0.06	8.68	1.43	101.43

Acetaminophen (ACE) from the *in vitro* experiments was assayed separately using a Lichrospher® 100 RP-8 reversed-phase column. The mobile phase comprised 88% citrate buffer 40 mM (pH 3.0) and 12% ACN. The flow rate and the injection volumes were 1.0 $ml.min^{-1}$ and 1-100 µL, respectively. ACE was detected by its UV absorbance at 243 nm. The LOD and LOQ were 1.81 and 5.05 ng, respectively.

Pharmacokinetic analysis

Estimates of the pharmacokinetic parameters for GST iontophoretic delivery were calculated using a one compartmental model (WinNolin® Professional, Version 5.2.1; Pharsight Corp., Mountain View, CA). The input (k_{01}) and elimination (k_{10}) rate constants were estimated using a Gauss-Newton algorithm with a Levenberg-Hartley modification.

Non-compartmental parameters such as AUC_{0_inf}, C_{max} and half-life were calculated in Microsoft Excel. The value of the volume of distribution after IV administration of GST was obtained from the literature (Chaturvedula *et al.*, 2005).

Pharmacokinetic models

Plasma profiles were fitted to the one compartmental model with zero-order absorption and first-order elimination using WinNonlin software version 5.2.1 as follows:

$$C_p = \left(\frac{k_{input}}{V_d k_{10}}\right)\left(1 - e^{-k_{10}t}\right) \quad if\ t \le t_{ionto}$$

where,C_p : plasma concentration of granisetron; V_d : volume of distribution; k_{input}: input rate; k_{10} : elimination rate constant; t : time; t_{ionto} : duration of current application (5 h).

Statistical analysis

Data were expressed as mean ± S.D. Outliers, determined using the Grubbs test (De Muth, 1999), were discarded. Analysis of variance (ANOVA) was employed to evaluate the difference between groups of data. Student's t-test was used to compare two data sets. The level of significance was fixed at $P < 0.05$.

RESULTS AND DISCUSSION

In vitro studies

The aim of the *in vitro* experiments was to investigate the effect of formulation and iontophoretic conditions on transport kinetics. Granisetron was stable in the presence of electrical current and epidermal skin samples during 7 h. However, it appeared to be subject to slight degradation (7%) in the presence of dermal skin; statistical analysis showed a significant difference between samples collected over the 7 h sampling period ($F = 3.31$; $F_{0.05,\ 11,\ 24} = 2.22$). The cumulative iontophoretic permeation profiles for GST as a function of concentration (5, 10, 20 and 40 mM) are shown in Figure 3. Doubling GST donor concentration from 20 to 40 mM resulted in a significant increase in the cumulative amount of GST delivered; however, cumulative delivery measured using 5 and 10 mM GST formulations was not statistically different (*Student t test*, p <0.05). According to Faraday's law, drug transport will depend on the products of the electrical mobility of charged species and their respective concentrations in the membrane.

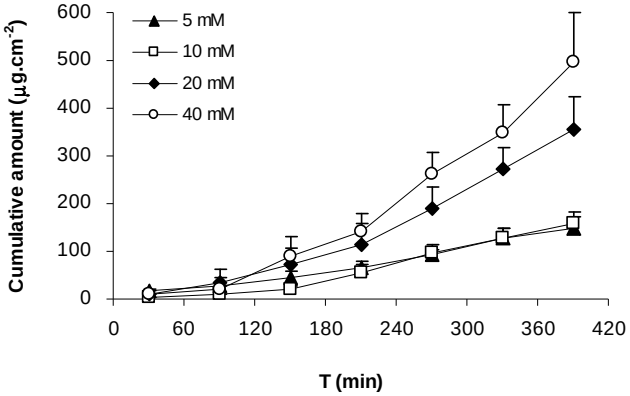

Figure 3. Cumulative iontophoretic permeation of GST during 7 h iontophoresis at 0.3 mA.cm^{-2} (Mean ± S.D.; n ≥ 3).

The presence of Na^+ in the formulation, which possesses higher mobility than GST, can reduce the delivery efficiency at lower concentrations, effectively negating any increase in

formulation concentration (Kasting, 1992; Phipps *et al.*, 1992). Co-iontophoresis of ACE enabled the estimation of the contributions of EM, EO and the calculation of an electroosmotic inhibition factor (IF; Table 2). Control values for ACE flux in the absence of drug were determined independently at 0.3 mA.cm^{-2}

Table 2. Iontophoretic flux of GST and the EM and EO contributions as a function of concentration (0.3 mA.cm^{-2}); IF is the inhibition factor reporting on the effect of GST delivery on skin permselectivity.

C (mM)	J_{tot} (µg.cm^{-2}min^{-1})	J_{EM} (µg.cm^{-2}min^{-1})	J_{EO} (µg.cm^{-2}min^{-1})	IF
5	0.39 ± 0.13	0.31	0.08	0.39 ± 0.17
10	0.57 ± 0.06	0.41	0.16	0.80 ± 0.24
20	1.41 ± 0.62	1.22	0.20	1.57 ± 0.60
40	2.50 ± 0.79	2.08	0.42	1.76 ± 0.85

J_{tot}= Total steady-state flux; J_{EM}= Electromigration flux; J_{EO}= Electroosmosis flux; IF= Inhibition factor.

The results showed that EM was the dominant transport mechanism accounting for 71-86% of transport over the concentration range studied (5 – 40 mM). GST iontophoresis resulted in a concentration-dependent decrease in ACE transport indicating that GST iontophoresis decreased skin permselectivity. Thus, the 4-fold increase in GST concentration from 10 to 40 mM resulted in a 2-fold reduction in ACE delivery (IF increased from 0.80 ± 0.24 to 1.76 ± 0.85).

In the absence of competing ion (Na^+) in the formulation, no dependence of iontophoretic flux on drug concentration was reported at 0.3 mA-cm^{-2} (*Student's t test*, P <0.05); experiments performed at 20 and 40 mM resulted in transport rates of 2.45 ± 0.63 µg.cm^{-2}.min^{-1} and 2.93 ± 0.62 µg.cm^{-2}.min^{-1}, respectively (Figure 4).

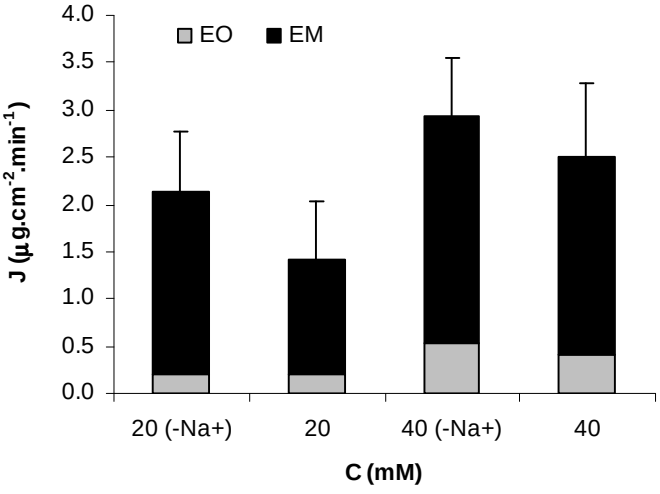

Figure 4. The effect of donor concentration on the iontophoretic transport of GST at 0.3 mA.cm^{-2} in the absence (-Na^+) and in the presence of competing ions. The data demonstrate that EM was the predominant iontophoretic transport mechanism. (Mean ± S.D.; n = 5).

Although the transport efficacy – as calculated transport numbers remains – effectively the same, the fraction of drug load delivered was higher at the lower formulation concentration (20 mM). It has been proposed that in the absence of competing cations, iontophoretic flux is independent of concentration and dependent only on the ratio of diffusivities of the cation and the main counterion (usually Cl^-) arriving in the donor compartment from beneath the skin (Kasting *et al.*, 1992). The impact of increasing current density from 0.1 to 0.3 $mA.cm^{-2}$ in the absence of competing ions is illustrated in Figure 5. As it can be seen, a 2-fold increase in applied current density from 0.1 to 0.2 $mA.cm^{-2}$ resulted in a ~4.2-fold increase in the EM and EO contributions; however, transport contributions at 0.2 and 0.3 $mA.cm^{-2}$ were not significantly different (*Student's t test, $p < 0.05$*). For small molecules, the flux due to electromigration, J_{EM}, should increase with the applied current (Lau *et al.*, 1994, Gupta *et al.*, 1998, Singh *et al.*, 1999). However, it has been suggested that at high current densities, the iontophoretic response saturates and once a limiting transport number is achieved, further increase in current has no effect (Kasting *et al.*, 1989). In order to compare the present results (40 mM GST concentration, 0.29 mA) with those obtained using hairless rat skin (Chaturvedula *et al.*., 2005; 57.3 mM GST, 0.2 mA), the *in vitro* GST fluxes from the two studies were current-normalized. Results showed that flux across porcine skin (10.28 $\mu g.mA^{-1}.cm^{-2}.min^{-1}$) was ~2-fold higher that that obtained across hairless rat skin (5.87 $\mu g.mA^{-1}.cm^{-2}.min^{-1}$). However, the observed iontophoretic flux in the latter study may have been at pre-steady-state since current was only applied for 2 h.

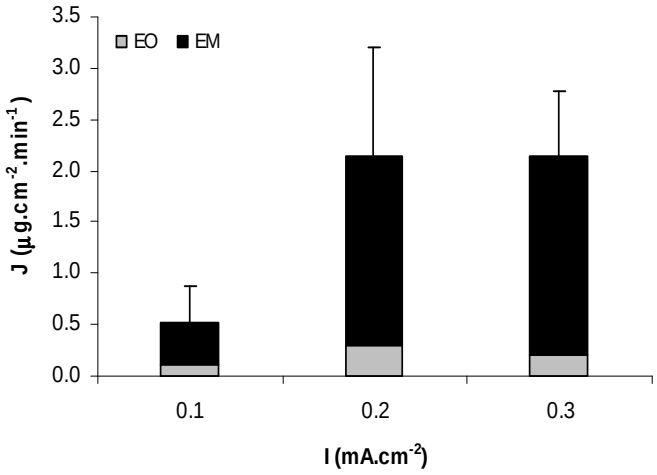

Figure 5. Iontophoretic transport of GST as a function of current density at constant donor concentration (20 mM). (Mean ± S.D.; n ≥ 4).

Radiofrequency (RF) induced thermal ablation has been used to enhance GST transport (GST 32 mM, ($-Na^+$)) across full thickness porcine ear skin (Sintov *et al.*, 2003); an array of small microchannels was created in the epidermis by microablating skin cells (100 $microchannels.cm^{-2}$). The results showed that pre-treatment with the RF microelectrodes enhanced delivery with respect to the control (untreated skin) resulting in a flux of

0.69 µg.cm^{-2}.min^{-1}. Comparison with the present study reveals that iontophoresis is the more efficient technique for GST delivery, resulting in a ~4-fold greater flux (2.45 ± 0.62 µg.cm^{-2}.min^{-1}; donor concentration = 20 mM (-Na^{+})).

Other approaches to increase the transdermal delivery of 5-HT$_3$ antagonists (ondansetron and granisetron) have involved the use of synthetic chemical enhancers such as surfactants, fatty acids (Ding *et al.*, 2000, Takahashi *et al.*, 2001, Dimas *et al.*, 2004) and solvents (Gwak *et al.*, 2004). A combination of oleic acid and ethanol was shown to significantly enhance the permeability of ondansetron through shed snake skin (Takahashi *et al.*, 2001); pretreatment with oleic acid followed by application of 60% ethanolic solution resulted in a flux of ~0.39 µg.cm^{-2}.min^{-1}. Similarly, an increase in the steady-state delivery of ondansetron (from 0.0012 to 0.06 µg.h^{-1}) was observed when oleic acid formulated in propylene glycol (5% (w/v)) was used as promoter (Ding *et al.*, 2000); however, extrapolation of these ondansetron transport rates suggests that delivery would probably be sub-therapeutic from a reasonably-sized patch. The use of mixtures of different solvents and fatty acids on the permeation of ondansetron has also been investigated; highest enhancement was observed by the addition of unsaturated fatty acids, oleic and linoleic acid, to propylene glycol (Gwak *et al.*, 2004).

Although these studies show that chemical permeation enhancers can increase 5-HT$_3$ antagonist transport, the extent of enhancement required to ensure delivery of therapeutic amounts is still limited *in vivo* by the risk of skin irritation. Encapsulation technologies (Krishnaiah *et al.*, 2009) and biochemical enhancers (Kim *et al.*, 2008) have also been suggested for the delivery of antiemetic dugs. Ethylene vinyl acetate (EVA) copolymer membranes prepared with polyethylene glycol 6000 (PEG6000 at 10% w/w) were found to be effective for ondansetron delivery (Krishnaiah *et al.*, 2009). The flux achieved across rat epidermis *in vitro* was 1.86 ± 0.02 µg.cm^{-2}.min^{-1}. The use of a hydroethanolic pre-treatment (60 % EtOH for 12 h) and magainin (a charged peptide) to increase GST transport across heat-separated human epidermis was recently reported (Kim *et al.*, 2008). However, highest delivery (~0.98 µg.cm^{-2}.min^{-1}, again less than that seen during iontophoresis) was observed at pH 10 – where both the magainin and GST were uncharged; given the conditions, and the fragility of epidermis, it remains to be seen how these data would extrapolate to human skin *in vivo*.

In vivo studies

Experimental and predicted values for the GST mean plasma concentration-time profile are shown in Figure 6. Granisetron was detected in the bloodstream at the first time-point (60 min) and maximum drug levels were 0.09 ± 0.004 µg.ml^{-1} at *t* = 300 min (Figure 6). The

standard deviations during current application were small; however, they increased immediately post-iontophoresis (t=360 and 420 min).

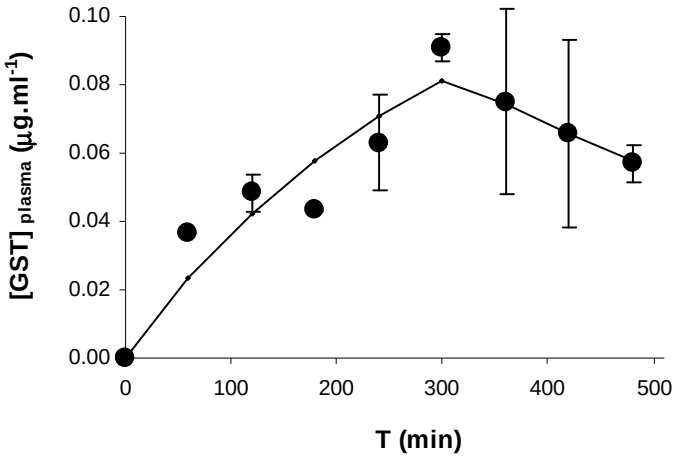

Figure 6. GST concentrations in plasma versus time in rats during and post-iontophoresis. A current density of 0.3 mA.cm^{-2} was applied for 5 h to an unbuffered 40 mM GST solution (pH 6.6) using Ag/AgCl electrodes and a salt bridge. The lines represent the predicted values (Mean ± S.D.; n = 3).

Granisetron levels decreased upon termination of current application but remained significant throughout the 5 - 8 h time-period indicating that reasonable levels of drug could be maintained for longer intervals than is currently possible with injectable formulations. Pharmacokinetic parameters obtained after iontophoretic delivery are given in Table 3.

Table 3. Pharmacokinetic parameters of GST following iontophoretic administration

Parameter	IV*	Iontophoresis
C_{max} (µg.ml^{-1})		0.092 ± 0.004
$AUC_{0\text{-}inf}$ (µg.min.ml^{-1})	26.21 ± 6.32	37.20 ± 7.67
Half-life (min)	80.23 ± 43.08	181.69 ± 10.00
Clearance (ml.min^{-1}.kg^{-1})	46.40 ± 10.41	
Volume of distribution (V_d) (l.kg^{-1})	5.81 ± 4.19	
Input rate constant (k_{input}) (µg.min^{-1})		0.83 ± 0.27
Elimination rate constant (k_{10}) (min^{-1})	0.011 ± 0.0006	0.0042 ± 0.003

*IV administration data from Chaturvedula *et al.*, 2005.

The goodness of the fit of the pharmacokinetic model can be observed through the correlations between the observed and predicted GST plasma concentrations versus time (Correlation (observed, predicted) = 0.9474) (Figure 6). The terminal half-life and $AUC_{0\text{-}inf}$ are slightly lower but not significantly different than the values previously reported (Chaturvedula *et al.*, 2005). The calculated input rate *in vivo* (k_{input}= 0.83 ± 0.27 µg.min^{-1}) was lower than the rate obtained *in vitro* across dermatomed porcine skin (2.79 ± 0.59 µg.min^{-1}); possibly due to differences in experimental conditions and interspecies variations (Kankkunen *et al.*, 2002, Li *et al.*, 2002).

CONCLUSIONS

The results confirm that GST is an excellent candidate for iontophoresis: its transport is governed by EM and there is negligible EO inhibition. It has also been shown that its transdermal flux increases essentially linearly as a function of GST concentration. The most favorable GST flux was obtained at 0.3 mA.cm^{-2} in the absence of Na^+, delivering drug at a rate of 2.93 ± 0.62 µg.cm^{-2}.min^{-1}; higher than that achieved with other transdermal methodologies. Pharmacokinetic data after iontophoretic delivery *in vivo* in rats showed an input rate constant of 0.83 ± 0.27 µg.min^{-1} (area of 1.33 cm^2) at 0.3 mA.cm^{-2}. The delivery profile was described by a one-compartment model with zero-order absorption. Based on these results and assuming that the upper limit for the daily systemic dose of GST can be approximated as 1.2 mg (daily dose 1-2 mg, with systemic bioavailability of ~60%; Sweetman, 2003), transdermal iontophoresis should be able to deliver therapeutic amounts of drug using a reasonably-sized (4 - 6 cm^2) patch. However, pharmacokinetic studies in human volunteers need to be performed to test this hypothesis.

ACKNOWLEDGEMENTS

The authors wish to thank the Swiss Cancer League (Berne, Switzerland) for financial support (OCS 01753-08-2005) and J. Cázares-Delgadillo also acknowledges financial support from CONACYT (Mexico). We are grateful to Roche Diagnostics GmbH (Mannheim, Germany) for the generous gift of granisetron hydrochloride. We would also like to acknowledge Pharsight Corporation (Mountain View, CA) for providing an academic program license for the WinNonlin® Professional software.

ABBREVIATIONS

ACE, acetaminophen
ACN, acetonitrile
AUC_{0_inf}, area under a curve from time 0 to time infinity
BA, bioavailability
C_{max}, maximum plasma concentration
C_p, plasma concentration of granisetron
EM, electromigration
EO, electroosmosis
GST, granisetron
HPLC, High Performance Liquid Chromatography
SB, salt bridge
IF, inhibition factor
IV, intravenous administration
J_{EM}, electromigration flux
J_{EO}, electroosmosis flux
J_{tot}, total steady state flux
k_{01}, input rate
k_{10}, elimination rate constant
LOD, limit of detection
LOQ, limit of quantification
S.D., standard deviation
t_{ionto}, time of current application
V_d, volume of distribution
V_w, solvent permeability coefficient

REFERENCES

Bopanna, V.K., 1995. Simultaneous determination of granisetron and its 7-hydroxymetbolite in human plasma by reversed-phase high-performance liquid chromatography utilizing fluorescence and electrochemical detection. J. Chromatogr. A. 692, 195-202.

Chaturvedula, A., Joshi, D.P., Anderson, C., Morris, R., Sembrowich, W.L., Banga, A. K., 2005. Dermal, subdermal, and systemic concentrations of granisetron by iontophoretic delivery. Pharm. Res. 22, 1313-1319.

De Muth, J.E., 1999. Basic Statistics and Pharmaceutical Statistical Applications, Marcel Dekker, New York.

Dimas, D.A., Dallas, P.P., Rekkas, D.M., 2004. Ion pair formation as a possible mechanism for the enhancement effect of lauric acid on the transdermal permeation of ondansetron. Pharm. Dev. Technol. 9, 311-320.

Ding, P., Yu, H., Wei, G., Zheng, J., 2000. Microdialysis sampling coupled to HPLC for transdermal delivery study of ondansetron hydrochloride in rats. Biomed. Chromatogr. 14, 141-143.

Food and Drug Administration, Center for Veterinary Medicine. Guidance for Industry Bioanalytical Method Validation, 2001.

Gupta, S.K., Southam, M., Sathyan, G., Klausner, M., 1998. Effect of current density on pharmacokinetics following continuous or intermittent input from a fentanyl electrotransport system. J. Pharm. Sci. 87, 976–981.

Gwak, H.S., Oh, I.S., Chun, I.K., 2004. Transdermal delivery of ondansetron hydrochloride: effects of vehicles and penetration enhancers. Drug. Dev. Ind. Pharm. 30, 187-194.

Hussain, A.A., Dakkuri, A., Itoh, S., 2000. Nasal absorption of ondansetron in rats: an alternative route of drug delivery. Cancer. Chemother. Pharmacol. 45, 432-434.

Kalia, Y.N., Naik, A., Garrison, J., Guy, R.H., 2004. Iontophoretic drug delivery. Adv. Drug. Deliv. Rev. 56, 619-658.

Kankkunen, T., Sulkava, R., Vuorio, M., Kontturi, K., Hirvonen, J., 2002. Transdermal iontophoresis of tacrine *in vivo*. Pharm. Res. 19, 705-708.

Kasting G.B., 1992. Theoretical models for iontophoretic delivery. Adv. Drug. Deliv. Rev. 9, 177– 199.

Kasting, G.B., Keister, J.C., 1989. Application of electrodiffusion theory for a homogeneous membrane to iontophoretic transport through skin. J. Control. Rel. 8, 195–210.

Kim., Y-C., Late, S., Banga, A.K., Ludovice, P.J., Prausnitz, M.R., 2008. Biochemical enhancement of transdermal delivery with magainin peptide: modification of electrostatic interactions by changing pH. Int. J. Pharm. 362, 20-28.

Krishnaiah, Y.S., Rama, B., Raghumurthy, V., Ramanamurthy, K.V., Satyanarayana, V., 2009. Effect of PEG6000 on the *in vitro* and *in vivo* transdermal permeation of ondansetron hydrochloride from EVA1802 membranes. Pharm. Dev. Technol. 14, 50-61.

Lau, D.T.W., Sharkey, J.W., Petryk, L., Mancuso, F.A., Yu, Z., Tse, F.L.S, 1994. Effect of current magnitude and drug concentration on iontophoretic delivery of octreotide acetate (Sandostatin\) in the rabbit. Pharm. Res. 11, 1742–1746.

Li, G.L., van der Geest, R., Chanet, L., van Zanten, E., Danhof M., Bouwstra J.A., 2002. In vitro iontophoresis of apomorphine across human stratum corneum: the structure/transport relationship of penetration enhancement, J. Control. Rel. 84, 49–57.

Phipps, J.B., Gyory, J.R., 1992. Transdermal ion migration, Adv. Drug. Deliv. Rev. 9, 137–176.

Singh, P., Boniello, S., Liu, P., Dinh, S., 1999. Transdermal iontophoretic delivery of methylphenidate HCl *in vivo*. Int. J. Pharm. 178, 121–128.

Sintov, A.C., Krymberk, I., Daniel, D., Hannan, T., Sohn, Z., Levin, G., 2003. Radiofrequency-driven skin microchanneling as a new was for electrically assisted transdermal delivery of hydrophilic drugs. J. Control. Rel. 89, 311-320.

Sweetman S (Ed), Martindale: The complete drug reference. London: Pharmaceutical Press. Electronic version, (33rd Edition [2003]).

Takahashi, K., Rytting, J. H., 2001. Novel approach to improve permeation of ondansetron across shed snake skin as a model membrane. J. Pharm. Pharmacol. 53, 789-794.

Comparing metoclopramide electrotransport kinetics *in vitro* and *in vivo*: relative contributions of electromigration and electroosmosis and the effect of drug transport on skin permselectivity

Jennyfer Cázares-Delgadillo[1], Inès Ben Aziza[1], Cristina Balaguer-Fernández[2], Aracely Calatayud-Pascual[2], Adriana Ganem-Rondero[3], David Quintanar-Guerrero[3], Alicia C. López Castellano[2], Virginia Merino[4], Yogeshvar N. Kalia[1]

[1] School of Pharmaceutical Sciences, University of Geneva, 30 Quai Ernest Ansermet, 1211 Geneva, Switzerland

[2] Departamento de Fisiología, Farmacologia y Toxicología, University Cardenal Herrera (CEU), Edificio Seminario s/n, 46113 Moncada, Valencia, Spain

[3] División de Estudios de Posgrado (Tecnología Farmacéutica), Facultad de Estudios Superiores Cuautitlán, Universidad Nacional Autónoma de México, Av. 1° de Mayo S/N Cuautitlán Izcalli, Estado de México 54704, Mexico

[4] Departamento de Farmacia y Tecnología Farmacéutica, Faculty of Pharmacy, University of Valencia, Avda. Vicente Andrés Estellés s/n, 46100 Burjassot, Valencia, Spain

Submitted to Pharmaceutical Research

ABSTRACT

Purpose: To investigate the transdermal iontophoretic delivery of metoclopramide and to determine (i) the dependence of electrotransport on current density and drug concentration, (ii) the relative contributions of electromigration and electroosmosis and (iii) the feasibility of administering therapeutic amounts of drug, using a drug-sparing iontophoretic configuration.
Methods: Iontophoretic delivery of metoclopramide (MCL) across dermatomed porcine ear skin was investigated *in vitro* as a function of concentration (10, 20, 40, 80 and 100 mM) and current density (0.1, 0.2 and 0.3 $mA.cm^{-2}$) using vertical flow through diffusion cells. *In vivo* studies were performed in Wistar rats (40 mM MCL, 0.3 $mA.cm^{-2}$, 5 h); the anodal and drug

formulation compartments were separated by a salt bridge. Blood samples were collected hourly for 8 h.

Results: Cumulative delivery *in vitro* after 7 h of current application (40 mM MCL; 0.3 $mA.cm^{-2}$) in the absence of electrolyte was 624.45 ± 99.45 $\mu g.cm^{-2}$ (flux – 2.55 ± 0.35 $\mu g.cm^{-2}.min^{-1}$). There was a linear relationship between flux and both current density (J_{tot} ($\mu g.cm^{-2}.min^{-1}$) = 8.88 i_d ($mA.cm^{-2}$) – 0.15; r^2 = 0.99) and drug concentration (J_{tot} ($\mu g.cm^{-2}.min^{-1}$) = 0.0178 C_{MCL} (mM) + 0.4595; r^2 = 0.88). Co-iontophoresis of acetaminophen confirmed that electromigration was the major transport mechanism (accounting for ~80% of MCL delivery). Electroosmotic inhibition, albeit modest, was only observed at the highest MCL concentration (100 mM). The delivery rate observed *in vivo* in male Wistar rats (1.21 ± 0.55 $\mu g.cm^{-2}.min^{-1}$) was lower than that observed *in vitro*.

Conclusions: The presence of a linear dependence of flux upon current density and drug concentration means that either parameter can be used to modulate MCL delivery rates and hence, the dose administered. *In vivo* results suggest that drug input rates would be sufficient to achieve therapeutic levels in humans using non-invasive transdermal iontophoresis.

Key words: metoclopramide, iontophoresis, transdermal delivery, pharmacokinetics.

INTRODUCTION

Metoclopramide (Figure 1; MCL, MW 299 Da; pKa 9.65) is a potent dopamine (D_2) receptor antagonist that acts on the chemoreceptor trigger zone (CTZ) in the brain (1). Systemic bioavailability following oral administration shows considerable inter-individual variability (30-100%); furthermore, oral delivery may be inconvenient for patients suffering from nausea or vomiting.

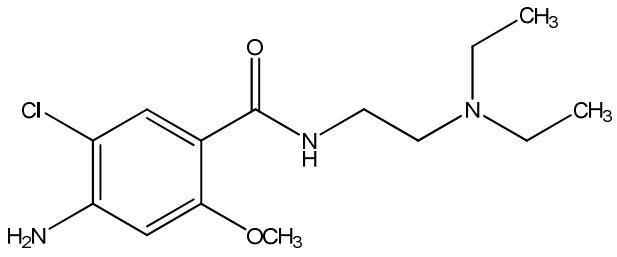

Figure 1. Molecular structure of metoclopramide (MW 299.8 Da; pKa 9.65; log P 2.22).

Transdermal iontophoresis is a convenient and painless means to enable controlled drug input rates. Previous *in vitro* studies using heat-separated human epidermis and

subsequent clinical trials in volunteers have suggested that therapeutic delivery might be possible with patch areas between 5-30 cm^2 using a low current density (0.1 $mA.cm^{-2}$) (2). However, the occurrence of local erythema meant that MCL was co-formulated with hydrocortisone (2). The irritation may have been due to the high local drug concentration (10% w/w MCL, 334 mM); MCL was also serving as the source of chloride ions to drive anodal electrochemistry. The objective of the present study was to investigate MCL electrotransport using an electrode configuration where the drug load was reduced by isolating the anodal and formulation compartments and NaCl was used to drive anodal Ag/AgCl electrochemistry without impacting on MCL transport. The specific aims were (i) to determine the dependence of MCL flux on current density and drug concentration – linear relationships would obviously be an advantage in order to modulate dosing and individualize treatment (ii) to investigate the relative contributions of electromigration and electroosmosis, this can impact on formulation design, (iii) to compare *in vitro* data using human and porcine skin and (iv) to measure iontophoretic MCL delivery in rats *in vivo* and to identify interspecies differences with the published human data.

METHODS

Materials

Metoclopramide hydrochloride, acetaminophen (ACE), agarose, sodium heptanesulfonate, silver wire and silver chloride used for the fabrication of electrodes were purchased from Sigma-Aldrich (Steinheim, Germany). HEPES buffer and sodium chloride were obtained from Fluka (Buchs, Switzerland). Silicon tubing (1.6 mm ID, 3.2 mm OD, 0.8 mm wall thickness) for collecting samples and PVC tubing (3 mm ID, 5 mm OD, 1 mm wall thickness) used to prepare salt bridge assemblies were obtained from Fisher Bioblock Scientific S.A. (Illkirch, France). Chromatographic reagents were obtained from VWR (Dietikon, Switzerland). All solutions were prepared using deionised water (resistivity > 18 MΩ.cm). All other chemicals were at least of analytical grade. Porcine ear skin was obtained from a local abattoir (STAC, Chambery, France). The skin was excised (thickness 750 µm) with an electro-dermatome (Zimmer, Etupes, France), wrapped in Parafilm™ and stored at -20℃ for a maximum period of 2 months.

Stability study

Metoclopramide stability was assessed prior to the iontophoretic studies in order to determine whether it was subject to metabolism by porcine skin and/or degradation by current application.

Stability in the presence of skin: A 200 µM MCL solution containing 133 mM NaCl and HEPES 25 mM (pH 7.4) and a 20 mM MCL solution (15 mM piperazine / 100 mM NaCl (pH 5.0)) were placed in contact with the dermal and epidermal skin surfaces, respectively. Samples were collected every hour for 7 h.

Stability in the presence of an electrical current: The electrical stability of MCL solutions was evaluated by subjecting a 20 mM MCL buffered solution (15 mM piperazine /100 mM NaCl (pH 5.0)) to a current density of 0.3 $mA.cm^{-2}$ over a 6 h period. Samples were collected hourly.

Stability in the presence of skin and an electrical current: A 3.34 mM MCL solution containing 100 mM NaCl and HEPES 25 mM (pH 7.4) was placed in contact with the dermal side of the skin for 7 h. A current density of 0.3 $mA.cm^{-2}$ was applied. Samples were collected hourly.

All experiments were performed in at least triplicate.

Iontophoretic delivery of MCL through dermatomed porcine skin *in vitro*

Skin was clamped in three compartment vertical flow-through diffusion cells (area = 0.95 cm^2). The cathodal and receptor compartments were filled with 1 and 6 ml of 25 mM HEPES / 133 mM NaCl (pH 7.4), respectively. After 40 min equilibration with HEPES / NaCl (pH 7.4), 1 ml of a buffered MCL solution (10, 20, 40, 80 and 100 mM MCL; 15 mM piperazine / 100 mM NaCl (pH 5.0)) containing 15 mM ACE was placed in the anodal compartment; ACE was used to report on the electroosmotic solvent flow. The samples were collected hourly using a syringe pump (SP220IZ, WPI, Sarasota, FL) which generated a continuous flow of buffer solution (1 $ml.h^{-1}$). A constant current density of 0.3 $mA.cm^{-2}$ was applied for 7 h via Ag/AgCl electrodes connected to a power supply (APH 1000M, Kepco, Flushing, NY). The effect of current density (0.1, 0.2 and 0.3 $mA.cm^{-2}$) on MCL transport was investigated in a separate study. A 40 mM MCL solution (15 mM piperazine (pH 5.0)) containing 15 mM ACE was used for these experiments. A salt bridge (SB) was used to isolate the formulation and anodal compartments; current was applied for 7 h. The experiments at 0.2 and 0.3 $mA.cm^{-2}$ were also used to provide information on MCL retention by the skin. For these experiments, after termination of current application, the formulation compartment was emptied and the MCL solution replaced with 25 mM HEPES / 1 33 mM NaCl buffer (pH 7.4). One sample was collected from the receiver compartment after 9 h of post-iontophoretic passive diffusion. All experiments were performed in at least quintuplicate. At the end of the experiments, MCL was extracted by soaking the tissues in

5 ml of mobile phase for 4 h. The extraction suspensions were membrane-filtered (0.45 µm, polypropylene micro-centrifuge tube filters, Whatman, Maidstone, England). MCL content was analyzed by HPLC.

The total iontophoretic flux (J_{tot}) of MCL, assuming negligible passive diffusion, is the sum of fluxes due to electromigration (EM) and electroosmosis (EO) (3):

$$J_{tot} = J_{EM} + J_{EO} \quad (1)$$

J_{EM} can be estimated directly from J_{tot} and J_{EO}, the latter is given by the product of the solvent permeability coefficient (V_W) and drug concentration C_{MCL}.

$$J_{EO} = V_W . C_{MCL} \quad (2)$$

For each experiment, co-iontophoresis of ACE also enabled the calculation of an inhibition factor (IF) to report on the effect of MCL transport on skin permselectivity:

$$IF = \frac{Q_{ACE,\ control}}{Q_{ACE}} \quad (3)$$

where $Q_{ACE,control}$ is the cumulative amount of ACE delivered calculated during 7 h of iontophoresis, and Q_{ACE} is the corresponding value when MCL was simultaneously iontophoresed.

Iontophoretic delivery of MCL in rats *in vivo*

The protocol was approved by the Ethics Committee for Animal Experimentation at the University of Valencia, Spain. Male Wistar rats weighing 260-300 grams were used for all of the experiments. Twenty four hours before iontophoresis, the rats were anesthetized by intraperitoneal administration of pentobarbital sodium (Dolethal solution, 40 $mg.kg^{-1}$, Vetoquinol, Madrid, Spain). The jugular vein was cannulated using medical grade silicon tubing (Silastic, Dow Corning Co.; ID 0.5 mm; OD 0.94 mm). Under anesthesia, 3.4 cm of the cannula was introduced into the jugular vein toward the heart and the free end was subcutaneously conducted to the dorsal base of the neck, where it emerged. The cannula was permanently filled with heparinized saline solution (20 $IU.ml^{-1}$) and closed with a polyethylene plug. On the day of the experiment, animals were again anesthetized (intraperitoneal injection of pentobarbital sodium, 20 $mg.kg^{-1}$) and mounted on a plastic support. Two glass chambers (1.33 cm^2) were then placed 2.5 cm apart on the animal's

abdomen (shaved beforehand) and fixed with glue. The donor formulation consisted of 0.7 ml of buffered MCL (40 mM; 15 mM piperazine (pH 5.0)) and was separated from the anodal compartment by means of a SB. The cathodal compartment was filled with 25 mM HEPES / 133 mM NaCl buffer solution (pH 7.4). Ag/AgCl electrodes were introduced in the respective solutions; the cathode was maintained at least 5 mm from the skin surface. Constant current (0.3 $mA.cm^{-2}$) was applied for 5 h via Ag/AgCl electrodes connected to a power supply (APH 1000M, Kepco, Flushing, NY). Blood samples (1.0 ml) were withdrawn into heparinized syringes from the jugular vein cannula at hourly intervals for 8 h and immediately centrifuged at 10,000 rpm; plasma collected was separated and stored at -20℃ until analysis by HPLC. After each sampling, the blood volume was replaced with the same volume of saline solution. At the end of each experiment, the animals were sacrificed by intraperitoneal administration of a lethal dose of pentobarbital sodium (200 $mg.kg^{-1}$). Iontophoretic studies were performed in triplicate.

Analytical method

A P680A LPG-4 pump equipped with an ASI-100 autosampler and a UV170U detector (Dionex, Voisins LeBretonneux, France) were used to assay MCL. Isocratic separation was performed using a Lichrospher® 100 RP-8 5 µm reversed-phase column. The flow-rate and injection volumes were 1.5 $ml.min^{-1}$ and 10-100 µl, respectively; the column temperature was kept at 30℃ (thermostated column compartment TCC-1 00, (Dionex, Voisins LeBretonneux, France)). Samples from the receiver compartment were eluted in phosphate buffer 0.01 M (pH 4.0) and acetonitrile (60:40 v/v). Drug was analyzed using its UV absorbance at 223 nm. The LOD and LOQ were 11.1 and 33.5 ng, respectively. ACE was assayed separately using a Lichrospher® 100 RP-8 reversed-phase column.

The mobile phase comprised 88% 40 mM citrate buffer (pH=3.0) and 12% acetonitrile. The flow rate and the injection volumes were 1.0 $ml.min^{-1}$ and 10-100 µl, respectively. ACE was detected by its UV absorbance at 243 nm. The LOD and LOQ were 9.0 and 27.2 ng, respectively.

Analysis of plasma extracts was performed using the same HPLC system coupled to a RF2000 fluorescence detector and a Sunfire™ 100 C-18 4.6 µm column. The flow rate was 2.0 $ml.min^{-1}$ (injection volume = 50 µl) and the column temperature was kept at 50℃. Samples were eluted in acetate buffer 0.1 M (pH 4.7) containing 2 g of sodium heptanesulfonate and 0.2 g EDTA, acetonitrile and deionised water (51:19:30 v/v). The excitation and emission wavelengths for detection of MCL were 316 and 359 nm, respectively, and the gain of the detector was set at unity. The extraction procedure was based on a one-step liquid-liquid technique (4, 5). Using Eppendorf vials, 50 µl NaOH (1 M) was added to 0.2 ml of plasma and the tube was shaken for 2 minutes. Immediately

thereafter, 1 ml of diethyl ether was added and the resulting mixture vortex-mixed for 15 minutes.

Table 1. Accuracy and precision for metoclopramide HPLC assay validation (n = 4).

Theoretical concentration ($\mu g.ml^{-1}$)	Experimental concentration (Mean ± S.D.) ($\mu g.ml^{-1}$)	Precision (%)	Accuracy (%)	Recovery (%)
Within-day (n=4)				
0.07	0.06 ± 0.01	9.79	12.95	87.06
0.31	0.28 ± 0.03	8.92	9.02	90.99
0.67	0.60 ± 0.04	6.83	10.72	89.28
1.78	1.77 ± 0.19	10.44	0.76	99.24
Between day (n=4)				
0.07	0.06 ± 0.01	12.69	4.60	95.40
0.31	0.29 ± 0.01	4.74	6.42	93.59
0.67	0.67 ± 0.03	4.83	0.72	100.72
1.78	1.51 ±0.10	6.75	15.12	84.88

After centrifugation at 10,000 rpm and separation, the organic layer was evaporated at 30°C. The residue was dissolved in 200 µl mobile phase and finally 50 µl injected into the chromatographic column. Calibration curves (n = 8) that spanned the range of MCL concentrations in the plasma samples were prepared in triplicate in order to validate the analytical method. The relative error and coefficient of variation were the parameters evaluated for accuracy and precision (Table 1). The mean recovery of MCL was 88.11 ± 5.27 % (n= 8). The LOQ was 44.17 $ng.ml^{-1}$. The long-term stability of MCL in plasma samples stored at -20°C was also investigated and it was found that after 5 weeks' storage, the percentage of drug degraded was only 7.5 % over a concentration range from 67 to 670 $ng.ml^{-1}$.

Pharmacokinetics

Pharmacokinetic parameters for the iontophoretic delivery of MCL were calculated using a one compartment model with zero-order absorption and first-order elimination as follows:

$$C_p(t) = \left(k_{input} / V_d \bullet k_{10}\right) * \left(1 - e^{-k_{10}t}\right) \quad \text{if } t \le t_{ionto} \tag{4}$$

$$C_p(t) = \left(k_{input} / V_d \bullet k_{10}\right) * \left(1 - e^{-k_{10}t}\right) * \left(e^{-k_{10}(t - t_{ionto})}\right) \quad \text{if } t \ge t_{ionto} \tag{5}$$

where,

$C_p(t)$ = plasma concentration of MCL at time (t)

V_d = volume of distribution

k_{input} = input rate

k_{10} = elimination rate constant

t = time

t_{ionto} = duration of current application (5 h)

The fitting was done using a Gauss-Newton algorithm with Levenberg-Hartley modification. Non-compartmental parameters such as C_{max}, half-life and $AUC_{0\text{-}inf}$ were calculated in Microsoft Excel. The volume of distribution of the drug was obtained from the literature (6).

Data treatment and statistical analysis

Experimental data reported represent the mean values ± standard deviation (S.D.). Outliers, determined using the Grubbs test, were discarded (7). Statistical analysis was conducted using analysis of variance (ANOVA) to evaluate the difference between groups of data. Student's t-test was used to compare two data sets. The level of significance was fixed at $P < 0.05$.

RESULTS

Susceptibility of MCL to degradation in the presence of skin and current application

The results showed that MCL in contact with the epidermis was stable; furthermore, the drug was also unaffected after 6 h of current application (*ANOVA test, p<0.05*). However, drug appeared to be degraded when in contact with the dermis. HPLC chromatograms (data not shown) displayed an unidentified peak that increased appreciably with time. Similarly, current application to MCL samples in contact with dermis further decreased drug stability (*ANOVA test, p<0.05*). Average MCL recovery (%) after simultaneous exposure to both conditions for 6 h was 81.5 ± 3.1 %.

Effect of experimental variables on skin permeation

Cumulative MCL permeation and the mean steady-state iontophoretic flux, as a function of donor concentration, are illustrated in Figure 2. Upon increasing drug concentration from 10 to 20 and 100 mM, cumulative delivery increased from 149.25 ± 56.09 to 218.24 ± 55.79 and 655.36 ± 185.97 $\mu g.cm^{-2}$, respectively. Similarly, flux increased from 0.48 ± 0.17 $\mu g.cm^{-2}.min^{-1}$ to 0.83 ± 0.23 and 2.41 ± 0.61 $\mu g.cm^{-2}.min^{-1}$, representing 1.7- and 5.0-fold increases, respectively. Regression analysis confirmed that electrotransport increased

linearly with concentration in the presence of background electrolyte, (J_{tot} (µg.cm^{-2}.min^{-1}) = 0.0178 C_{MCL} (mM) + 0.4595; r^2 = 0.88).

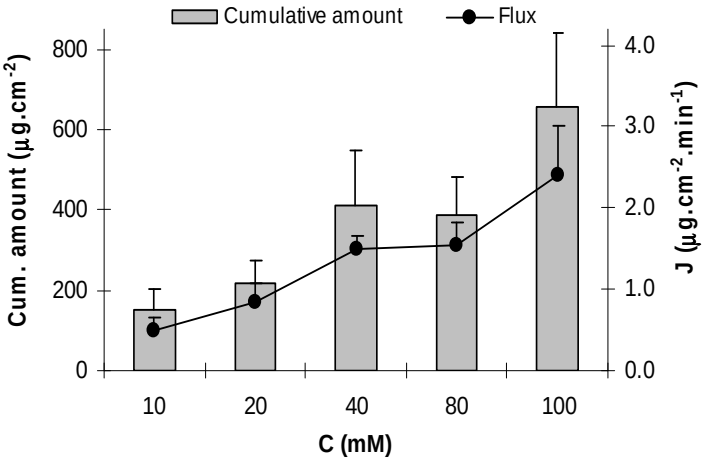

Figure 2. Cumulative amount permeated and steady-state flux of MCL as a function of donor concentration during 7 h of transdermal iontophoresis at 0.3 mA.cm^{-2} (Mean ± S.D.; n ≥ 5).

Drug extraction from the skin carried out at the end of the iontophoretic experiments at 80 and 100 mM MCL, showed that significant amounts of drug were retained in the skin (1.34 ± 0.26 and 0.65 ± 0.27 mg, respectively).

Co-iontophoresis of ACE was used to determine the relative contributions of EM and EO to MCL transport (Figure 3); EM was the dominant mechanism, accounting for 80% of total iontophoretic transport. ACE transport was also used to show that convective solvent flow was only affected at the highest MCL concentration (100 mM) with an IF of 2.8, suggesting that MCL was not prone to interacting with fixed negative charges in the skin.

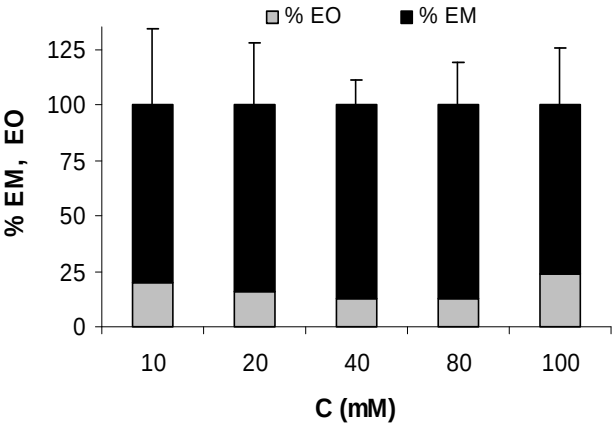

Figure 3. Relative contributions of EM and EO to the total MCL flux as a function of donor concentration (Mean ± S.D.; n ≥ 5).

Figure 4 compares current-normalized iontophoretic transport rates for MCL with those of other moderately lipophilic cations – lidocaine (L; MW 224 Da, pKa 8.53, log P 2.36), propranolol (P; MW 259 Da, pKa 9.14, log P 3.10), quinine (Q; MW 324 Da, pKa 9.28, log P 3.44) iontophoresed at the same concentrations (10 and 40 mM, presence of competing ions) across dermatomed porcine skin *in vitro*. At the lower concentration (10 mM), transport for all of the molecules is equivalent suggesting that interactions with the transport pathway

are limited and the absence of drug-drug interactions that might favor aggregation. The four-fold increase in concentration to 40 mM results in a proportionate increase in lidocaine flux; for metoclopramide, there is a three-fold increase in flux. However, transport rates of propranolol and quinine show only a two-fold increase in response to the four-fold change in concentration; it has been shown that both of these molecules display considerable EO inhibition (IF of 6.1 and 5.2, respectively, (8)) and they may also aggregate in the transport pathway. Molecular modeling studies are underway to investigate the effect of structure and the spatial distribution of hydrophilicity / lipophilicity on drug transport.

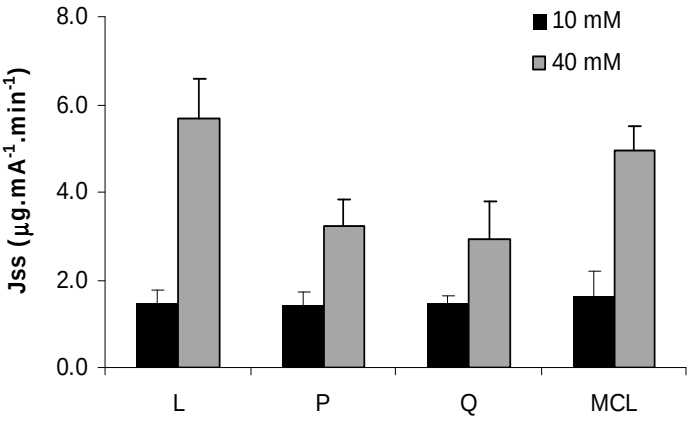

Figure 4. Comparison of the current-normalized transport rates of MCL, lidocaine (L), propranolol (P) and quinine (Q) as a function of concentration (10 and 40 mM) across dermatomed porcine skin *in vitro*.

The impact of increasing current density from 0.1 to 0.3 mA.cm^{-2} on MCL transport in the absence of competing electrolyte is reported in Table 2. A linear dependence of MCL flux on current density was observed (J_{tot} (µg.cm^{-2}.min^{-1}) = 8.88 i_d (mA.cm^{-2}) – 0.15; r^2 = 0.99).

Table 2. The impact of current density on the iontophoretic transport of MCL at constant donor concentration (40 mM) (n ≥ 5).

I (mA.cm^{-2})	Cum. amount (µg.cm^{-2})	J_{tot} (µg.cm^{-2}min^{-1})	Transport efficiency (%)
0.1	175.94 ± 6.46	0.77 ± 0.04	0.74
0.2	425.42 ± 100.71	1.56 ± 039	1.81
0.3	624.45 ± 99.35	2.55 ± 0.35	2.65

I = current intensity; Cum. amount = cumulative amount; J_{tot} = total iontophoretic flux

The effect of competing ions (Na^+) on MCL transport under various experimental conditions is further illustrated in Figure 5. Cumulative iontophoretic delivery at 0.3 mA.cm^{-2} from a 40 mM MCL solution in the presence (A) and absence (B) of NaCl (100 mM) was 411.71 ±

136.82 and 624.45 ± 99.35 µg.cm^{-2}, respectively; similarly, MCL flux also increased by ~50% (1.49 ± 0.17 and 2.55 ± 0.35 µg.cm^{-2}.min^{-1}, respectively). Delivery from the unbuffered 40 mM solution (B) was equivalent to that achieved at the same current density from a 100 mM MCL that contained background electrolyte (100 mM NaCl; solution C). These data confirmed the relevance of formulation composition and the need to reduce the presence of competing ions for the optimization of iontophoretic systems.

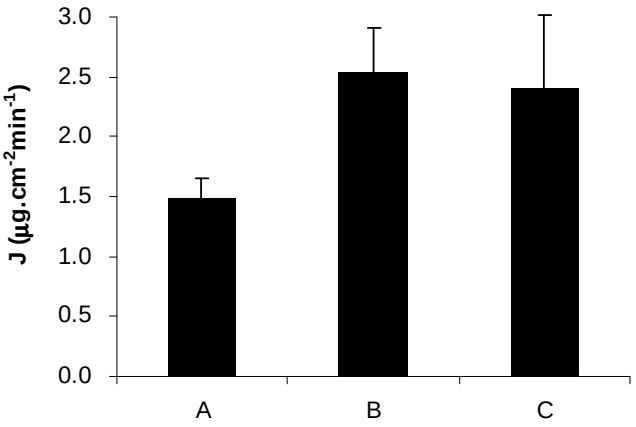

Figure 5. MCL fluxes as a function of experimental conditions. Formulation A = 40 mM MCL and 100 mM NaCl; Formulation B = 40 mM MCL (-Na$^+$); Formulation C = 100 mM MCL and 100 mM NaCl. All experiments were conducted at 0.3 mA.cm^{-2}. (Mean ± S.D.; n ≥ 5).

As mentioned above, significant amounts of drug were retained in the skin; a post-iontophoretic passive diffusion study for 9 h was carried out following current application for 7 h at 0.2 and 0.3 mA.cm^{-2} using a formulation containing 40 mM MCL (-Na$^+$) in order to determine whether the bound drug was released post-iontophoresis into the receptor compartment (Figure 6). Total cumulative permeation increased from 425.42 ± 100.71 to 611.09 ± 60.77 and from 624.45 ± 99.35 to 1011.04 ± 225.52 µg.cm^{-2}, at 0.2 and 0.3 mA.cm^{-2}, respectively. Given the amount of drug stored within the skin, delivery efficiency at the higher current density was calculated to be ~4.3%. In order to compare our results with those obtained previously using heat-separated human epidermis (0.1 mA.cm^{-2}, 334 mM MCL), the MCL fluxes were current-normalized (2). The normalized steady-state flux across human epidermis was 21.85 ± 4.50 µg.mA^{-1}.min^{-1} (area not given); for comparison, the highest MCL flux across dermatomed porcine skin (0.3 mA.cm^{-2}, 40 mM MCL (-Na$^+$), area 0.95 cm^2) was 8.50 ± 1.17 µg.mA^{-1}.min^{-1}. The ~2.6-fold difference may be attributed to differences in the diffusional surface area, superior permeability of epidermal membrane and the 8.3-fold higher MCL concentration in the study with human epidermis.

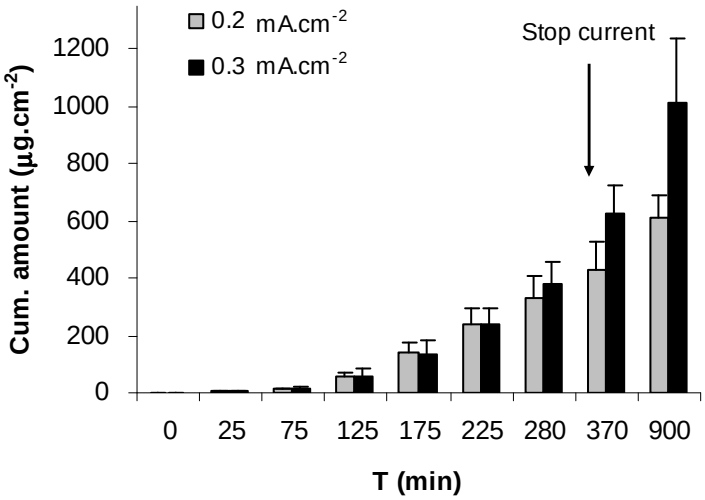

Figure 6. Post-iontophoretic passive diffusion of MCL during 9h after 7 h iontophoresis at 0.2 and 0.3 $mA.cm^{-2}$. (Mean ± S.D.; n ≥ 5).

Iontophoretic delivery of MCL *in vivo*

Figure 7 shows the mean plasma concentration-time curve of MCL during and following iontophoretic current application (0.3 $mA.cm^{-2}$, (40 mM; $-Na^{+}$), 5 h). The plasma levels of MCL rose gradually during iontophoresis and reached a maximum of 0.31 ± 0.04 $\mu g.ml^{-1}$ at 300 min when current application was terminated. Although drug levels decreased after system removal, they remained appreciable up to the 8 h time-point. Inter-animal variability, as indicated by the standard deviation about the mean drug levels, was lower during current application than in the post-iontophoretic phase. The low plasma concentration (0.082 $\mu g.ml^{-1}$) of one animal at t = 240 min increased the standard deviation at this time-point. Pharmacokinetic parameters obtained from the iontophoretic delivery including *AUC*, half-life and elimination rate constant are listed in Table 3. The goodness of the fit of the pharmacokinetic model can be observed in Figure 7. The iontophoretic input rate was 1.21 ± 0.55 $\mu g.cm^{-2}.min^{-1}$ (equivalent to 1.61 ± 0.73 $\mu g.min^{-1}$).

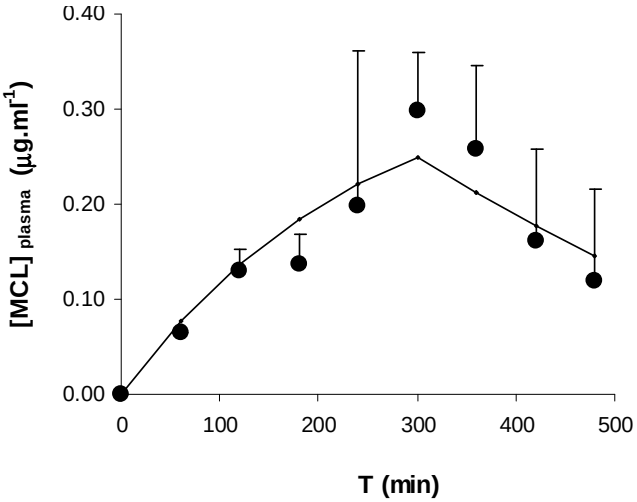

Figure 7. The observed and predicted mean plasma concentration-time profiles in rats after iontophoretic administration (Mean ± S.D.; n=3)

For comparison, the mean absorption rate in human volunteers following iontophoresis at 0.1 mA.cm^{-2} and using a 10% w/w MCL solution (334 mM) containing 0.5% hydrocortisone (w/w) was estimated to be 1.67 µg.cm^{-2}.min^{-1} (2). Given the differences in current density and drug loading, there is reasonable agreement given the different nature of the skin barriers. It is conceivable that, under equivalent conditions, iontophoretically-controlled transdermal delivery may reduce some of the interspecies variability that can be seen during passive transdermal administration; although this hypothesis requires further validation.

In conclusion, although delivery *in vivo* was lower than that predicted from the *in vitro* data, the input rates may still be sufficient to achieve therapeutic delivery. Clinically, MCL doses range between 10-15 mg t.i.d./q.i.d (9); therefore, assuming a mean systemic MCL bioavailability of ~75%, transdermal iontophoresis would probably be able to deliver therapeutic amounts of MCL from a patch size of 10-20 cm^2.

Table 3. Mean pharmacokinetic parameters of metoclopramide following iontophoretic administration to three male rats. Data are presented as mean and inter-individual variability (S.D.).

Parameter	Mean ± S. D.
C_{max} (µg.ml^{-1})	0.31 ± 0.04
T_{max} (min)	300.0 ± 60.0
Half-life (min)	74.89 ± 54.53
$AUC_{(0-8)}$ (µg.min.ml^{-1})	70.98 ± 1.13
AUC_{0-inf} (µg.min.ml^{-1})	85.54 ± 20.56
k_{input} (µg.min^{-1})	1.61 ± 0.73
k_{10} x10 $^{-2}$ (min^{-1})	0.43 ± 0.31

ACKNOWLEDGEMENTS

The authors wish to thank the Swiss Cancer League (Berne, Switzerland) for financial support (OCS 01753-08-2005) and J. Cázares-Delgadillo also acknowledges financial support from CONACYT (Mexico). We would also like to acknowledge Pharsight Corporation (Mountain View, CA) for providing an academic program license for the WinNonlin® Professional software.

ABBREVIATIONS

ACE, acetaminophen

AUC $_{(0-8)}$, area under a curve from time = 0 to time t = 8h

AUC_{0_inf}: area under a curve from time = 0 to time infinity

C_{max}, maximum plasma concentration

C_p, plasma concentration

Cum. amount, cumulative amount

EM, electromigration

EO, electroosmosis

HPLC, High Performance Liquid Chromatography

I, current intensity

IV, intravenous administration

J_{tot}, total iontophoretic flux

k_{input}, input rate

k_{10}, elimination rate constant

MCL, metoclopramide

Na^+, presence of electrolyte

$-Na^+$, absence of electrolyte

SB, salt bridge

S.D., standard deviation

T_{max}, time point of the maximum concentration

V_w, solvent permeability coefficient

REFERENCES

1. L. Lohr. Chemotherapy-induced nausea and vomiting. Cancer J. 14: 85–93. (2008).
2. M. Cormier, S. T. Chao, S. K. Gupta and R. Haak. Effect of transdermal iontophoresis codelivery of hydrocortisone on metoclopramide pharmacokinetics and skin-induced reactions in human subjects. J Pharm Sci. 88: 1030-1035 (1999).
3. Y. N. Kalia, A. Naik, J. Garrison and R. H. Guy. Iontophoretic drug delivery. Adv Drug Deliv Rev. 56: 619-658 (2004).
4. A. Leucuta, L. Vlase, D. Farcău and M. Nanulescu. Pharmacokinetic interaction study between ranitidine and metoclopramide. Rom J Gastroenterol. 13: 211-214 (2004).
5. A. Chmielewska, L. Konieczna, A. Plenis and H. Lamparczyk. Sensitive quantification of chosen drugs by reverser-phase chromatography with electrochemical detection at a glassy carbon electrode. J Chromatogr B. 839: 102-111 (2006).
6. V. K. Tam, J. E. Axelson, B. McErlane, R. Ongley and J. O. E. Price. Dose-dependent pharmacokinetics of metoclopramide in rat: An effect of hemoperfusion? J Pharmacol Exp Ther. 21 7: 764-769 (1981).

7. J. E. De Muth. Basic Statistics and Pharmaceutical Statistical Applications, Marcel Dekker, New York, 1999.
8. D. Marro, Y. N. Kalia, M. B. Delgado-Charro, and R. H. Guy. Contributions of electromigration and electroosmosis to iontophoretic drug delivery, Pharm Res. 18: 1701– 1708 (2001).
9. Sweetman (Ed.), Martindale: The Complete Drug Reference, Pharmaceutical Press; 35th Edition (2006).

Transdermal iontophoretic delivery of dexamethasone sodium phosphate *in vitro* and *in vivo*: effect of experimental parameters and skin type on drug transport kinetics

J. Cázares-Delgadillo[1], Cristina Balaguer-Fernández[2], Aracely Calatayud-Pascual[2], A. Ganem-Rondero[3], D. Quintanar-Guerrero[3], A. C. López Castellano[2], V. Merino[4], Y. N. Kalia[1]

[1] School of Pharmaceutical Sciences, University of Geneva & University of Lausanne, 30 Quai Ernest Ansermet, 1211 Geneva, Switzerland

[2] Departamento de Fisiología, Farmacologia y Toxicología, University Cardenal Herrera (CEU), Edificio Seminario s/n, 46113 Moncada, Valencia, Spain

[3] División de Estudios de Posgrado (Tecnología Farmacéutica), Facultad de Estudios Superiores Cuautitlán, Universidad Nacional Autónoma de México, Av. 1° de Mayo S/N Cuautitlán Izcalli, Estado de México 54704, Mexico

[4] Departamento de Farmacia y Tecnología Farmacéutica, Faculty of Pharmacy, University of Valencia, Avda. Vicente Andrés Estellés s/n, 46100 Burjassot, Valencia, Spain

European Journal of Pharmaceutics and Biopharmaceutics, in press

ABSTRACT

The aim of this study was to investigate the cathodal iontophoresis of dexamethasone sodium phosphate (DEX-P) *in vitro* and *in vivo* and to determine the feasibility of delivering therapeutic amounts of the drug for the treatment of chemotherapy-induced emesis. Stability studies, performed to investigate the susceptibility of the phosphate ester linkage to hydrolysis, confirmed that conversion of DEX-P to dexamethasone (DEX) upon exposure to samples of human, porcine and rat dermis for 7 h was limited (82.2 ± 0.4 %, 72.5 ± 4.8 % and 78.6 ± 6.0 % remained intact) and did not point to any major interspecies differences. Iontophoretic transport of DEX-P across dermatomed porcine skin (0.75 cm thickness was studied *in vitro* as a function of concentration (10, 20, 40 mM) and current density (0.1, 0.3, 0.5 $mA.cm^{-2}$) using flow-through diffusion cells. As expected, increasing concentration of DEX-P from 10 to 40 mM resulted in a ~4-fold increase in cumulative permeation (35.65 ±

23.20 and 137.90 ± 53.90 µg.cm^{-2}, respectively). Good linearity was also observed between DEX-P flux and the applied current density (i_d; 0.1, 0.3, 0.5 mA.cm^{-2}; J_{DEX} (µg.cm^2.h^{-1}) = 237.98i_d – 21.32, r^2=0.96). Moreover, separation of the DEX-P formulation from the cathode compartment by means of a salt bridge – hence removing competition from Cl^- ions generated at the cathode – produced a 2-fold increase in steady-state iontophoretic flux (40 mM, 0.3 mA.cm^{-2}; 20.98 ± 7.96 and 41.82 ± 11.98 µg.cm^{-2}.h^{-1}, respectively).
Pharmacokinetic parameters were determined in Wistar rats (40 mM DEX-P; 0.5 mA.cm^{-2} for 5 h with Ag/AgCl electrodes and salt bridges). Results showed that DEX-P was almost completely converted to DEX in the bloodstream and significant DEX levels were achieved rapidly. The calculated input rate (k_{01}) and maximum plasma concentration (C_{max}) were 2.21 ± 0.27 µg.min^{-1} and 1.62 ± 0.36 µg.ml^{-1}, respectively. The results suggest that DEX-P delivery rates would be sufficient for the management of chemotherapy-induced emesis.

Key words: dexamethasone sodium phosphate, iontophoresis, transdermal, pharmacokinetics, antiemetics

INTRODUCTION

Dexamethasone (DEX) is a highly potent glucocorticoid that is often used in combination therapy to treat acute and delayed emesis in patients receiving chemotherapy. Its mechanism of action is not fully understood; studies in animal models suggest that it may affect prostaglandin activity. A report on the ability of dexamethasone to antagonize cisplatin-induced acute and delayed emesis in the ferret suggested that inflammatory mediators may contribute to the vomiting response [1]. However, in earlier studies, no increase in prostaglandin activity was observed in patients receiving treatment with cisplatin [2]. Dexamethasone is usually administered orally – but this is not always convenient for patients who, in addition to enduring nausea and vomiting, frequently suffer from oral mucositis.
Dexamethasone sodium phosphate (DEX-P) (Figure 1) is a water soluble prodrug that is administered parenterally. The presence of the phosphate ester means that there are two ionisable groups (pKa1 and pKa2 are 2.0 and 6.0, respectively). Thus, under physiological conditions, DEX-P exists principally as a di-anion. Its aqueous solubility and charge render DEX-P a much better candidate for transdermal iontophoretic delivery than the parent molecule (DEX) [3].

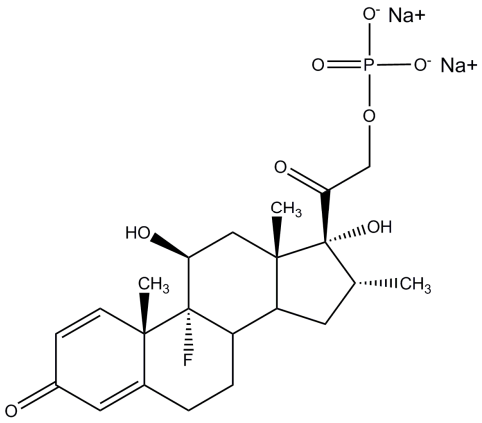

Figure 1. Chemical structure of dexamethasone sodium phosphate (MW 516.4 Da; pKa 2.04 and 6).

Iontophoresis is ideally suited to the delivery of hydrophilic charged molecules and its major advantage, as compared to other transdermal technologies, is that modulation of the intensity and duration of current application enables precise control of drug delivery kinetics [3, 4]. Different iontophoretic devices and "fill-on-site patches" are currently used in clinical practice – in particular in physical therapy – to deliver corticosteroids locally [5, 6]; pre-filled iontophoretic patch systems for lidocaine and fentanyl have also been approved by the US FDA [3, 4, 7, 8].

The first administration of DEX-P by anodal iontophoresis was accomplished in the 80's for the treatment of localized tissue inflammation [9]. Drug levels were measurable levels in deep underlying structures following anodal delivery at a current density of 0.94 $mA.cm^{-2}$. Petelenz *et al.* compared anodal and cathodal DEX-P iontophoresis in the presence of lidocaine [10]. Surprisingly, their results indicated that although cathodal iontophoresis was more efficient *in vitro*, there was no difference between anodal and cathodal delivery *in vivo*. More recently, Sylvestre *et al.* evaluated the effect of different experimental variables on the transdermal iontophoresis of DEX-P *in vitro* [11, 12].

The main objective of the present work was to investigate cathodal iontophoretic delivery of DEX-P *in vitro and in vivo* using an electrode configuration where the electrode and formulation compartments were separated in order to optimize DEX-P transport. Cathodal iontophoresis using Ag/AgCl results in the liberation of Cl^- ions from the electrode that compete with drug anions to transport current; the progressive increase in the Cl^- concentration during current application results in a decrease in drug delivery – as reported for different nonsteroidal anti-flammatory drugs [13-16] – hence the interest in separating the formulation and electrode compartments.

The specific aims of the investigation were: (a) to examine the *ex vivo* stability of DEX-P using different skin species – in order (i) to identify any interspecies differences and (ii) to confirm that the ester linkage and hence the charged moiety was retained during transport (early hydrolysis would release the neutral DEX molecule which cannot be delivered by cathodal iontophoresis), (b) to study cathodal iontophoresis of di-anionic DEX-P as a function of current density and formulation composition and (c) to investigate the feasibility of delivering therapeutic amounts of drug *in vivo* for the treatment of chemotherapy-induced nausea and vomiting (CINV).

MATERIALS AND METHODS

Dexamethasone 21-disodium phosphate salt, dexamethasone, agarose, silver wire and silver chloride used for the fabrication of electrodes were purchased from Sigma-Aldrich (Buchs, Switzerland). HEPES buffer and sodium chloride were obtained from Fluka (Buchs, Switzerland). Silicon tubing (1.6 mm ID, 3.2 mm OD, and 0.8 mm wall) for collecting samples and PVC tubing (3 mm ID, 5 mm OD, 1 mm wall thickness) used to prepare salt bridge assemblies were obtained from Fisher Bioblock Scientific S.A. (Illkirch, France). Chromatographic reagents were obtained from VWR (Dietikon, Switzerland). All solutions were prepared using deionised water (resistivity > 18 MΩ.cm). All other chemicals were at least of analytical grade.

Porcine ear skin was obtained from two abattoirs (STAC; Chambery, France and Carre Coopérative des Abattoirs de Rolle, Switzerland). The skin was excised (thickness 750 µm) with an electro-dermatome (Zimmer; Etupes, France). Rat skin was obtained from the Animal Experimental Research Centre at the University of Valencia (Spain). Human skin was acquired from the Department of Plastic Reconstructive Surgery and Aesthetics, Geneva University Hospital (Geneva, Switzerland). All tissue samples were wrapped in Parafilm® and stored at -20°C for a maximum period of 2 months.

Experimental protocol *in vitro*

Evaluation of DEX-P stability

The influence of skin metabolism on DEX-P stability was examined *in vitro* using different skin species. A 200 µM DEX-P solution (in 25 mM HEPES / 133 mM NaCl, pH 7.4) was placed in contact with the dermal surfaces of samples of human, rat and porcine skin for 7 h. Aliquots were collected after 30, 60, 90, 120, 180, 240, 300, 360 and 420 min.

The stability of DEX-P in the presence of dermatomed porcine skin and heat separated epidermis was also compared in a separate study. Briefly, heat separated epidermis was prepared by first heating skin samples to 60°C for 30 s in water; then the epidermis was

carefully separated from underlying tissue by using forceps and transferred to Petri dishes filled with phosphate buffer saline solution (pH 7.4). The internal surfaces of dermatomed porcine skin and heat separated porcine epidermis were placed in contact with a solution containing 20 mM DEX-P in water (~pH 7.8). Samples were withdrawn over a period 7 h at the same time-points mentioned above.
The stability experiments were performed in triplicate.

Effect of concentration

Dermatomed porcine skin was clamped in three compartment vertical flow-through diffusion cells (A = 0.95 cm^2). The electrode and receptor compartments were filled with buffer solution (comprising 25 mM HEPES + 133 mM NaCl, pH 7.4). After equilibration, 1 ml of unbuffered DEX-P solution 10, 20 or 40 mM (pH ~7.8) was placed in the cathodal compartment; at this pH, the molecule existed principally in the di-anionic form. A constant current density of 0.3 $mA.cm^{-2}$ was applied for 7 h via Ag/AgCl electrodes connected to a power supply (APH 1000M, Kepco, Flushing, NY). Samples were collected hourly from the receptor compartment using a syringe pump (SP220IZ, WPI, Sarasota, FL), which provided a continuous flow of buffer solution (1 $ml.h^{-1}$).

Effect of current density

This was investigated in separate studies at 0.1, 0.3, and 0.5 $mA.cm^{-2}$ using a 40 mM unbuffered DEX-P solution. Salt bridges (SB) were included to separate the cathodal and donor compartments and eliminate competition from Cl^- ions. Current was applied for 7 h. All other aspects of the protocol were the same as those outlined above.

Skin extraction

DEX-P was extracted from the skin by soaking the tissues in 5 ml of mobile phase for 4 h at ambient temperature. The extraction suspensions were membrane-filtered (nylon membranes 0.22 µm, Whatman, Maidstone, England). DEX-P content was analyzed by HPLC (see below). Experiments were typically performed in sextuplicate.

Experimental protocol *in vivo*

Male Wistar rats (260-280 g) were supplied by the Animal Experimental Research Centre at the University of Valencia, Spain. Experimental protocols were approved by the Ethical Committee for Animal Experimentation at the University of Valencia. Twenty four hours before iontophoresis, the rats were anesthetized by intraperitoneal administration of pentobarbital sodium (Dolethal solution, 40 $mg.kg^{-1}$; Vetoquinol, Madrid, Spain). The jugular

vein was cannulated using medical grade silicon tubing (Silastic, Dow Corning Co.; inner diameter 0.5 mm; outer diameter, 0.94 mm).

For iontophoretic administration of DEX-P, animals were anesthetized (pentobarbital sodium, 40 $mg.kg^{-1}$) and mounted on a plastic support. Two glass chambers (A = 1.33 cm^2) were then placed 2.5 cm apart on the animal's abdomen (shaved beforehand) and fixed with glue. The cathodal, anodal and receptor compartments contained buffer solution (25 mM HEPES / 133 mM NaCl, pH 7.4). The DEX-P formulation (0.7 ml of unbuffered 40 mM DEX-P solution; pH ~7.8) was separated from the cathode by a SB. A power supply (APH 1000M, Kepco, Flushing, NY) delivered a constant, direct current of 0.66 mA (0.5 $mA.cm^{-2}$) for 5 h. Blood samples (1.0 ml) were withdrawn at hourly intervals and immediately centrifuged at 10,000 rpm; the plasma collected was separated and stored at -20°C until analysis by HPLC. After each sampling time the blood volume was replaced with the same volume of saline solution. At the end of each experiment, the animals were sacrificed using pentobarbital sodium at a dose of 200 $mg.kg^{-1}$.

Analytical method

A P680A LPG-4 pump equipped with an ASI-100 autosampler (Dionex, Voisins LeBretonneux, France) and a UV detector (UVD 170/340-U) was used to quantify both the prodrug (DEX-P) and dexamethasone (DEX). Isocratic separation was performed using a 125 mm x 4 mm column packed with 5 µm C_{18} endcapped silica reversed-phase particles (Lichrocart, Merck KGaA, Germany). The flow-rate was 1.0 $ml.min^{-1}$ and the column temperature was kept at 30°C. The mobile phase consisted of 50% 0.01 M oxalic acid and 50% methanol pH = 6.0. The injection volume was 5-100 µl. The UV absorbance at 240 nm was used for detection. The limits of detection (LOD) and quantification (LOQ) for DEX were 87 and 262 ng, and for DEX-P, 12 and 37 ng, respectively.

Plasma extraction

The extraction procedure was based on a one-step liquid-liquid technique [17]. Diethyl ether (1 ml) was added to 200 µl of plasma and the resulting mixture was vortex-mixed for 15 min. After centrifugation at 12,000 rpm and separation, the organic layer was evaporated at 30°C. The residue was dissolved in 200 µl of mobile phase and finally 50 µl injected into the chromatographic column. Calibration curves (n = 6) that spanned the range of DEX concentrations in the plasma samples were prepared in triplicate in order to validate the analytical method. A linear correlation was obtained and the intercept was not significantly different from zero (r^2 = 0.999). The mean recovery of DEX averaged 84.0 ± 6.1 % (n = 8); the LOQ was 262 ng.

The relative error and coefficient of variation were the parameters evaluated for accuracy and precision and are shown in Table 1 (US Food and Drug Administration, 2001). The stability of DEX in plasma stored at -20℃ during 3 weeks was also evaluated. The relative variation was ~5 % over a concentration range from 0.035 to 0.750 $\mu g.ml^{-1}$.

Table 1. Accuracy and precision for DEX assay validation.

Theoretical concentration ($\mu g.ml^{-1}$)	Experimental concentration (Mean ± S.D.) ($\mu g.ml^{-1}$)	C.V. (%)	Deviation from theoretical value (%)
Intra-day (n=3)			
0.075	0.072 ± 0.009	11.892	4.617
0.350	0.370 ± 0.008	2.168	5.726
0.750	0.812 ± 0.009	1.087	8.244
2.000	2.242 ± 0.130	5.812	12.090
Inter-day (n=3)			
0.075	0.068 ± 0.002	3.658	9.467
0.350	0.338 ± 0.032	9.584	3.543
0.750	0.750 ± 0.048	6.415	0.020
2.000	2.261 ± 0.150	6.612	13.064

Pharmacokinetic analysis

Pharmacokinetic parameters for the iontophoretic delivery of DEX were calculated using a one compartment model with zero-order absorption and first-order elimination (WinNonlin software version 5.2.1; Pharsight, Inc., Apex, NC) as follows:

$$C_p = \left(\frac{k_{input}}{V_d \bullet k_{10}} \right) * \left(1 - e^{k_{10}t} \quad if \;\; t \le t_{ionto} \right) \tag{1}$$

$$C_p = \left(\frac{k_{input}}{V_d \bullet k_{10}} \right) * \left(1 - e^{k_{10}t} \right) * \left(e^{-k_{10}(t - t_{ionto})} \right) \;\; if \;\; t \ge t_{ionto} \tag{2}$$

where C_p is the plasma concentration of DEX at time (t), V_d is the volume of distribution, k_{input} is the input rate and k_{10} is the elimination rate constant.

Plasma profiles were fitted using a Gauss-Newton algorithm with Levenberg-Hartley modification. Non-compartmental parameters such as C_{max}, half-life and $AUC_{0\text{-}inf}$ were calculated in Microsoft Excel. The volume of distribution of the drug was obtained from the literature [18].

Data analysis and statistics

Values were expressed as mean ± S.D. Outliers determined using the Grubbs test were discarded [19]. Statistical analysis was conducted using analysis of variance (ANOVA) to evaluate the difference between multiple data sets. Student's t-test was used to compare two data sets. The level of significance was fixed at $P < 0.05$.

RESULTS AND DISCUSSION

Skin metabolism of DEX-P

Figure 2 shows the extent of metabolism of the prodrug when in contact with human, porcine and rat dermis; the average recovery of intact DEX-P after 7 h was 82.2 ± 0.4 %, 72.5 ± 4.8 % and 78.6 ± 6.0 %, respectively. The HPLC chromatograms showed only one additional peak, which increased with time and was identified as the hydrolysis product, dexamethasone (DEX).

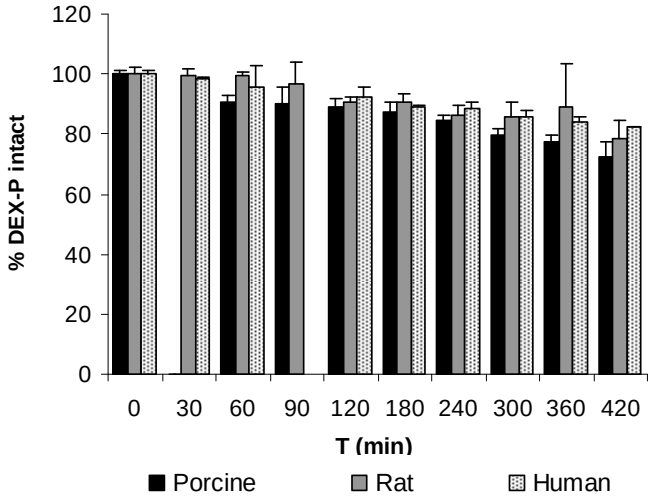

Figure 2. Stability of DEX-P when placed in contact porcine, rat and human dermis *in vitro*. (Mean ± SD; n =3).

Overall, DEX-P displayed good stability and there was little interspecies variation. It has previously been reported that both animal and human skins possess esterase activity and can hydrolyse corticosteroid 21-monoesters – although typically the ester (e.g., valerate or (di)propionate) is used as a means to increase the lipophilicity of the molecule and facilitate partitioning into the stratum corneum rather than introduce a hydrophilic charged moiety as

is the case here [20]. More generally, there are several studies that point to the ability of cutaneous esterases to hydrolyse many different ester prodrugs [20-25] – including valaciclovir, the charged amino-ester derivative of aciclovir [26] – although the rate and extent of hydrolysis can vary depending on the structure and physicochemical properties of the molecules. It should also be borne in mind that there may be differences between the cutaneous activities and distribution of esterases and phosphatases. When DEX-P was placed in contact with the external and internal surfaces of porcine epidermis, the drug appeared to be essentially unaffected (*t test, p<0.05*). There was no statistically significant difference in DEX-P recovery after 7 h after exposure to the internal surfaces of dermatomed skin and heat-separated epidermis (96.46 ± 1.92 and 96.88 ± 14.50 %, respectively). This is significant since electromigration through the epidermis and subsequent entry into the dermis depends on the presence of the negatively charged phosphate group – thus, cleavage of this moiety should only occur in the dermis or once the molecule is in the bloodstream itself.

Iontophoretic delivery of DEX-P

***In vitro* transport**

Control passive diffusion experiments with DEX from a commercial formulation (Dexolan, 0.1% ointment; G Streuli & Cie. SA Uznach, Switzerland) during 7 h resulted in very poor permeation and skin retention; DEX levels were below the limit of detection. In contrast, cathodal DEX-P iontophoresis using a 10 mM solution (~0.5%) resulted in significant drug transport; cumulative permeation was 35.65 ± 23.20 µg.cm^{-2}.

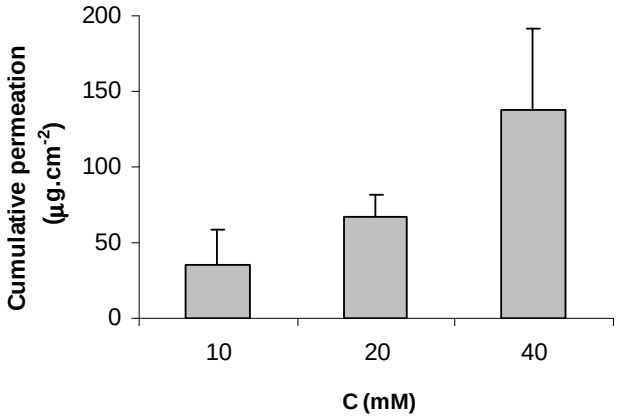

Figure 3. Cumulative permeation of DEX-P during 7 h of iontophoresis at 0.3 mA.cm^{-2} as a function of concentration. (Mean ± SD; n ≥ 3)

The effect of drug concentration on DEX-P iontophoresis from unbuffered solutions is shown in Figure 3; an increase from 10 to 40 mM resulted in a ~4-fold increase in cumulative permeation (at 40 mM, DEX-P delivery was 137.90 ± 53.90 µg.cm^{-2}). Drug extraction from

the skin carried out at the end of the iontophoretic experiments using 10, 20 and 40 mM DEX-P, showed that significant amounts of DEX-P were also retained in the membrane (171.56 ± 109.20, 484.67 ± 290.40, and 520.92 ± 409.75 µg.cm^{-2}, respectively). The calculated delivery efficiencies based on the sum of the cumulative amount permeated and retained within the skin using the 10, 20 and 40 mM formulations were 0.93, 2.99 and 3.58%, respectively.

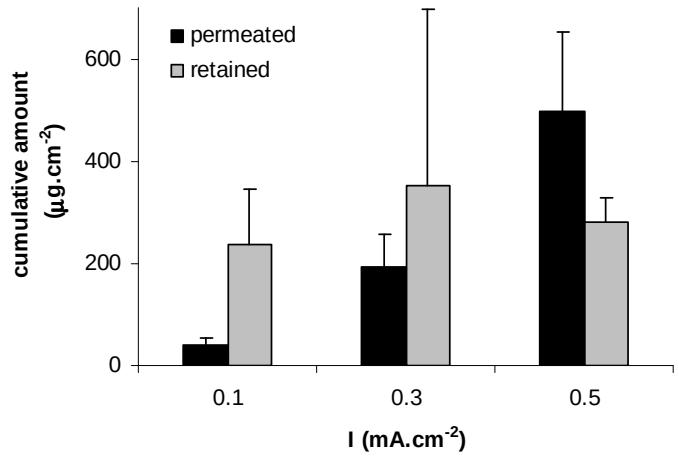

Figure 4. Cumulative permeation and skin deposition of DEX-P as a function of current density after 7 h iontophoresis at 0.1, 0.3 and 0.5 mA.cm^{-2}. (Mean ± SD; n ≥ 3)

The impact of increasing current density on DEX-P transport is illustrated in Figure 4. Good linearity was observed between the cumulative amount of DEX-P permeated and the applied current density (i_d; 0.1, 0.3, 0.5 mA.cm^{-2}) (J_{DEX} (µg.cm^2.h^{-1}) = 237.98i_d – 21.32, r^2 = 0.96). Although an increase in current density from 0.1 to 0.5 mA.cm^{-2} resulted in a ~12–fold increase in DEX-P permeation following 7 h of iontophoresis, there was no statistically significant difference between the amounts of DEX-P extracted from the skin at 0.1, 0.3 and 0.5 mA.cm^{-2} (Figure 4)**.**

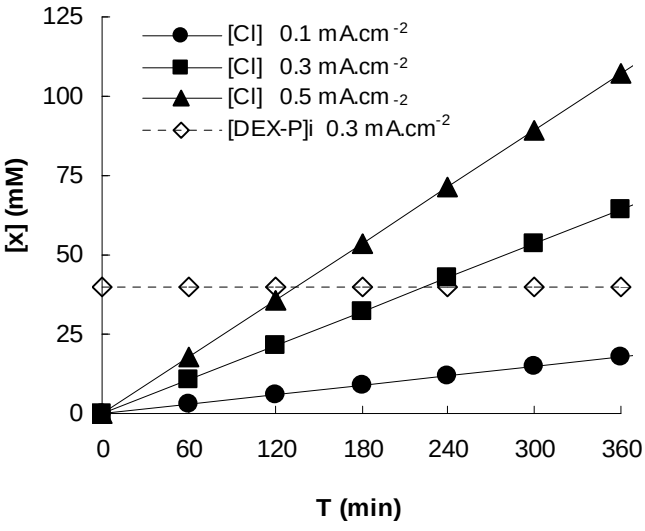

Figure 5. Concentration profile of chloride ions generated at the cathode compartment (1 cm^3) during 7 h of iontophoresis as a function of current density. $[DEX\text{-}P]_i$ = initial concentration of DEX-P.

The release of mobile chloride ions from the Ag/AgCl cathode during iontophoresis will impact upon the transport efficiency of drug anions [13-16]. The theoretical evolution of chloride ion concentration in the cathodal compartment over 7 h at the different current densities used in these experiments is depicted in Figure 5. Clearly, the transport of DEX-P would be progressively hampered by the increasing levels of more mobile chloride ions. Isolation of the DEX-P formulation from the cathode by means of a SB can reduce competition from Cl^-.

This is illustrated in Figure 6, which shows the doubling of iontophoretic fluxes (and hence transport number) when using the SB assembly ($P < 0.05$).

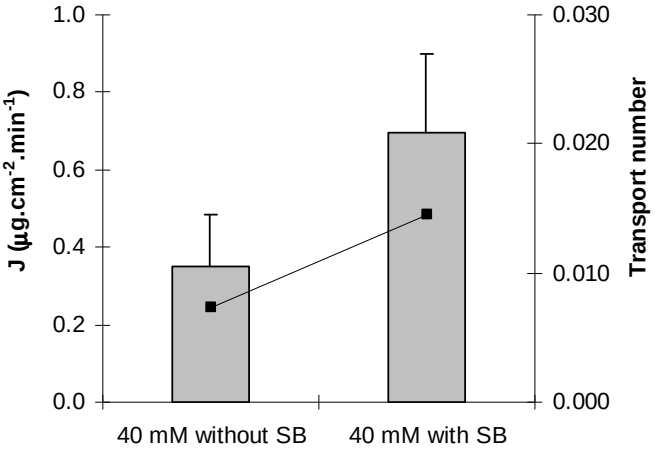

Figure 6: Improving DEX-P transport efficiency upon eliminating competition from Cl^- ions by using a salt bridge (SB). (Mean ± SD; n >3).

Dexamethasone pharmacokinetic study

The *in vivo* data confirmed that, in contrast to its relative stability in contact with skin, DEX-P was rapidly hydrolysed by phosphatases in the blood and only the active steroid (DEX) was detected in the bloodstream.

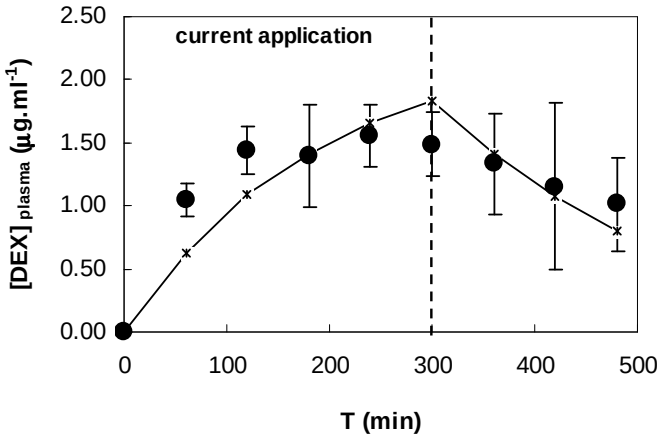

Figure 7. Mean DEX concentrations in plasma (± SD) from four animals after iontophoretic administration of DEX-P for 5 h (40 mM; 0.5 $mA.cm^{-2}$ with a SB). The solid line represents the predicted values.

The mean DEX concentration–time profile upon iontophoretic administration at 0.5 mA.cm^{-2} and the fitted curve are shown in Figure 7. Significant DEX levels (~1 µg.ml^{-1}) were achieved at 1 h, reflecting the fast input kinetics of the phosphate prodrug (Table 3). Furthermore, the DEX concentration remained significant throughout the post-iontophoretic period between t = 5 - 8 h. The goodness of the fit can be clearly seen through the correlation between the observed and predicted DEX-P plasma concentrations versus time (Correlation ($_{observed,\ predicted}$) = 0.91). The estimated pharmacokinetic parameters after iontophoretic delivery are given in Table 2. The calculated input rate (1.66 ± 0.20 µg.cm^{-2}.min^{-1}) was not statistically different from the flux obtained *in vitro* across dermatomed porcine skin (1.79 ± 0.49 µg. cm^{-2}.min^{-1}).

Table 2: Pharmacokinetic parameters for DEX after cathodal iontophoresis for 5 h at 0.5 mA.cm^{-2} (n=4).

Parameter	
C_{max} (µg.ml^{-1})	1. 62 ± 0.36
$AUC_{0\text{-}inf}$ (µg.min.ml^{-1})	914.33 ± 378.27
Half-life (min)	235.12 ± 165.83
Input rate (k_{input}) (µg.min^{-1})	2.21 ± 0.27
Elimination rate constant (k_{10}) (min^{-1})	0.006 ± 0.002

CONCLUSIONS

The results presented here suggest that DEX-P can be delivered efficiently by cathodal iontophoresis and that transport is further enhanced by eliminating competition with Cl^- ions generated at the cathode. Moreover, DEX-P flux increased linearly as a function of donor concentration and current density. This offers a significant advantage in modulating delivery rates. Pharmacokinetic analysis using a one-compartment model estimated the input rate constant for DEX at 0.5 mA.cm^{-2} as 2.21 ± 0.27 µg.min^{-1} (for an application area of 1.33 cm^2). The usual initial adult dosing of dexamethasone for treating delayed CINV ranges from 4 - 12 mg *per os*, depending on the patient response. Based on our results, it should be possible to deliver therapeutic amounts of DEX for the treatment of CINV using moderately-sized iontophoretic systems containing DEX-P with an application area of 10 cm^2 at reasonable current densities.

ACKNOWLEDGEMENTS

We thank the Swiss Cancer League (Berne, Switzerland) for financial support (OCS 01753-08-2005) and J. Cázares-Delgadillo also acknowledges financial support from CONACYT (Mexico). We would also like to acknowledge Pharsight Corporation (Mountain View, CA) for providing an academic license for the WinNonlin® Professional software.

REFERENCES

1) T.S. Sam, S.W. Chan, J.A. Rudd, J.H. Yeung, Action of glucocorticoids to antagonize cisplastin-induced acute and delayed emesis in the ferret, Eur. J. Pharmacol. 417 (2001) 231-237.
2) S.L. Curry, J. Rine, C.W. Whitney, W.A. Nahhas, R. Mortel, L.M. Demers, The role of prostaglandins in the excessive nausea and vomiting after intravascular cis-platinum therapy. Gynecol. Oncol. 12 (1981) 89-91.
3) Y.N. Kalia, A. Naik, J. Garrison, R.H. Guy, Iontophoretic drug delivery, Adv. Drug. Deliv. Rev. 56 (2004) 619-658.
4) J.A. Subramony, A. Sharma, J.B. Phipps, Microprocessor controlled transdermal drug delivery, Int. J. Pharm. 317 (2006) 1-6.
5) A.K. Banga, P.C. Panus, Clinical applications of iontophoretic devices in rehabilitation medicine, Critical Reviews in Physical and Rehabilitation Medicine, 10 (1998) 147-179.
6) H. Hamann, M. Hodges, B. Evans, Effectiveness of iontophoresis of anti-inflammatory medications in the treatment of common musculoskeletal inflammatory conditions: a systematic review, Phys. Ther. Rev. 11(2006) 190-194.
7) W.T. Zempsky, J. Sullivan, D.M. Paulson, S.B. Hoath, Evaluation of low-dose lidocaine iontophoresis system for topical anesthesia in adults and children: a randomized controlled trial, Clin. Ther. 26 (2004) 1110-1119.
8) E.R. Viscusi, M. Siccardi, C.V. Damaraju, D. J. Hewitt, P. Kershaw, The safety and efficacy of fentanyl iontophoretic transdermal system compared with morphine intravenous patient-controlled analgesia for postoperative pain managemement: an analysis of pooled data from three randomized, active-controlled clinical studies, Anesth. Analg. 105 (2007) 1428-1436.
9) J.M. Glass, R.L. Stephen, S.C. Jacobson, The quantity and distribution of radiolabeled dexamethasone delivered to tissue by iontophoresis, Int. J. Pharm. 19 (1998) 519-525.
10) T.J. Petelenz, J.A. Buttke, C. Bonds, L. B. Lloyd, J. E. Beck, R. L. Stephen, S. C. Jacobsen, P. Rodriguez, Iontophoresis of dexamethasone: laboratory studies, J. Control. Release. 20 (1992) 55-66.

11) J.-P. Sylvestre, R.H. Guy, M.B. Delgado-Charro, *In vitro* optimization of dexamethasone phosphate delivery by iontophoresis, Phys. Ther. 88 (2008) 1177-1185.

12) J.-P. Sylvestre, C. Díaz-Martín, M.B. Delgado-Charro, R.H. Guy, Iontophoresis of dexamethasone phosphate: competition with chloride ions, J. Control. Release. 131 (2008) 41-46.

13) C.L. Gay, P.G. Geen, R.H. Guy, M.L. Francoeur, Iontophoretic delivery of piroxicam across the skin in vitro, J. Control. Release. 22 (1992) 57-67.

14) X. Hui, A. Anigbogu, P. Singh, G. Xiong, N. Poblete, P.Lieu, H.I. Maibach, Pharmacokinetic and local tissue disposition of [14C] sodium diclofenac following iontophoresis and systemic administration in rabbits, J. Pharm. Sci. 90 (2001) 1269-1276.

15) Y. Katori, M. Erickson, J.A. Subramony, R. Padmanabhan, J.B. Phipps, Transdermal iontophoretic delivery of ketoprofen. 34th Annual Meeting and Exposition of the Controlled Release Society. Long Beach (CA), July 7-11, 2007.

16) A. Romand, J. Cázares-Delgadillo, Y. G. Bachhav, Y. N. Kalia, Optimizing iontophoretic delivery kinetics of diclofenac *in vitro*. 6th World Meeting on Pharmaceutics, Biopharmaceutics and Pharmaceutical Technology. Barcelona, Apr 7-10, 2008.

17) A. Chmielewska, L. Konieczna, A. Plenis, H. Lamparczyk, Sensitive quantification of chosen drugs by reversed-phase chromatography with electrochemical detection at a glassy carbon electrode, J. Chromatrogr. B 839 (2006) 102-111.

18) M.N. Samtani, W.J. Jusko, Comparison of dexamethasone pharmacokinetics in female rats after intravenous and intramuscular administration, Biopharm. Drug. Dispos. 26 (2005) 85-91.

19) J. E. De Muth, Basic Statistics and Pharmaceutical Statistical Applications, Marcel Dekker, New York, 1999.

20) U. Taüber, K. L. Rost, Esterase activity of the skin including species variation In B. Shroot and H. Schaefer B. Shroot H. Schaefer (eds.), Pharmacology and the Skin Vol. 1, Skin Pharmacokinetics, Karger, Basel, 1987, pp. 170-183.

21) A. L. Stinchcomb, A. Paliwal, R. Dua, H. Imoto, R. W. Woodward, G. L. Flynn, Permeation of buprenorphine and its 3-alkyl-ester prodrugs through human skin, Pharm. Res. 13 (1996) 1519-1523.

22) H. Bundgaard, N. Mork, A. Hoelgaard, Enhanced delivery of nalixidic acid through human skin via acyloxymethyl ester prodrugs, Int. J. Pharm. 55 (1989) 91-97.

23) G. Nicolau, A Yacobi, Transdermal absorption and skin metabolism of vipristol, a synthetic prostaglandin E2 analogue, Drug Metab. Rev. 21 (1990) 401-425.

24) T. Seki, T. Kawaguchu, K. Juni, Enhanced delivery of zidovidudine through rat and human skin via ester prodrugs, Pharm. Res. 7 (1990) 948-952.
25) O. Pillai, M. O. Hamad, P. A. Crooks, A. L. Stinchcomb, Physicochemical evaluation, in vitro hum skin diffusion and concurrent biotransformation of 3-O-alkyl carbonate prodrugs of naltrexone. Pharm. Res. 21 (2004) 1146-1152.
26) N. Abla, A. Naik, R. H. Guy, Y. N. Kalia, Topical iontophoresis of valaciclovir hydrochloride improves cutaneous acyclovir delivery, Pharm. Res. 23 (2006) 1842-1849.

ABBREVIATIONS

AUC_{0_inf}: area under a curve from time = 0 to time infinity
Cl^-, chloride ion
C, concentration
C_{max}, maximum plasma concentration
C_p, plasma concentration
C.V., coefficient of variation
DEX-P, dexamethasone sodium phosphate
HPLC, High Performance Liquid Chromatography
I, current intensity
IV, intravenous administration
J_{tot}, iontophoretic flux
k_{input}, input rate
k_{10}, elimination rate constant
SB, salt bridge
S.D., standard deviation

New therapeutic approaches to treat chemotherapy induced emesis: simultaneous co-iontophoresis of granisetron, metoclopramide and dexamethasone sodium phosphate *in vitro* and *in vivo*

Jennyfer Cázares-Delgadillo[1], Adriana Ganem-Rondero[2], David Quintanar-Guerrero[2], Alicia C. López Castellano[3], Virginia Merino[4], Yogeshvar N. Kalia[1]

[1] School of Pharmaceutical Sciences, University of Geneva & University of Lausanne, 30 Quai Ernest Ansermet, 1211 Geneva, Switzerland

[2] División de Estudios de Posgrado (Tecnología Farmacéutica), Facultad de Estudios Superiores Cuautitlán, Universidad Nacional Autónoma de México, Av. 1° de Mayo S/N Cuautitlán Izcalli, Estado de México 54704, Mexico

[3] Departamento de Fisiología, Farmacología y Toxicología, University Cardenal Herrera (CEU), Edificio Seminario s/n, 46113 Moncada, Valencia, Spain

[4] Departamento de Farmacia y Tecnología Farmacéutica, Faculty of Pharmacy, University of Valencia, Avda. Vicente Andrés Estellés s/n, 46100 Burjassot, Valencia, Spain

Submitted to Journal of Controlled Release

ABSTRACT

The objective was to investigate the co-iontophoretic delivery of granisetron (GST), metoclopramide (MCL) and dexamethasone sodium phosphate (DEX-P), medications that are routinely used in combination to treat chemotherapy-induced emesis. Two preliminary *in vitro* studies using porcine skin were performed: Study 1 – effect of formulation composition on anodal co-iontophoresis of GST and MCL and Study 2 – combined anodal iontophoresis of GST (10 mM) and MCL (110 mM) and cathodal iontophoresis of DEX-P (40 mM). The results from Study 1 demonstrated the dependence of GST/MCL transport on their respective concentrations when co-iontophoresed at 0.3 $mA.cm^{-2}$. Although they possess similar physicochemical properties, MCL seemed to be a more efficient charge carrier ($J_{MCL} = 0.0591*C_{MCL}$ cf. $J_{MCL} = 0.0414*C_{GST}$). In study 2, as expected based on their relative

concentrations, MCL permeation was markedly superior to that of GST (2324.83 ± 307.85 and 209.83 ± 24.84 µg.cm^{-2}, respectively); DEX-P permeation was 336.94 ± 71.91 µg.cm^{-2}. Subsequent *in vivo* studies in Wistar rats (10 mM GST, 110 mM MCL and 40 mM DEX-P (0.5 mA.cm^{-2} for 5 h with Ag/AgCl electrodes and salt bridges) demonstrated that significant drug levels were achieved rapidly for each drug; most visibly for dexamethasone (DEX; N.B., DEX-P was not detected in the plasma) where relatively constant plasma levels were obtained from the 1 h to 5 h time-points. The calculated input rates *in vivo* (k_{01}; area 1.33 cm^2) for GST, MCL and DEX were 0.60 ± 0.07, 4.03 ± 0.64 and 2.62 ± 0.56 µg.min^{-1}, respectively. These results showed that therapeutic amounts of the three antiemetic agents could be co-administered by non-invasive transdermal iontophoresis.

Key words: iontophoresis, antiemetics, transdermal route, pharmacokinetics

INTRODUCTION

Treatment of chemotherapy-induced nausea and vomiting (CINV) represents a considerable challenge due to its complex etiology. Although the first-generation 5-HT$_3$ receptor antagonists have shown substantial efficacy, almost 50% of patients continue to suffer both acute and delayed emesis despite prophylactic treatment with these agents [1-3]. A number of clinical trials have demonstrated the superiority of combined therapy with dexamethasone and a 5-HT$_3$ antagonist over monotherapy with a 5-HT$_3$ antagonist alone [4-7]. Recent guidelines have also recommended the combination of metoclopramide (D_2 receptor antagonist) and dexamethasone as the antiemetic regimen of choice for the prevention of cisplatin-induced delayed emesis [8].

At present, these polytherapies are administered either orally or via the intravenous route. Obviously, the latter requires trained personnel and rigorous device care; in contrast, oral administration is convenient but systemic bioavailability in these patients can be severely reduced. The goal of this work was to investigate the co-iontophoretic delivery of granisetron (GST; MW 312.4 & pKa 9.4), metoclopramide (MCL; MW 299.8 & pKa 9.3) and dexamethasone sodium phosphate (DEX-P; MW 392.5), in order to optimize transdermal administration of the three antiemetics for the treatment of CINV. These data also provide mechanistic information on the effect of simultaneous anodal iontophoresis of two cationic drugs and the factors influencing their delivery.

The specific aims of the study were (i) to investigate the anodal co-iontophoresis of GST and MCL formulated at different concentrations and determine the impact of competition between the cations on their respective transport rates *in vitro*, (ii) to investigate co-iontophoretic

administration of GST, MCL and DEX-P *in vitro* and (iii) to explore the feasibility of delivering therapeutic amounts of the three antiemetics *in vivo*.

MATERIALS AND METHODS

Materials

Granisetron hydrochloride was a gift from Roche Diagnostics GmbH (Mannheim, Germany). HEPES buffer and sodium chloride were obtained from Fluka (Buchs, Switzerland). Metoclopramide hydrochloride, dexamethasone, dexamethasone 21-disodium phosphate salt, acetaminophen (ACE), agarose, sodium heptanesulfonate, silver wire and silver chloride were purchased from Sigma-Aldrich (Steinheim, Germany). Silicon tubing (1.6 mm ID, 3.2 mm OD, and 0.8 mm wall) for collecting samples and PVC tubing (3 mm ID, 5 mm OD, 1 mm wall thickness) used to prepare salt bridge assemblies were obtained from Fisher Bioblock Scientific S.A. (Illkirch, France).

Chromatographic reagents were obtained from VWR (Dietikon, Switzerland). All solutions were prepared using deionised water (resistivity > 18 MΩ.cm). All other chemicals were at least of analytical grade.

In vitro studies

Skin preparation

Porcine ear skin was obtained from a nearby abattoir (Carre Coopérative des Abattoirs de Rolle, Switzerland). The skin was excised (thickness 750 µm) with an electro-dermatome (Zimmer; Etupes, France), wrapped in Parafilm™ and stored at -20°C for a maximum period of 2 months.

Co-iontophoresis of GST and MCL

Skin was clamped in three compartment vertical flow-through diffusion cells (area 0.95 cm^2). After equilibration with buffer (25 mM HEPES / 133 mM NaCl, pH 7.4), 1 ml of each unbuffered formulation containing GST and MCL (compositions given in Table 1) was placed in the anodal compartment. Acetaminophen (ACE; 15 mM) was included in the formulations to report on electroosmosis (EO) and the effect of cation transport on skin permselectivity. The cathodal and receptor compartments were filled with 1 and 6 ml of 25 mM HEPES / 133 mM NaCl (pH 7.4) buffer solution. Samples were collected from the receiver compartment hourly using a syringe pump SP220IZ (WPI, Sarasota, FL), which generated a continuous flow of buffer solution (1 $ml.h^{-1}$). A constant current density of 0.3 $mA.cm^{-2}$ was applied for 7h via Ag/AgCl electrodes connected to a power supply (APH 1000M; Kepco, Flushing, NY).

Co-iontophoresis of GST, MCL and DEX-P

An unbuffered solution containing 10 mM GST and 110 mM MCL was placed in the anodal compartment. The cathodal compartment, which contained 25 mM HEPES / 133 mM NaCl (pH 7.4) was separated from the DEX-P formulation (40 mM DEX-P unbuffered solution; pH ~7.8) by a salt bridge. A constant current (0.5 $mA.cm^{-2}$) was applied for 7 h via Ag/AgCl electrodes. All other aspects of the protocol were the same as those outlined above.

Table 1. GST and MCL content in the different formulations used in the anodal co-iontophoresis experiments *in vitro*

Drug	Formulation			
(mM)	A	B	C	D
GST	10	40	60	80
MCL	110	80	60	40

The total flux (J_{tot}) of a charged species (i) during iontophoresis, can be represented as the sum of the component fluxes due to electromigration and electroosmosis (J_{EM} and J_{EO}) assuming negligible passive diffusion [9]:

$$J_{tot} = J_{EM} + J_{EO} = \left(\frac{t_i I}{z_i F} \right) + V_W c_i \quad (1)$$

where t_i is transport number (the fraction of the total applied current density carried across the skin by the ion), I is the total current density, z_i the charge of the ion, F Faraday's constant, c_i the drug concentration and V_w the solvent permeability coefficient.

Inhibition factor

Co-iontophoresis of ACE also enabled the calculation of an inhibition factor (*IF*) to quantify the effect of cation transport on skin permselectivity:

$$IF = \frac{Q_{ACE,\ control}}{Q_{ACE}} \quad (2)$$

where $Q_{ACE,control}$ is the cumulative amount of ACE delivered calculated during 7 h of iontophoresis at a given current density and Q_{ACE} is the corresponding value when GST and MCL were simultaneously iontophoresed.

***In vivo* protocol**

The pharmacokinetic protocol was approved by the Ethics Committee for Animal Experimentation at the University of Valencia (Valencia, Spain). Male Wistar rats (300-312 g) were used for the experiments. Twenty four hours before iontophoresis, the rats were anesthetized by intraperitoneal administration of pentobarbital sodium (Dolethal solution, 40 $mg.kg^{-1}$, Vetoquinol, Madrid, Spain). The jugular vein was cannulated using medical grade silicon tubing (Silastic, Dow Corning Co.; ID 0.5 mm; OD, 0.94 mm). The cannula was permanently filled with heparinized saline solution (20 $IU.ml^{-1}$) and closed with a polyethylene plug. Immediately prior to the co-iontophoresis experiments, the animals were re-anesthetized (Dolethal solution, 40 $mg.kg^{-1}$) and mounted on a plastic support. Two glass chambers (area 1.33 cm^2) were then placed 2.5 cm apart on the animal's abdomen (shaved beforehand) and fixed with glue. The anodal formulation comprised 0.7 ml of unbuffered 10 mM GST and 110 mM MCL solution (pH ~6.0), Ag/AgCl electrodes were introduced in the respective solutions; the cathodal compartment, which contained buffer solution (25 mM HEPES / 133 mM NaCl, pH 7.4), was separated from the DEX-P formulation (40 mM DEX-P unbuffered solution, pH 7.8) by a salt bridge. A power supply (APH 1000M; Kepco, Flushing, NY) was used to deliver a constant direct current of 0.66 mA (0.5 $mA.cm^{-2}$) for 5 h. Blood samples (1.0 ml) were withdrawn at hourly intervals and immediately centrifuged at 10,000 rpm; plasma collected was separated and stored at -20°C until analysis by HPLC. After each sampling time the blood volume was replaced with the same volume of saline solution. At the end of each experiment, the animals were sacrificed using pentobarbital sodium (200 $mg.kg^{-1}$).

HPLC Assay

A P680A LPG-4 pump equipped with an ASI-100 autosampler, a RF-2000 fluorescence detector and a UV detector (UVD 170/340-U) (Dionex, Voisins LeBretonneux, France) was used to quantify the three molecules. Isocratic separation of GST and MCL was performed using a Sunfire™ 100 C_{18} 5 µm column. The flow-rate was 2.0 $ml.min^{-1}$ and the column temperature was kept at 50°C. For the *in vitro* experiments, the mobile phase consisted of acetate buffer (0.1 M pH 4.7; 0.2% sodium heptanesulfonate and 0.02% EDTA) and acetonitrile (73:27 v/v) and the injection volume was 1-100 µl. The excitation and emission wavelengths for detection of GST were 305 and 350 nm, respectively, and the gain of the detector was set at unity. MCL was analyzed by UV detection at 273 nm. The limits of detection (LOD) and quantification (LOQ) were 11 and 34 ng, and 17 and 52 ng for GST and MCL, respectively.

Plasma samples were eluted using a mobile phase containing acetate buffer, acetonitrile and deionised water (51:19:30 (v/v)) and the injection volumes for GST and MCL were 10 and 50 µl, respectively. GST and MCL were analyzed by fluorescence detection; the excitation and emission wavelengths were 305 and 350 nm for GST and 316 and 359 nm for MCL. The LOD and LOQ and were 12 and 36 ng and 15 and 44 ng for GST and MCL, respectively.

DEX-P and DEX were assayed using a 123 mm x 4 mm column packed with 5 µm C_{18} endcapped silica reversed-phase particles (Lichrocart; Merck KGaA, Germany). The flow rate was kept at 1.0 $ml.min^{-1}$ and the column temperature was kept at 30°C. Samp les were eluted with oxalic acid (0.01 M) and methanol (50:50 v/v); the pH was adjusted to 6.0 and the injection volume was 5-100 µl. The UV absorbance at 240 nm was used for detection. The LOD and LOQ were 10 and 31 ng, and 87 and 262 ng for DEX-P and DEX, respectively.

ACE transport from the *in vitro* experiments was assayed separately using a Lichrospher 100 RP-8 reversed-phase column. The mobile phase comprised 88% citrate buffer (40 mM, pH 3.0) and 12% acetonitrile. The flow rate and the injection volumes were 1.0 $ml.min^{-1}$ and 1-100 µl, respectively. ACE was detected by its UV absorbance at 243 nm. The LOD and LOQ were 2 and 6 ng, respectively.

All solvents were filtered (0.45 µm pore size nylon membrane filter) and degassed prior to use and the columns were equilibrated for at least 1 h.

Plasma extraction

GST plasma samples were extracted using a method adapted from literature [10]. A volume of 200 µl of ACN was added to plasma (100 µl) and the mixture was vortex-mixed for 5 min and centrifuged at 10,000 rpm for 2 minutes at 5°C. An aliquot of the supernatant (10 µl) was injected directly into the HPLC column.

The extraction procedure for MCL and DEX was based on a one-step liquid-liquid technique [11]. Briefly, 50 µl of 1 M NaOH was added to 200 µl of plasma and the tube was shaken for 2 minutes. Immediately thereafter, 1 ml of diethyl ether was added and the resulting mixture was then vortex-mixed for 15 min. After centrifugation at 10,000 rpm and separation, the organic layer was evaporated at 30°C. The residue was dissolved in 200 µl of mobile phase and finally 50 µl injected into the chromatographic column. DEX was extracted following the same protocol without alkalinization of the supernatant; plasma samples were centrifuged at 12,000 rpm. Calibration curves spanning the plasma concentration range for each drug were prepared in triplicate in order to validate the analytical method. The mean recoveries for GST, MCL and DEX averaged 102.2 ± 4.4 % (n = 7), 88.11 ± 5.27% (n = 7) and 84.0 ± 6.07 % (n = 8), respectively.

Pharmacokinetic models

Plasma profiles were fitted using a one compartment model with zero and first-order absorption and first-order elimination (WinNonlin® Professional (version 5.2.1; Pharsight, Corp., Mountain View, CA)).

During iontophoretic current application, the drug concentration in plasma at time *t* can be calculated assuming a zero-order drug input from the system into the skin (based on a constant iontophoretic driving force):

$$C_p = \frac{k_{input}}{V_d \bullet k_{10}} \{1 - \exp(-k_{10} t)\} \qquad t \le 5\,h \tag{3}$$

where, C_p = plasma concentration of drug ; V_d = volume of distribution; k_{input}= input rate

Transport during the post-iontophoretic period can be modeled using two different conditions. First, if it assumed that there is no further mass input into the systemic circulation after terminating current application at time t_{ionto}, then the drug concentration can be written as:

$$C_p = \frac{k_{input}}{V_d \bullet k_{10}} \{1 - \exp(-k_{10} t)\} * \{\exp(-k_{10}(t - t_{ionto}))\} \qquad t \ge 5\,h \tag{4}$$

On the other hand, if serum levels continue to increase after t_{ionto}, then drug release from the skin into the plasma is a passive process determined by a first-order skin release rate constant. In this situation C_p will be defined by Eq. (5):

$$C_p = \frac{F \bullet k_a}{V_d \bullet (k_a - k_{10})} [\{\exp(-k_{10}(t - t_{ionto}))\} - \{\exp(-k_a(t - t_{ionto}))\}] \qquad t \ge 5\,h \tag{5}$$

where F represents the fraction of the dose that accumulates in the skin and k_a the absorption constant.

The fitting was done using a Gauss-Newton algorithm with a Levenberg-Hartley modification. Basic pharmacokinetic parameters such as AUC_{0_inf}, C_{max} and half-life were calculated in Microsoft Excel. The volume of distribution of each drug was obtained from the literature [12-14].

Statistical analysis

The results were derived from at least triplicate experiments. Outliers determined using the Grubbs test [15], were discarded. Statistical differences were determined by Student's *t*-test and analysis of variance (ANOVA). The level of statistical significance was fixed at $P < 0.05$.

RESULTS AND DISCUSSION

Effect of formulation composition on GST and MCL co-iontophoretic transport rates

The cumulative permeation and steady state fluxes for GST and MCL from formulations A–D (Table 1) after iontophoresis at 0.3 mA.cm^{-2} for 7 h are presented in Figures 1 and 2, respectively. The results demonstrate that both cumulative permeation and flux increase with drug concentration. However, the dependence of drug transport on concentration is different for GST and MCL – $J_{GST} = 0.0414*C_{GST}$ and $J_{MCL} = 0.0591* C_{MCL}$ – therefore, for a given concentration $J_{MCL} = 1.43*J_{GST}$. For example, comparison of the data for formulations B (80 mM MCL, 40 mM GST) and D (40 mM MCL, 80 mM GST) shows that doubling the concentration of GST and MCL in the formulation resulted in 2.0 and 3.7-fold increases in their respective fluxes. GST and MCL have similar molecular weights, log P and pKa values (see above); however, based on the flux-concentration relationship, MCL seems to be a more efficient charge carrier. This was tentatively attributed to MCL having superior electric mobility; however, capillary zone electrophoresis measurements showed that the difference in mobility was minimal (138 ± 0.97 and 136 ± 0.68 10^{-6}cm^2.s^{-1}.V^{-1} for MCL and GST, respectively) [16].

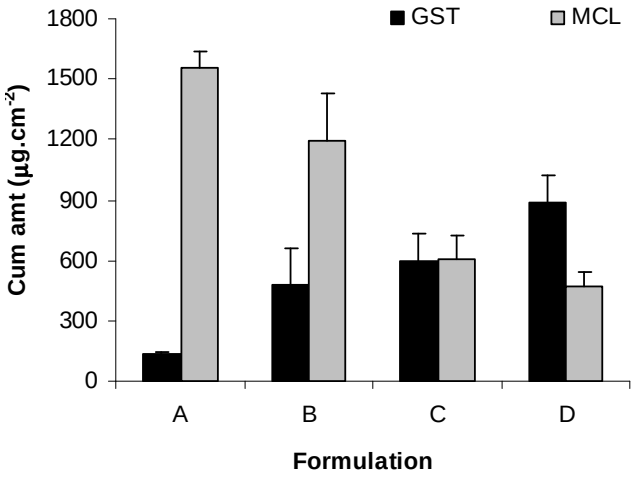

Figure 1. Influence of formulation composition (see Table 1) on GST and MCL delivery after 7 h of iontophoresis at 0.3 mA.cm^{-2}. (Mean ± SD; n>4).

However, computational analysis of the physicochemical properties over the molecular surface and in three dimensions showed that MCL has a higher polar surface area (PSA; 110.8 cf. 36.0) and a smaller dipole moment (15.8 cf. 20.9).

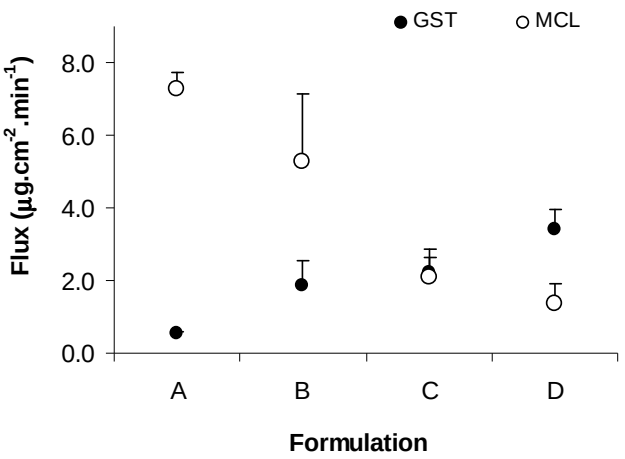

Figure 2. Steady-state fluxes of GST and MCL from the different formulations (Table 1) after 7 h of iontophoresis at 0.3 mA.cm^{-2}. (Mean ± SD; n ≥ 5).

It has previously been reported that increasing hydrophilic surface area is advantageous for iontophoretic transport (i.e, higher PSA) and whereas localized charge (evidence by a higher dipole moment) is unfavorable due to the increased propensity to interact with oppositely charged structures in the transport pathway [17].

The relative contributions of electromigration (EM) and electroosmosis (EO) to MCL and GST electrotransport from each formulation are shown in Figure 3; EM was the principal transport mechanism for both cations, accounting for between 60 to 80% of total delivery. Inhibition of ACE transport (IF, 1.71), evidenced by a decrease in convective solvent flow, was observed only for formulation C where both cations were formulated at 60 mM.

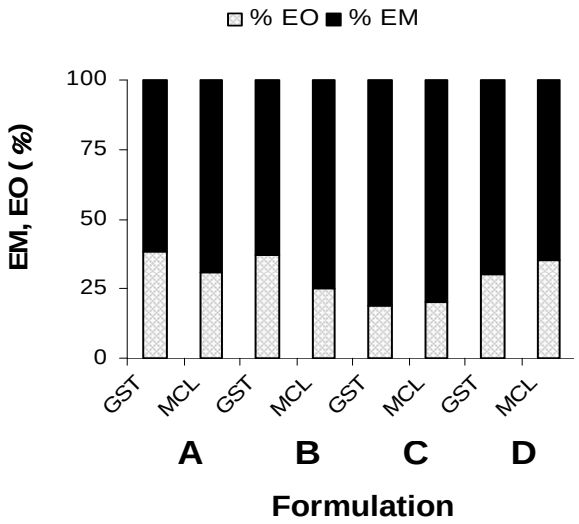

Figure 3. Relative contributions of electromigration (EM) and electroosmosis (EO) to the total flux of GST and MCL formulations.

The delivery efficiency of both cations as calculated from the respective transport numbers is shown in Table 2. For each formulation (A–D), the total concentration of MCL and GST was maintained at 120 mM and although increasing the concentration of each drug in the formulation clearly increased its own delivery, cation transport only accounted for ~5-7% of

total charge transfer. As expected Cl^- from the receiver phase was the predominant charge carrier and accounted for > 90% of current flow.

Table 2. Iontophoretic transport efficiency of GST and MCL delivered from formulations A-D in the anodal co-iontophoresis experiments *in vitro* (0.3 $mA.cm^{-2}$ applied for 7 h; n > 4).

Formulation	Transport numbers x 10^{-2}		
	GST	MCL	Total
A	0.55	6.64	7.18
B	1.96	5.08	7.04
C	2.56	2.57	5.13
D	3.68	1.99	5.67

Simultaneous anodal and cathodal co-iontophoresis of GST, MCL and DEX-P

The second phase of this work explored the feasibility of combining anodal iontophoresis of GST and MCL with cathodal delivery of DEX-P. The anodal compartment contained GST (10 mM) and MCL (110 mM), hence obviating the need for NaCl to drive anodal electrochemistry. Cathodal iontophoresis of DEX-P (40 mM) was performed using a salt bridge to separate the cathodal and formulation compartments and so eliminate the effect of competition from Cl^- produced at the cathode; thus, the principal competition to DEX-P transfer came from Na^+ present in the receiver compartment – which, due to its concentration and high mobility, was the main charge carrier. Figure 4 shows the cumulative permeation profile for the three drugs when co-iontophoresed at 0.5 $mA.cm^{-2}$. MCL delivery was approximately 11-fold higher than that of GST (2324.83 ± 307.85 and 209.83 ± 24.84 $\mu g.cm^{-2}$, respectively) corresponding the difference in their respective concentrations. DEX-P permeation was 336.94 ± 71.91 $\mu g.cm^{-2}$.

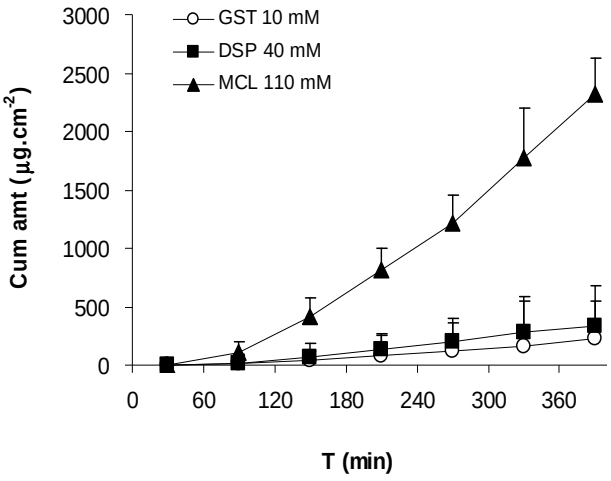

Figure 4. Cumulative permeation of DEX-P (40 mM), GST (10 mM) and MCL (110 mM) after 7 h of coiontophoresis at 0.5 $mA.cm^{-2}$. (Mean ± SD; n = 5).

It should be noted that despite its 4-fold higher concentration, DEX-P delivery was only 1.6-fold higher than that of GST. Steady-state fluxes and transport numbers (calculated from the cumulative amounts permeated) are shown in Table 3.

Table 3. Steady-state fluxes and transport numbers of GST, MCL and DEX-P after 7 h of co-iontophoresis at 0.5 mA.cm^{-2} (Mean ± SD; n =5).

Drug	C (mM)	Flux (µg.cm^{-2}.min^{-1})	Transport number x 10^{-2}
MCL	110	9.25 ± 2.43	5.94
GST	10	0.69 ± 0.06	0.51
DEX-P	40	1.05 ± 0.15	0.99

Although the total concentration of MCL and GST in the anodal compartment was 120 mM (cf. 133 mM Cl^- in the receiver compartment) cation transport still only accounted for ~7 % of total charge transfer. Thus, Cl^- transfer from the receiver to the anodal compartment was primarily responsible for current flow (~93%) as given by:

$$t_{Cl^-}^{c\to a} = \left(1-\left(t_{GST}^{a\to c} + t_{MCL}^{a\to c}\right) = 0.93 \right. \quad (6)$$

where t = transport number of the respective ion; a = anode; c = cathode.

Delivery of DEX-P accounted for only ~0.5% of the total charge transfer at the cathode-skin interface.

***In vivo* delivery**

The plasma concentration–time profiles of the three antiemetics upon iontophoretic administration at 0.5 mA.cm^{-2} are shown in Figure 5. DEX-P was found to be completely hydrolysed by esterases in the blood and only the concentration of the active steroid (DEX) was measured during this experiment. Significant drug levels were achieved rapidly; most visibly for DEX where steady state plasma levels were observed between the 1 and 5 h time-points. However, there was significant interindividual variation resulting in $AUC_{0\text{-inf}}$ values varying by approximately 50% (Table 4). Upon terminating current application, the DEX plasma concentration dropped as expected; however, GST and MCL plasma concentrations continued to increase. This suggested that drug had been retained in the skin and was slowly released post-iontophoresis.

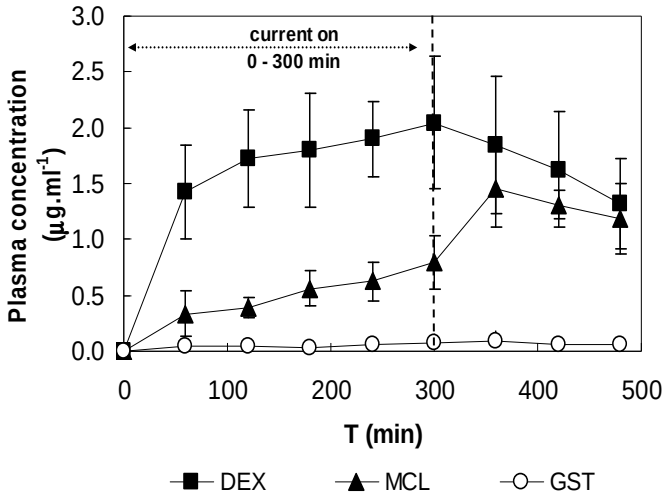

Figure 5. Plasma levels of GST, MCP and DEX obtained after 5 h of iontophoretic administration at 0.5 mA.cm^{-2}. (Mean ± SD; n = 3).

The calculated input rate *in vivo* for GST was slightly lower than the obtained *in vitro* (Tables 3 and 4) however, MCL levels achieved in plasma were ~3-fold less than predicted from the results obtained *in vitro* (Table 3). In contrast, iontophoretic delivery of DEX was more efficient *in vivo* (Table 3) and the calculated flux of 1.96 ± 0.42 µg.cm^{-2}.min^{-1} was ~2-fold higher than that of DEX-P *in vitro* (1.05 ± 0.15 µg.min^{-1}.cm^{-2}).

Table 4. Pharmacokinetic parameters of MCP, GST and DEX after constant current iontophoresis at 0.5 mA.cm^{-2} for 5 h (n = 3).

Parameter	MCL	GST	DEX
	0.5 mA.cm^{-2}	**0.5 mA.cm^{-2}**	**0.5 mA.cm^{-2}**
C_{max} (µg.ml^{-1})	1.49 ± 0.29	0.09 ± 0.03	2.10 ± 0.50
$AUC_{0\text{-}inf}$ (µg.min.ml^{-1})	900.67 ± 438.60	33.11 ± 6.57	1515.19 ± 711.34
Half-life (min)	281.44 ± 162.04	132.69 ± 25.86	363.85 ± 211.36
K_{input} (µg.min^{-1})	4.38 ± 0.22	0.60 ± 0.07	2.61 ± 0.56
K_{10} x10 $^{-2}$ (min^{-1})	0.34 ± 0.19	0.35 ± 0.11	0.50 ± 0.04
Calculated flux (µg.min^{-1}.cm^{-2})	3.29 ± 0.17	0.45 ± 0.05	1.96 ± 0.42

It has been previously reported that *in vitro* flux measurements can underestimate the transport of certain low molecular weight ions *in vivo* [18]. This may be due, for example, to the use of higher NaCl concentrations in the receiver compartment *in vitro* than would be present in the epidermis *in vivo* [18]. However, if this were the only factor, then it would presumably affect GST and MCL equally and this does not appear to be the case. In contrast, Van der Geest *et al*, demonstrated that apomorphine concentrations achieved in plasma were lower than the concentration obtained *in vitro* [19]. It is also probable that the

in vitro / *in vivo* correlation is highly dependent on the experimental conditions and the skin models used for the *in vitro / in vivo studies* [20]. Nevertheless different drug molecules may be affected to different extents by the differences between experimental conditions – most likely the nature of the membrane – and is probably dependent on their intrinsic physicochemical properties. Indeed, several mechanisms may contribute to the total transport and may affect *in vitro* and *in vivo* delivery rates to a different extent. Skin metabolism plays an important role on the percutaneous penetration of several molecules. Differences may take place in the skin residence time of the substrate and enzyme activity. MCL appeared to be degraded (~20%) when in contact with porcine dermis and electrical current *in vitro* [21]. Hydrolysis of MCL in contact with rat skin during iontophoresis *in vivo* might be higher if there is increased enzymatic activity and would therefore to lead to a decrease in transport. The *in vitro* stability studies with DEX-P demonstrated that the prodrug was partially metabolized (~27%) when exposed to porcine dermis after 7 h; when in contact with rat skin (experiment carried out in our laboratory under the same conditions), it was found that ~21% of the drug was degraded. The breakdown of phosphate ester prodrugs in contact with skin *in vitro* normally occurs at a very slow rate ($t_{1/2}$ is in hours) [22]. The slow rate of hydrolysis may be due in part to the prodrug's ionic nature which means it cannot readily diffuse into cells where most metabolizing enzymes are usually present Biotransformation is far more rapid and essentially complete once the prodrug, DEX-P, is exposed to circulating esterases; the reported half-life *in vivo* of various corticosteroids in the bloodstream is less than 10 minutes [23].

The thickness of stratum corneum and epidermis [24] and follicular density [25 have also been reported to play a role in the iontophoretic transport of drugs and these two factors must also be considered when *in vitro* / *in vivo* comparisons are made between different species and body sites [20]. Studies in hairless rats might be more consistent for comparison with porcine or human skin.

GST pharmacokinetics were similar to the values obtained in an earlier study [12] and confirmed that iontophoresis at these conditions would be capable of achieving therapeutic delivery. In order to compare the pharmacokinetics of MCL in rats (0.5 $mA.cm^{-2}$, 110 mM MCL ($-Na^{+}$), area 1.33 cm^2) and humans (~0.1 $mA.cm^{-2}$, 334 mM MCL, area 5 cm^2 [26]), the *in vivo* MCL fluxes from the two studies were current-normalized. Results showed that MCL flux in volunteers was ~2.5-fold higher (16.6 $\mu g.mA^{-1}.min^{-1}$) than that obtained in rats (6.58 ± 0.34 $\mu g.mA^{-1}.min^{-1}$).

The efficiency of cathodal DEX-P iontophoresis, as evidenced by DEX levels in the bloodstream confirms the superiority of cathodal electromigration over anodal electroosmosis for the delivery of steroid prodrugs. The results support an earlier report that more dexamethasone was delivered per mA.min by electromigration than by electroosmosis

– in other words, the same amount of drug could be administered in a shorter time from the negative electrode [27].

CONCLUSIONS

The results confirmed the feasibility of delivering therapeutic amounts of granisetron, metoclopramide and dexamethasone sodium phosphate simultaneously across the skin by non-invasive transdermal iontophoresis. Pharmacokinetic analysis using a one-compartment model estimated the input rate constants for GST, MCL and DEX at 0.5 $mA.cm^{-2}$ as 0.60 ± 0.07, 4.38 ± 0.22 and 2.61 ± 0.56 $\mu g.min^{-1}$, respectively. Drug depot formation in the skin was observed for MCL and GST and was most likely responsible for prolonged absorption observed after terminating current application. The daily dosing requirements to achieve a therapeutic response can be estimated as 1.2 mg q.d. (BA ~60%), 10 mg t.i.d. (BA~75%) and 4-20 mg q.d. for GST, MCL and DEX, respectively [28]. Based on the data presented here, anodal iontophoresis of GST and MCL coupled with cathodal delivery of DEX-P for 12 h would be capable of delivering therapeutic drug levels from a reasonably sized (10 cm^2) patch. The next step will be to investigate the delivery kinetics in larger animal models before determining the pharmacokinetics in human volunteers.

ABBREVIATIONS

a, anode
ACE, acetaminophen
ACN, acetonitrile
AUC_{0_inf}, area under de curve from time 0 to time infinity
c, cathode
C_{max}, maximum plasma concentration
C_p, plasma concentration
DEX, dexamethasone sodium phosphate
DEX-P, dexamethasone
EM, electromigration
EO, electroosmosis
GST, granisetron
HPLC, high performance liquid chromatography
SB, salt bridge
IF, inhibition factor

IV, intravenous administration
J_{EM}, electromigration flux
J_{EO}, electroosmosis flux
J_{tot}, total steady state flux
K_{input}, input rate
k_{10}, elimination rate constant
LOD, limit of detection
LOQ, limit of quantification
MCL, metoclopramide
Na^+, presence of electrolyte
$-Na^+$, absence of electrolyte
S.D., standard deviation
t_{ionto}, time of current application
V_d, volume of distribution
V_w, solvent permeability coefficient

ACKNOWLEDGEMENTS

The authors wish to thank the Swiss Cancer League (Berne, Switzerland) for financial support (OCS 01753-08-2005) and J. Cázares-Delgadillo also acknowledges financial support from CONACYT (Mexico). We are grateful to Roche Diagnostics GmbH (Mannheim, Germany) for the generous gift of granisetron hydrochloride. We would also like to acknowledge Pharsight Corporation (Mountain View, CA) for providing an academic license for the WinNonlin® Professional software. We also thank Dr. S. Rudaz, Dr. J. Schappler and S. Comte of the Laboratory of Analytical Chemistry (School of Pharmacy, University of Geneva) for performing the capillary zone electrophoresis studies.

REFERENCES

[1] P.J. Hesketh, Comparative review of 5-HT3 receptor antagonists in the treatment of acute chemotherapy-induced nausea and vomiting, Cancer. Invest. 18 (2000) 163–173.
[2] J.T. Hickok, J.A. Roscoe, G.R. Morrow, D.K. King, J.N. Atkins, T.R. Fitch, Nausea and emesis remain significant problems of chemotherapy despite prophylaxis with 5-hydroxytryptamine-3 antiemetics: a University of Rochester James P Wilmot Cancer Center

Community Clinical Oncology Program Study of 360 cancer patients treated in the community, Cancer. 97 (2003) 2880–2286.

[3] S.M. Grunberg, R.R. Deuson, P. Mavros, O. Geling, M. Hansen, G. Cruciani, B. Daniele, G. De Pouvourville, E.B. Rubenstein, G. Daugaard, Incidence of chemotherapy-induced nausea and emesis after modern antiemetics, Cancer. 100 (2004) 2261–2268.

[4] IGAR, A double-blind randomized study comparing intramuscular (i.m.) granisetron with i.m. granisetron plus dexamethasone in the prevention of delayed emesis induced by cisplatin, Anticancer Drugs. 5 (1999) 465–470.

[5] C. Gridelli, G.P. Ianniello, G. Ambrosini, G. Mustacchi, T. Pedicini, A. Farris, S. Iacobelli, G. Rossi, G. Moretti *et al.*, A multicentre, double-blind, randomized trial comparing ondansetron versus ondansetron plus dexamethasone in the prophylaxis of cisplatin-induced delayed emesis, Int. J. Oncol. 10 (1997) 395–400.

[6] The Italian Group for Antiemetic Research, Dexamethasone alone or in combination with ondansetron for the prevention of delayed nausea and vomiting induced by chemotherapy, N. Engl. J. Med. 342 (2000) 1554-1159.

[7] M. Saito, K. Aogi, I. Sekine, H. Yoshizawa, Y.O. Yanagita, H. Sakai, K. Inoue, Ch. Kitagawa, T. Ogura, S. Mitsuhashi, Palonosetron plus dexamethasone versus granisetron plus dexamethasone for prevention of nausea and vomiting during chemotherapy: a double-blind, double-dummy, randomised, comparative phase III trial, Lancet. Oncol. 10 (2009) 115–124.

[8] American Society of Clinical Oncology, M.G. Kris , P.J. Hesketh, M.R. Somerfield, P. Feyer, R. Clark-Snow, J.M. Koeller, G.R. Morrow, L.W. Chinnery, M.J. Chesney, R.J. Gralla, S.M. Grunberg, American Society of Clinical Oncology guideline for antiemetics in oncology: update 2006, J. Clin. Oncol. 24 (2006) 2932 – 2947.

[9] Y.N. Kalia, A. Naik, J. Garrison, R.H. Guy, Iontophoretic drug delivery, Adv. Drug. Deliv. Rev. 56 (2004) 619-658.

[10] A.A. Hussain, A. Dakkuri, S. Itoh, Nasal absorption of ondansetron in rats: an alternative route of drug delivery, Cancer Chemother. Pharmacol. 45 (2000) 432-434.

[11] A. Chmielewska, L. Konieczna, A. Plenis, H. Lamparczyk, Sensitive quantification of chosen drugs by reversed-phase chromatography with electrochemical detection at a glassy carbon electrode, J. Chromatrogr. B 839 (2006) 102-111.

[12] A. Chaturvedula, D.P. Joshi, C. Anderson, R. Morris, W.L. Sembrowich, A.K. Banga, Dermal, subdermal, and systemic concentrations of granisetron by iontophoretic delivery. Pharm. Res. 22 (2005) 1313-1319.

[13] V. K. Tam, J. E. Axelson, B. McErlane, R. Ongley, J.D. Price, Dose-Dependent Pharmacokinetics of Metoclopramide in Rat: An Effect of Hemoperfusion?, J. Pharmacol. Exp. Ther. 217 (1981) 764-769.

[14] M.N. Samtani, W.J. Jusko, Comparison of dexamethasone pharmacokinetics in female rats after intravenous and intramuscular administration, Biopharm. Drug. Dispos. 26 (2005) 85 – 91.

[15] J.E. De Muth, Basic Statistics and Pharmaceutical Statistical Applications, Marcel Dekker, New York, 1999.

[16] N. Abla, L. Geiser, M. Mirgaldi, A. Naik, J.-L. Veuthey, R. H. Guy, Y. N. Kalia, Capillary zone electrophoresis for the estimation of transdermal iontophoretic mobility, J. Pharm. Sci. 94 (2005) 2667-2675.

[17] Y. B. Schuetz, P.-A. Carrupt, A. Naik, R. H. Guy, Y. N. Kalia, Structure-permeation relationships for the non-invasive transdermal delivery of cationic peptides by iontophoresis, Eur. J. Pharm. Sci. 29 (2006) 53-59.

[18] B. J. Phipps, R. J. Gyory, Transdermal ion migration, Adv.Drug Deliv. Rev. 9 (1992) 137–176.

[19] R. van der Geest, T. van Laar, J.M. Gubbens-Stibbe, H.E. Boddé, M. Danhof, Iontophoretic delivery of apomorphine II: An *in vivo* study in patients with parkinson's disease, Pharm. Res. 14 (1997) 1804 – 1810.

[20] Jakasa I., Kezic S., Evaluation of *in vivo* animal and *in vitro* models for prediction of dermal absorption in man, Hum. Exp. Toxicol. 27 (2008) 281-288.

[21] J. Cázares-Delgadillo, I. Ben Aziza, A. Ganem-Rondero, D. Quintanar-Guerrero, Y. N. Kalia, Electrotransport kinetics of metoclopramide across porcine skin in vitro, 34th Annual Meeting and Exposition of the Controlled Release Society. Long Beach, 7-11 July, 2007.

[22] H. Derendorf, P. Rohdewald, G. Hochhaus, H. Mollmann, HPLC determination of glucocorticoid alcohols, their phosphates and hydrocortisone in aqueous solutions and biological fluids, J. Pharm. Biomed. Anal. 4 (1986)197–206.

[23] H. Mollmann, S. Balbach, G. Hochhaus, J. Barth, H. Derendorf, Pharmacokinetic–pharmacodynamic correlations of corticosteroids, in: H. Derendorf, G: Hochhaus, (Eds.). Handbook of pharmacokinetic/pharmacodynamic correlation, Boca Raton, FL: CRC Press, 1995, pp 323–361.

[24] N.A. Monteiro-Riviere, D.G. Bristol, T.O. Manning, R.A. Rogers, J.E. Riviere, Interspecies and interregional analysis of the comparative histologic thickness and laser Doppler blood flow measurements at five cutaneous sites in nine species, J. Invest. Dermatol. 95 (1990) 582-586.

[25] R. Panchagnula, K. Stemmer, W.A. Ritchel, Animal models for transdermal drug delivery, Methods Find. Exp. Clin. Pharmacol. 19 (1997) 335–341.

[26] M. Cormier, S. T. Chao, S. K. Gupta, R. Haak, Effect of transdermal iontophoresis co-delivery of hydrocortisone on metoclopramide pharmacokinetics and skin-induced reactions in human subjects, J. Pharm. Sci. 88 (1999) 1030-1035.

[27] T.J. Petelenz, J.A. Buttke, C. Bonds, L.B. Lloyd, J.E. Beck, R.L. Stephen, S.C. Jacobsen, P. Rodriguez, Iontophoresis of dexamethasone: laboratory studies, J. Control. Rel. 20 (1992) 55 - 66.

[28] Sweetman S (Ed), Martindale: The complete drug reference (33rd Edition), Pharmaceutical Press, London, Electronic version, 2003.

Transdermal delivery of cytochrome c – a 12 kDa protein- across intact skin by constant-current iontophoresis

J. Cázares-Delgadillo[1,2], A. Naik[1,2,4], A. Ganem-Rondero[3], D. Quintanar-Guerrero[3], and Y. N. Kalia[1,2,5]

[1]School of Pharmaceutical Sciences, University of Geneva & University of Lausanne, 30 Quai Ernest Ansermet, 1211 Geneva, Switzerland.
[2]Centre Interuniversitaire de Recherche et d'Enseignement, "Pharmapeptides", 74160 Archamps, France.
[3]División de Estudios de Posgrado (Tecnología Farmacéutica), Facultad de Estudios Superiores Cuautitlán, Universidad Nacional Autónoma de México, Av. 1° de Mayo S/N Cuautitlán Izcalli, Estado de México 54704, Mexico.
[4]Present address: Triskel Integrated Services SA, 4 rue des Terreaux-du-Temple, 1201 Geneva, Switzerland.

Pharmaceutical Research, Vol. 24, No. 7 (2007): 1360-1368

ABSTRACT

Purpose: To demonstrate the transdermal iontophoretic delivery of a small (12.4 kDa) protein across intact skin.
Methods: The iontophoretic transport of Cytochrome c (Cyt c) across porcine ear skin *in vitro* was investigated and quantified by HPLC. The effect of protein concentration (0.35 and 0.7 mM), current density (0.15, 0.3 or 0.5 mA.cm^{-2} applied for 8 h) and competing ions was evaluated. Co-iontophoresis of acetaminophen was employed to quantify the respective contributions of electromigration (EM) and electroosmosis (EO).
Results: The data confirmed the transdermal iontophoretic delivery of intact Cyt c. Electromigration was the principal transport mechanism, accounting for ~90 % of delivery; correlation between EM flux and electrophoretic mobility was consistent with earlier results using small molecules. Modest EO inhibition was observed at 0.5 mA.cm^{-2}. Cumulative permeation at 0.3 and 0.5 mA.cm^{-2} was significantly greater than that at 0.15 mA.cm^{-2}; fluxes

using 0.35 and 0.7 mM Cyt c in the absence of competing ions (J_{tot} = 182.8 ± 56.8 and 265.2 ± 149.1 µg.cm^{-2}.h^{-1}, respectively) were statistically equivalent. Formulation in PBS (pH ~ 8.2) confirmed the impact of competing charge carriers; inclusion of ~170 mM Na^+ resulted in a 3.9-fold decrease in total flux.

Conclusions: Significant amounts (~0.9 mg.cm^{-2} over 8 hours) of Cyt c were delivered non-invasively across intact skin by transdermal electrotransport.

Key words

Iontophoresis; protein delivery; skin permeation; electromigration; cytochrome c

INTRODUCTION

The physicochemical properties of peptides and proteins, namely, high molecular weight, charge and hydrophilicity, severely restrict their uptake by the lipid-rich stratum corneum and limit passive diffusion through the intercellular lipid matrix. However, charge and hydrophilicity facilitate peptide electrotransport through the skin via primarily aqueous transport pathways by transdermal iontophoresis (1): a non-invasive technology that uses a mild electric current to increase the mobility of charged molecules across the skin (2, 3).

Although there are reports of the iontophoretic enhancement of different peptide hormones with molecular weights (MW) in the 1-6 kDa range including luteinising hormone releasing hormone (4, 5), calcitonin (6, 7), growth hormone releasing hormone (8), human parathyroid hormone (9) and insulin (10, 11), the effect of molecular size and protein structure on iontophoretic transport has not been well characterized. For a series of fluorescently-labeled poly-L-lysines (FITC-PLLs) ranging in MW from 4 to 26 kDa, iontophoresis enhanced the penetration of the 4 kDa analog but did not have any effect on the transport of the larger 26 kDa FITC-PLL (12).

The transdermal iontophoretic flux of an unidentified cationic protein (“Protein X”) with molecular weight of ~12 kDa at an applied current density of 0.1 mA.cm^{-2} (concentration not given, assayed by radioactive-labelling), was measured to be ~15 µg.cm^{-2}.h^{-1} (13). It was subsequently reported that “Protein X” was in fact Cytochrome c (14). Comparison of the normalized iontophoretic fluxes of a series of negatively charged compounds across hairless mouse skin (HMS) *in vitro* as a function of MW suggested that electrotransport decreased with increasing molecular size (15). It has also been proposed that large, bulky ions will only carry a small fraction of the charge passing across the skin and hence can only be transported by electroosmosis; thus, as cation MW increases, there will be a transition in the dominant iontophoretic transport mechanism from electromigration (EM) to electroosmosis (EO) (16). Our recent work has demonstrated that the ratio of charge to MW, which

determines electric mobility, is a key parameter in governing iontophoretic peptide transport rates (17). A comparison of lysine and H-Lys-Lys-OH transport revealed that the 2-fold increase in molecular weight (149 to 274 Da) was compensated by doubling the charge (J_{tot} = 225 ± 48 and 218 ± 40 nmol. $cm^{-2}.h^{-1}$, respectively); in contrast, H-His-Lys-OH, with approximately the same molecular weight as H-Lys-Lys-OH but unit charge (at pH 7.4), had a significantly lower flux (107 ± 29 $nmol.cm^{-2}.h^{-1}$).

For dipeptides of a given MW, e.g., H-Tyr-D-Arg-OH (MW = 337 Da, +1) and H-Tyr-D-Arg-NH_2 (MW = 336 Da, +2), the increment in charge led to a significant difference in total flux (150 ± 26 and 237 ± 35 $nmol.cm^{-2}.h^{-1}$, respectively). Furthermore, we have also shown that there is a correlation between EM flux across skin and electrophoretic mobility measured by capillary zone electrophoresis (CZE): increasing mobility resulted in increased EM flux for a series of small molecules that did not interact with the skin transport pathway (18). Thus, it seemed appropriate to investigate whether the principle of using molecular charge to facilitate electrotransport by compensating for molecular weight, and hence increasing electric mobility, could be extended to proteins. If this were the case, it would obviously increase the range of molecules that could be considered as candidates for non-invasive iontophoretic administration across the skin.

Horse heart cytochrome c (Cyt c, Figure 1) was chosen as a model protein (19). It has a compact globular structure consisting of a single polypeptide chain, which houses a central, heme group. It has a MW of ~12.4 kDa, an isoelectric point of 10.2, (the protein contains a total of twenty-one amino acids with positively charged side-chains (Arg and Lys), twelve amino acids with negatively charged side-chains (Asp and Glu), and three His residues. The aim of the present work was (i) to evaluate the feasibility of delivering intact Cyt c across the skin by transdermal iontophoresis, (ii) to demonstrate that electromigration and not electroosmosis was the key transport mechanism and (iii) to investigate the effect of experimental variables including protein concentration, applied current density, and the presence of competing charge carriers, on iontophoretic transport rates in order to establish whether these factors, which govern small molecule delivery, affected macromolecular transport in the same way.

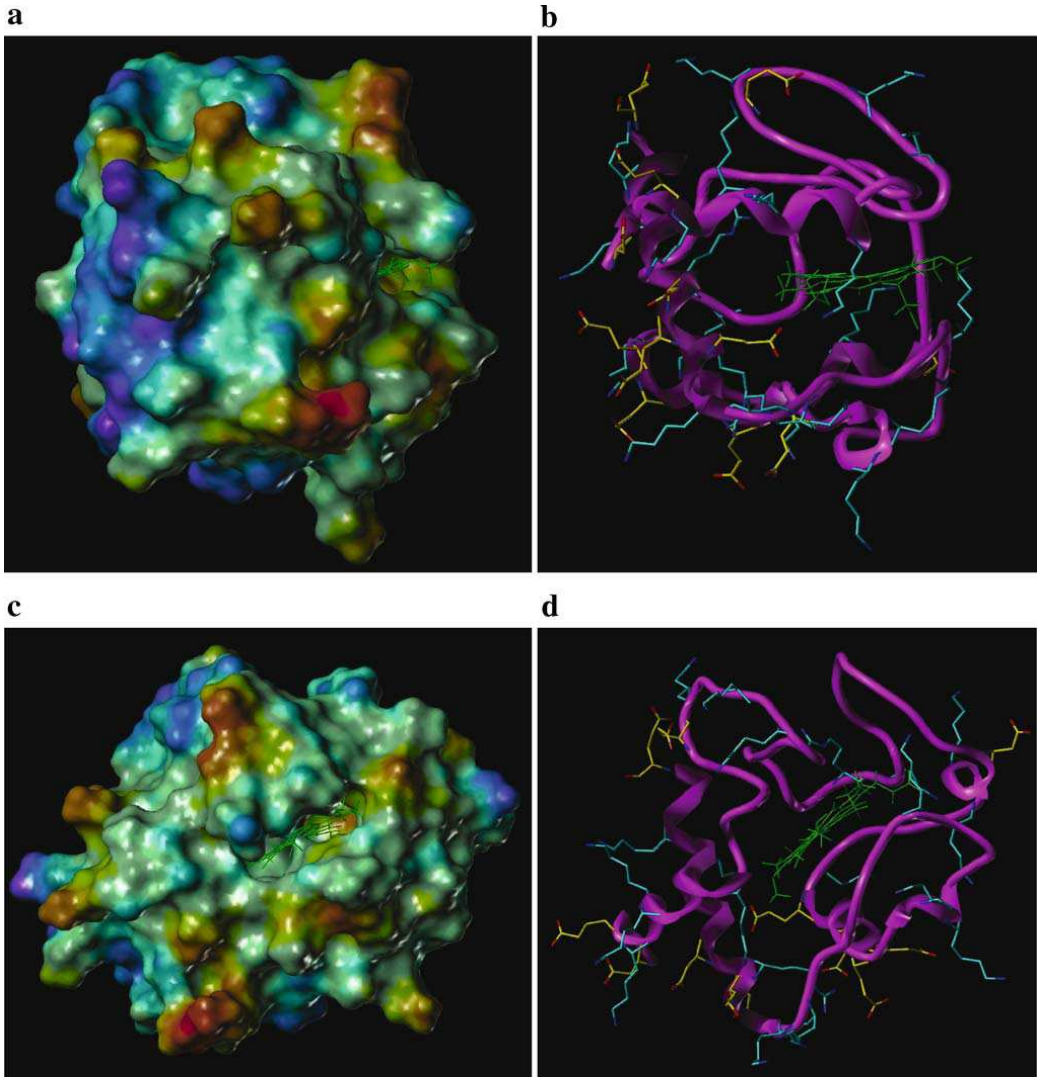

Figure 1. Three-dimensional structure of horse heart Cytochrome c (Cyt c; 12.4 kDa, +9 at pH 8.2); the compact globular structure of the protein is readily discernable (the heme group is shown in green). (1a) and (1c) present different views of the solvent accessible (Connolly) surface showing the electrostatic potential distribution across the molecular surface (red and blue colours represent regions of high positive and negative charge density, respectively). Distinct areas of positive and negative charge density can be clearly seen in (1a); a more homogenous surface charge distribution is shown in (1c). The corresponding views of the protein backbone, tertiary structure and the distribution of positively (Arg and Lys; cyan) and negatively (Asp and Glu; yellow) charged amino acid residues are shown in (1b) and (1d). The charged amino acids are predominantly located on the protein surface; the presence of negative charge density may inhibit electrostatic interactions between Lys or Arg residues and negative charge sites in the transport pathway (see Discussion); thus, reducing the effect of Cyt c passage on skin permselectivity. The 1hrc pdb file (Author Y Luo and G.D. Brayer (19) was downloaded from www.rcsb.org. Molecular modelling and graphics were done using SYBYL® 7.1 (Tripos Inc., 1699 South Hanley Rd., St. Louis, Missouri, 63144, USA).

MATERIALS AND METHODS

Materials

Horse heart Cyt c (MW ~12.4 kDa; charge ~+9 at pH 8.2), acetaminophen (ACE), sodium chloride, di-sodium hydrogen phosphate, potassium dihydrogen phosphate, trifluoroacetic acid (TFA), and citric acid were all purchased from Fluka (Saint Quentin Fallavier, France). Silver wire and silver chloride used for the fabrication of electrodes and acetonitrile (Acetonitrile Chromasolv® HPLC, gradient grade) were purchased from Sigma-Aldrich (St. Quentin Fallavier, France). Silicon tubing (3.2 mm ID, 6 mm OD, 1 mm wall) for collecting samples and PVC tubing (3 mm ID, 5 mm OD, 1 mm wall) used to prepare salt bridge assemblies were obtained from Fisher Bioblock Scientific S.A. (Illkirch, France). All solutions were prepared using deionised water (resistivity > 18 MΩ.cm). All other chemicals were at least of analytical grade.

Protein stability

Solution stability: The stability of Cyt c in solution as a function of temperature was investigated by periodic sampling of solutions (10 and 100 $\mu g.ml^{-1}$ in phosphate buffered saline pH 7.4 (PBS); 16.8 mM Na_2HPO_4 / 1.4 mM KH_2PO_4 / 136.9 mM NaCl) in order to ensure the integrity of the protein in the putative receptor phase for a period of 48 h. Cyt c formulations were stored at 5℃ and 25℃. Samples were assayed after 8, 24 and 48 h and were run twice.

Electrical stability: The impact of electrical current on the stability of Cyt c solutions was evaluated prior to the iontophoretic permeation studies. 5 ml of unbuffered protein solution (8.7 $mg.ml^{-1}$ (0.7 mM), typical concentration for the permeation studies, pH ~8.2) was subjected to a current density of 0.5 $mA.cm^{-2}$ using salt bridges (20). Samples were collected and analysed every hour for a period of 8 h. Experiments were performed in triplicate.

Stability in the presence of skin: The influence of porcine ear skin on Cyt c stability in solution was assessed by preparing *(a)* 1 $mg.ml^{-1}$ Cyt c in 10 mM NaCl (pH ~ 8.2) and *(b)* 100 $\mu g.ml^{-1}$ Cyt c in PBS at pH 7.4. Dermatomed epidermal and dermal skin surfaces were placed in contact with solutions *(a)* and (*b)*, respectively during 8 h. Samples were evaluated separately and experiments were performed in triplicate.

Iontophoretic permeation

Protocol: Porcine ears were obtained from a local abattoir (STAC, Chambery, France). The skin was excised (thickness 750 µm) with an electro-dermatome (Zimmer, Etupes, France), wrapped in Parafilm ^{PM} and stored at −20 °C for a maximum period of 2 months. Dermatomed skin was clamped in three-compartment vertical flow-through diffusion cells (area 0.85 cm^2). The anode (containing PBS buffer at pH 7.4) was isolated from the donor solution via a salt bridge (SB) assembly (3% agarose in 0.1 M NaCl) to minimize the effect of competing ions (20). After a 40 minute equilibration period with PBS, 1 ml of unbuffered peptide solution containing Cyt c (0.7 mM, pH ~ 8.2) and ACE (15 mM) was placed in the donor compartment. ACE was used to report on the electroosmotic solvent flow (20). The cathodal and receptor compartments were filled with 1 and 6 ml of PBS (pH 7.4), respectively. A syringe pump (model SP220IZ, WPI, Sarasota, FL) generated a continuous flow of buffer solution (1 $ml.h^{-1}$) through the receiver compartment, and samples were collected hourly from the second hour onwards. Constant current densities of 0.15, 0.3 and 0.5 $mA.cm^{-2}$ were applied for 8 h via Ag/AgCl electrodes connected to a power supply (Kepco® APH 1000M, Flushing, NY).

Effect of concentration: This was investigated in a separate study, where the donor compartment contained a solution comprising 0.35 mM Cyt c and 15 mM ACE. All other aspects of the protocol were the same as those outlined above.

Effect of competing ions: Cyt c solution (0.7 mM) was prepared using PBS buffer at ~pH 8.2 in order to investigate the effect of competing cations. These formulations contained ~170 mM Na^+; transport experiments were conducted at a current density of 0.5 $mA.cm^{-2}$.
The permeation experiments were performed in at least quadruplicate.

HPLC analysis

A P680A LPG-4 pump equipped with an ASI-100 auto sampler and a UV-Vis detector (UVD 170/340-U) (Dionex, Voisins LeBretonneux, France) was used to quantify Cyt c. Isocratic separation was performed using a 150 mm × 4.6 mm base stable (from pH 2.0-10) column packed with 5 µm C4 silica reversed-phase particles (Phenomenex, Le Pecq, France). The flow-rate and the injection volume were 1.0 $ml.min^{-1}$ and 10-100 µl, respectively; the column temperature was kept at 30 °C using a thermostat (TCC-100, Dionex GmbH, Germany). The mobile phase consisted of 66.0% of the aqueous component (0.1% TFA (v/v) in water pH 2.0 and 34.0% of the organic phase (0.1% TFA (v/v) in a 90:10 mixture of MeCN:water) (adapted from (21)). The column was equilibrated for at least 1 h. All solvents were filtered (0.45 µm pore size nylon membrane filter) and degassed prior to use. The UV absorbance

at 400 nm was used to detect the protein. The limit of quantification (LOQ) and detection (LOD) were 190.0 ng and 62.7 ng, respectively. ACE was assayed separately using a Lichrospher® 100 RP-8 5 µm reversed-phase column (125 mm x 4 mm; Lichrocart) with pre-filter. The mobile phase comprised 88% citrate buffer 40 mM (pH=3.0) and 12% MeCN. Fresh buffer solution was prepared daily. The flow rate and the injection volume were 1.0 $ml.min^{-1}$ and 10-100 µl, respectively. All the samples were diluted (1:20) prior to the analysis. ACE was detected by its UV absorbance at 243 nm. The LOQ and LOD were 8.9 ng and 2.9 ng, respectively.

The amount of Cyt c retained in the skin samples during the iontophoretic permeation experiments at 0.3 and 0.5 $mA.cm^{-2}$ was estimated by skin extraction using the HPLC mobile phase as the extraction medium. We used 5 and 10 ml of mobile phase comprising 66.0% of the aqueous phase (0.1% TFA (v/v) in water pH 2.0) and 34.0% of the organic phase (0.1% TFA (v/v) in a 90:10 mixture of MeCN: water 90:10) for the samples from the experiments at 0.3 and 0.5 $mA.cm^{-2}$, respectively. The skin samples were cut and immersed in the solvent for 4 h under constant stirring at ambient temperature. The samples were analysed using HPLC and the experiments were performed in at least triplicate.

Theory

Estimation of EM and EO contributions

The total iontophoretic flux ($J_{tot,\ Cyt\ c}$) of Cyt c, assuming negligible passive diffusion, is the sum of the fluxes dues to electromigration ($J_{EM,\ Cyt\ c}$) and electroosmosis ($J_{EO,\ Cyt\ c}$) and is given by Equation 1 (22):

$$J_{tot,Cytc} = J_{EM,Cytc} + J_{EO,Cytc} = \left(\frac{i_d}{F} \bullet \frac{u_{Cytc}}{\sum_{1}^{i} z_i u_i c_i} + V_W \right) c_{Cytc} \qquad (1)$$

$J_{EM,Cyt\ c}$ is related to the current density (i_d), by Faraday's constant (F) and is proportional to $u_{Cyt\ c}$ and $c_{Cyt\ c}$, the mobility and concentration, respectively of the protein in the membrane; z_i, u_i, and c_i refer to the corresponding values for the other charge carriers in the system.

The EO contribution, $J_{EO,\ Cyt\ c}$, is proportional to the volume flow induced by the applied potential gradient and is the product of the solvent permeability coefficient (V_W) and the protein concentration, $c_{Cyt\ c}$; the former can be estimated from Equation 2 (20):

$$V_W = \frac{J_{ACE}}{c_{ACE}} \qquad (2)$$

where J_{ACE} is the ACE flux and c_{ACE} is its concentration in the donor compartment.

Inhibition factor

For each experiment, an inhibition factor (IF) was calculated using the following equation:

$$IF = \frac{V_{W,control}}{V_{W,Cytc}} \quad (3)$$

where $V_{w,control}$ is the solvent permeability coefficient calculated during 8 h of iontophoresis in the absence of protein, and $V_{w,Cyt\ c}$ is the corresponding value when Cyt c was simultaneously iontophoresed.

Statistical analysis

Data were expressed as mean ± S.D. Outliers, determined using the *Grubbs test* (23), were discarded. The results were evaluated statistically using analysis of variance (ANOVA); *Student's t-test* was used to compare two data sets. The level of significance was fixed at $P < 0.05$.

RESULTS

Cytochrome c stability

HPLC analysis confirmed that Cyt c response (retention time, peak width, and symmetry) was unaffected by current application (0.5 $mA.cm^{-2}$) for 8 h. Furthermore, Cyt c was also stable in the presence of both epidermal and dermal skin samples (*Student's t-test, $P < 0.05$*). Similarly, the solution stability experiments carried out at different temperatures also showed that the protein was unchanged; statistical tests did not show any significant difference between the samples stored for 48 h at 5℃ and 25℃. These results suggested that Cyt c would be stable under the conditions to be used for the permeation experiments.

Iontophoretic delivery

In the first series of Cyt c transport experiments, the impact of increasing current density from 0.15 to 0.5 $mA.cm^{-2}$ was tested using a protein concentration of 0.7 mM. The cumulative amount permeated and the iontophoretic flux at 0.15, 0.3 and 0.5 $mA.cm^{-2}$ are shown in Figure 2. The measured steady-state fluxes were 90.91 ± 45.07, 157.77 ± 140.13, and 265.15 ± 149.05 $\mu g.cm^{-2}.h^{-1}$, respectively. A two-fold increase in applied current resulted in an approximately proportional flux enhancement; however, Cyt c flux at 0.3 and 0.5 $mA.cm^{-2}$ was not significantly different (*Student t test, $p < 0.05$*). From Equation 1, it is

clear that the flux due to electromigration, J_{EM}, should increase with the applied current and this is the case for several small molecules and some peptides, both *in vitro* and *in vivo* (24-27). It has been suggested that at high current densities, the iontophoretic response saturates and once a limiting transport number is achieved, further increase in current has no effect (28).

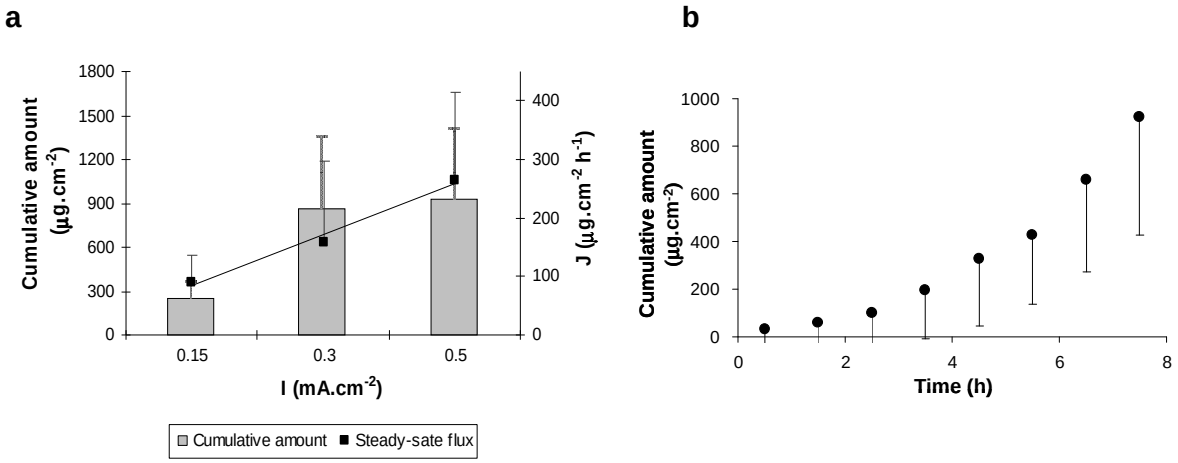

Figure 2. (a) Cumulative amounts permeated and steady-state fluxes (J_{tot}) of Cyt c across porcine skin during 8 h of transdermal iontophoresis at 0.15, 0.3 and 0.5 mA.cm^{-2}. (Mean±SD) (n ≥ 5) and (b) Cumulative Cyt c permeation as a function of time during 8 h iontophoresis at 0.5 mA.cm^{-2}. (Mean±SD) (n = 12).

Similarly, the cumulative permeation of Cyt c at 0.3 and 0.5 mA.cm^{-2} was greater than that at 0.15 mA.cm^{-2}. Figure 3 shows the amounts of Cyt c extracted from the skin after completion of the permeation experiments. Although greater amounts of protein were recovered from the skin samples used in the experiments at 0.3 mA.cm^{-2} (2060.82 ± 367.53 µg.cm^{-2}) than at 0.5 mA.cm^{-2} (951.55 ± 201.08 µg.cm^{-2}); the sum of the amounts extracted and permeated at the two current densities was not statistically different.

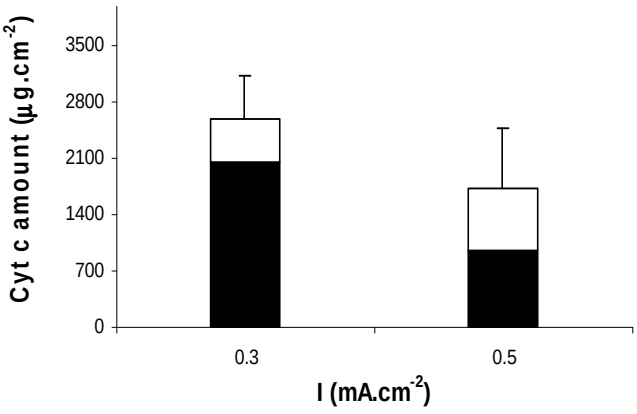

Figure 3. Effect of current density on the cumulative amount of Cyt c permeated across porcine skin (❑) and retained within the membrane (■). (Mean±SD) (n ≥ 3)

Co-iontophoresis of ACE enabled the estimation of the contributions of EM, EO and the calculation of an electroosmotic inhibition factor (IF) (Table 1). Control values for ACE flux in the absence of Cyt c were determined independently with applied current densities of 0.15, 0.3 or 0.5 mA.cm^{-2}. Calculation of the EO contribution and subtraction from the total flux showed that EM was the dominant mechanism, accounting for ~90 % of total Cyt c delivery. A two-fold increase (0.15 to 0.3 mA.cm^{-2}) in current produced an approximately proportional increase in the EM and EO contributions.

Table 1. Iontophoretic transport kinetics of horse heart Cytochrome c and the relative contributions of electromigration and electroosmosis. (n ≥ 4)

I (mA cm^{-2})	J_{tot} (µg cm^{-2} h^{-1})	J_{EM} (µg cm^{-2} h^{-1})	J_{EO} (µg cm^{-2} h^{-1})	$10^4 V_{W, Cyt\ c}$ (cm h^{-1})	$10^4 V_{W,\ control}$ (cm h^{-1})	IF
0.15	90.91 ± 45.07	82.00	8.91	8.61 ± 4.91	16.61 ± 7.45	1.93 ± 1.40
0.30	157.77 ± 140.13	137.93	19.84	20.94 ± 7.92	21.40 ± 2.73	1.02 ± 0.47
0.50	265.15 ± 149.05	248.71	16.44	18.41 ± 10.81	90.72 ± 29.34	4.93 ± 3.08

I: Current density; J_{EM}: Electromigration contribution; J_{EO}: Electroosmotic contribution; J_{tot}: Total steady-state flux; $V_{W,Cyt\ c}$: solvent permeability coefficient in the presence of Cyt c; $V_{W,\ control}$: solvent permeability coefficient; *IF*: Inhibition factor (calculated according to Equation 3).

Inhibition of ACE transport, caused by reduction of convective solvent flow was only noticeable at the highest current density (0.5 mA.cm^{-2}), with an IF ~5; however, this did not have a significant impact on Cyt c transport since EM was by far the dominant transport mechanism (Figure 4). Moreover, although significant amounts of Cyt c were extracted from the skin following iontophoresis at 0.3 mA.cm^{-2}, there was no concomitant effect on ACE transport and hence convective solvent flow (as evidenced by IF ~1, Table 1).

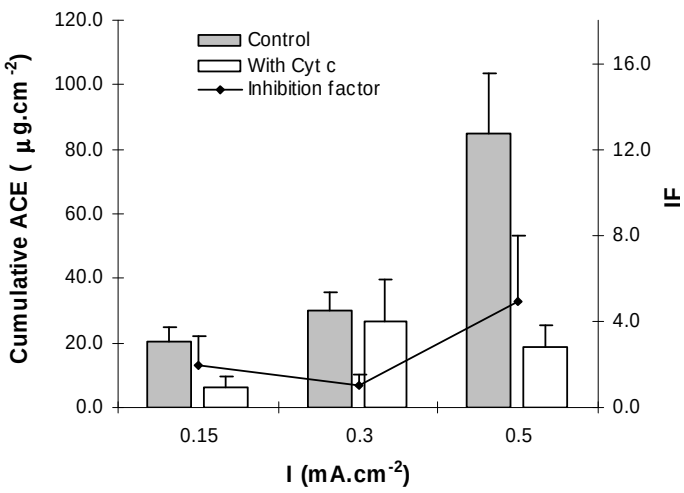

Figure 4. Cumulative amount of acetaminophen (ACE) delivered across the skin after 8 h of transdermal iontophoresis at 0.15, 0.3 and 0.5 mA.cm^{-2} in the presence and in the absence of Cyt c. The inhibition factor (IF) is calculated according to Equation 3. (Mean±SD) (n ≥ 4)

Thus, Cyt c accumulation in the membrane at 0.3 mA.cm^{-2} was not in itself a sufficient condition for significant EO inhibition; this may point to Cyt c aggregation or to the presence of intermolecular interactions that do not involve the fixed negative charges responsible for skin permselectivity.

The effect of concentration on the iontophoretic transport of Cyt c was examined in the second series of experiments. Figure 5 shows that increasing the donor concentration from 0.35 to 0.7 mM Cyt c, in the absence of competing ions, affected neither the cumulative permeation (594.0 ± 257.4 and 923.0 ± 496.1 µg.cm^{-2}, respectively; *t*-test, $p < 0.05$) nor the flux (J_{tot} = 182.8 ± 56.8 and 265.2 ± 149.1 µg.cm^{-2}.h^{-1}, respectively; *t*-test, $p < 0.05$).

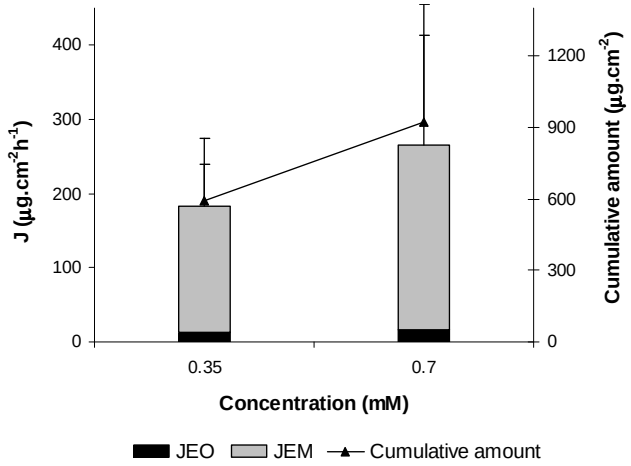

Figure 5. Iontophoretic transport of Cyt c at constant current (0.5 mA.cm^{-2}) was independent of donor concentration (0.35 and 0.7 mM Cyt c) in the absence of competing ions. (Mean±SD) (n ≥ 6)

Similarly, ACE transport was not affected by the two-fold difference in donor concentration and the solvent permeability coefficient, V_W, was effectively unchanged ((27.9 ± 19.0) and (18.4 ± 10.8) 10^{-4}cm.h^{-1} respectively) at the two concentrations. At the lower concentration, EM was again the dominant transport mechanism governing the iontophoretic transfer of Cyt c, accounting for >90% of total flux; thus, there was no change in the relative contributions of EM and EO to overall electrotransport. (*Student's t-test, P < 0.05*). Under the experimental conditions used, Cyt c was the sole cation in the anodal formulation; the majority of the charge transfer was due to Cl^- ions moving from the receiver compartment towards the anode. The electrodiffusion model developed by Kasting and Keister (28) suggests that, in the absence of competing cations, iontophoretic flux is independent of concentration and dependent only on the ratio of diffusivities (or mobilities) of the cation and the main counterion (usually Cl^-) arriving from beneath the skin. The addition of buffer or an increase in the ionic strength of the formulation by the addition of background electrolyte increases competition between charge carriers and generally decreases iontophoretic drug flux (29-31). The effect of Na^+ on the iontophoretic transport of Cyt c (0.7 mM) was confirmed by formulating the protein in PBS (pH ~ 8.2). The estimated flux and the transport efficiency as a function of experimental conditions are shown in Figure 6. The presence of ~170 mM Na^+

resulted in a 3.9-fold decrease in J_{tot} (67.5 ± 15.7 µg.cm^{-2}.h^{-1}) which was entirely due to a decrease in the EM contribution to Cyt c electrotransport. Calculation of the Cyt c transport number for the two experimental conditions showed that inclusion of Na^+ (at >200-fold excess as compared to the protein) caused Cyt c transport efficiency to decrease from 0.048% to 0.010%. Although the presence of competing ions resulted in a significant decrease in Cyt c delivery, it did not impact on EO flow.

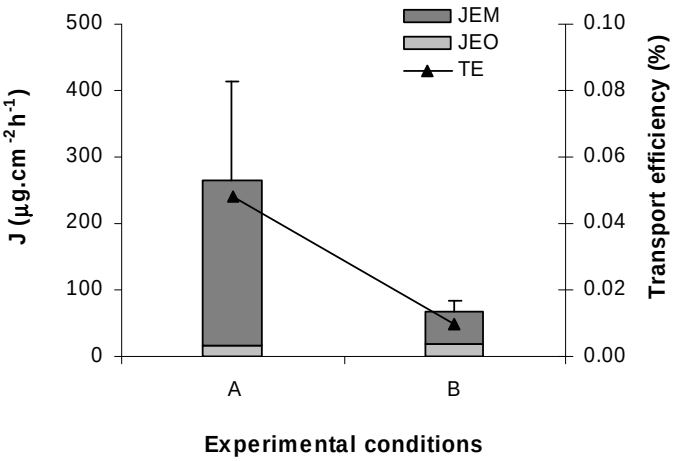

Figure 6. The impact of ion competition on Cyt c electrotransport at 0.5 mA.cm^{-2}. Formulation in PBS containing ~170 mM Na^+ caused a significant decrease in flux. Electromigration contribution (EM); Electroosmosis contribution (EO); Transport efficiency (TE). Experimental setup: A = with salt bridge; B = without salt bridge. (Mean±SD) (n≥5)

DISCUSSION

Electric mobility governs Cyt c electrotransport

The relative contributions of EM and EO (Table 1) to Cyt c electrotransport across the skin show that EM accounted for ~90% of total delivery despite the molecular weight of the protein; providing clear evidence that EO does not *per se* govern peptide or protein iontophoretic transport rates (27).

The dominant transport mechanism will depend on the physicochemical properties of the macromolecule, in particular, its electric mobility. Figure 7 shows the normalized steady state electromigratory flux (J_{EM}^{norm}) of lidocaine, propranolol, quinine and a series of lysine- and tyrosine-containing dipeptides as a function of electrophoretic mobility (adapted from (18)). Inclusion of the corresponding normalized flux for Cyt c using the same current density and similar conditions (0.5 mA.cm^{-2}, 0.7 mM, PBS pH 8.2) and assuming a mobility of 4 x 10^{-5} cm^2.V^{-1}.s^{-1} (32) shows that despite its much greater MW, Cyt c electromigration displays the same correlation with its electrophoretic mobility ($J_{EM}^{norm} = 92.76u_i + 0.0031$, r^2 = 0.97). The normalized EM flux of Cyt c (0.7 mM buffered in PBS, 0.5 mA.cm^{-2}) shows the same dependence on its electric mobility (average value of 4 x 10^{-5} cm^2.V^{-1}.s^{-1} (32)) (filled circle); for example, its mobility is approximately four-fold less than that of YdR-NH_2 and it shows a corresponding four-fold lower normalized flux.

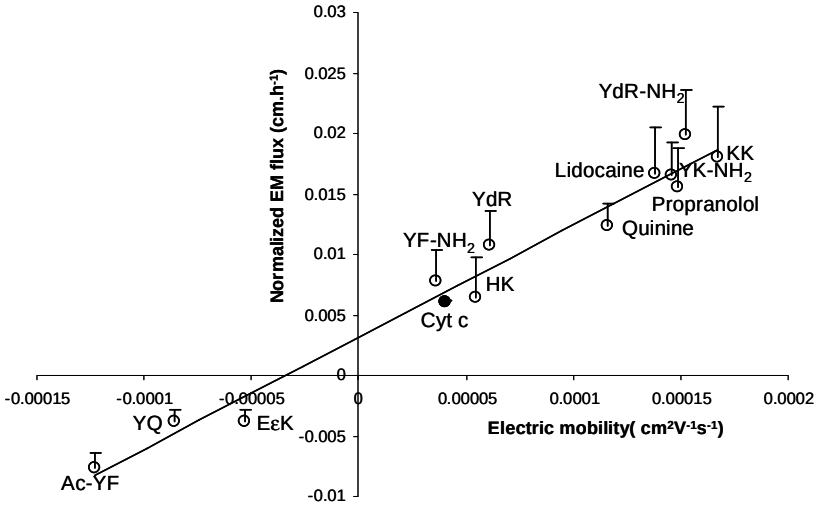

Figure 7. Correlation between normalized EM flux (J_{EM}^{norm}, cm.h^{-1}) and electrophoretic mobility (u_i, cm^2.V^{-1}.s^{-1}) for a series of small molecules and dipeptides (hollow circles) (10 mM, 0.5 mA.cm^{-2}, adapted from (18)).

As for the smaller molecules and dipeptides, under these iontophoretic conditions, Cyt c does not interact with the transport pathway in the skin; hence, its electrophoretic mobility as measured by CZE is a good predictor of the flux due to electromigration. ($J_{EM}^{norm} = 92.76u_i + 0.0031$, r^2=0.97). High molecular weight peptides and small proteins with multiple exposed charged amino acid side chains or available hydrophobic surfaces may interact strongly with structures in the transport pathway, either through electrostatic or van der Waals' type interactions. If these associations are accompanied by neutralization of the fixed negative charges in the skin, this will result in reduced convective flow. These interactions with the biological transport pathway will also reduce the reliability of electrophoretic mobility as a predictor for peptide or protein electrotransport. Increasing current density causes more protein to be transported into the skin and increases the likelihood of interaction: for Cyt c, inhibition of skin permselectivity was only significant at a current density of 0.5 mA.cm^{-2}. However, since EM was by far the dominant transport mechanism it had negligible impact on total flux.

Feasibility of delivering small proteins by transdermal iontophoresis

Comparison of our results with those of "Protein X" (13) is difficult, given the lack of experimental details; however, assuming similar protein concentrations in the respective formulations (and the presence of competing ions), then the current-normalized fluxes are similar (~150 µg.mA.h^{-1} for "Protein X" and ~135 µg.mA.h^{-1} for Cyt c in the present study - 0.7 mM, 0.5 mA.cm^{-2}, PBS pH 8.2). Laser scanning confocal microscopy studies using FITC-

labelled poly-L-lysines with molecular weights of 4, 7 and 26 kDa showed that although iontophoresis (0.5 $mA.cm^{-2}$ at 0.05 mM polypeptide) enhanced delivery of the 4 kDa derivative it had little or no effect on the transport of the larger species; after 8 h iontophoresis at 0.5 $mA.cm^{-2}$, cumulative permeation of the 4 and 7 kDa poly-L-lysines was 3.84 ± 1.48 and 0.44 ± 0.12 µg, respectively (12).

Iontophoresis of 2.7, 8.2 and 20 kDa poly-L-lysines (0.5 $mA.cm^{-2}$ and 3.7, 1.2 and 0.5 mM, respectively) decreased skin permselectivity as measured by mannitol flux (by up to 30-fold in the case of the 20 kDa derivative (33)): the pronounced EO inhibition suggesting the presence of the polypeptide in the transport pathway. These poly-L-lysine results are very different to those observed with Cyt c both in terms of cumulative protein delivery (784.52 ± 421.64 µg after 8 h at 0.5 $mA.cm^{-2}$) and the effect on convective solvent flow (only a ~5-fold decrease in ACE transport under the same conditions).

Furthermore, for comparison, PL_{83}, a poly-L-lysine containing 83 Lys residues, with a molecular weight of ~12.5 kDa, is reported to have an electrical mobility of 16 x 10^{-5} $cm^2.V^{-1}.s^{-1}$ (34), which is four times greater than that of Cyt c; therefore, why does the latter show superior iontophoretic transport kinetics? The poly-L-lysine experiments were conducted using hairless mouse skin (HMS) whereas the iontophoretic transport of Cyt c was investigated across porcine ear skin. The nature of the membrane can have a significant impact on iontophoretic drug transport rates. For example, although the variation of the current-normalized convective solvent flow across both HMS and porcine ear skin (PES) as a function of propranolol concentration, as reported by mannitol flux, is similar (Figure 8a), propranolol transport kinetics are completely different (Figure 8b) (3, 35, 36).

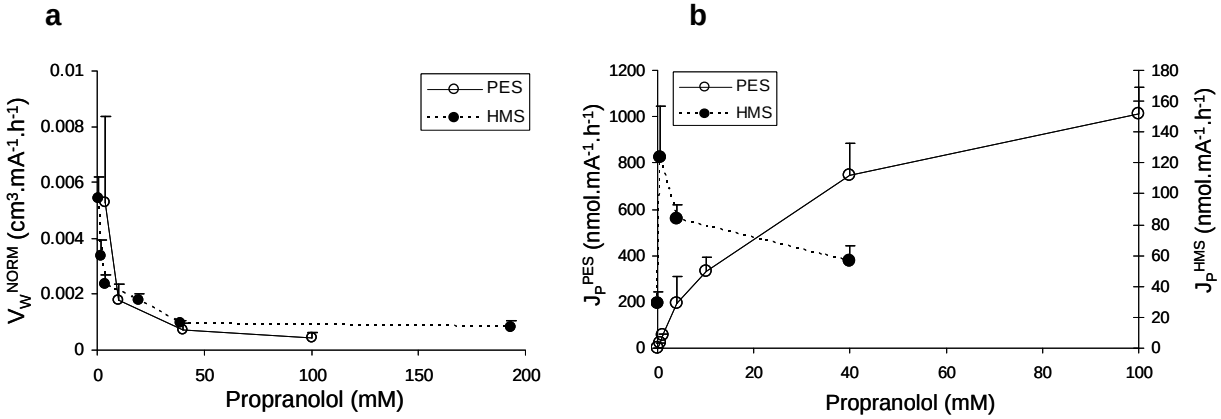

Figure 8. (a) Variation of the current-normalized convective solvent flow across porcine ear skin (PES) and hairless mouse skin (HMS) in the presence of propranolol as a function of drug concentration in the formulation. A similar exponential decrease is observed with both membranes. (b) Variation of the current-normalized propranolol flux across PES and HMS as a function of drug concentration is strikingly different. Although a "plateau" is observed with PES as the concentration increases, the flux across HMS passes through a sharp maximum at a low concentration (0.4 mM).

Thus, although increasing propranolol concentration in the formulation has a similar effect on skin permselectivity in both membranes, the presence of drug-drug or drug-pathway interactions causes current-normalized propranolol flux across HMS to decrease sharply after reaching a maximum at 0.4 mM. By analogy, poly-L-lysines may have a greater propensity to bind to structures along the transport route or to self-aggregate during iontophoresis across HMS than is the case for Cyt c in PES. Thus, the nature of the biological barrier can have a significant on molecular electrotransport. Data from (35) and (36). Cyt c and the poly-L-lysines also have very different structures and solution conformations. Under physiological conditions, poly-L-lysine has a dynamic random coil structure in solution; in contrast, Cyt c possesses a compact globular structure (2.5 x 2.5 x 3.7 nm, (37)) with a well-defined three-dimensional conformation containing three major and two minor helices separated by strands with more random structure, folded around a heme group (19) (Figure 1). A 20 kDa poly-L-lysine contains ~130 lysine residues in a polypeptide chain with a random coil structure. The Lys side-chains will be extensively exposed to the solution so that the side chain ε-NH_2 group can interact with anions or form hydrogen-bonds with surrounding water molecules – these groups will also be predisposed to interacting with accessible sites of negative charge density present in the iontophoretic transport pathway. Although Cyt c is rich in Arg and Lys residues (~21 residues), that are also found at the protein surface, solvent-accessible and whose side-chains show considerable flexibility (Figure 1b and 1d), the more rigid three-dimensional structure of the protein backbone restricts the number of possible side-chain-membrane interactions. Furthermore, the presence of surface negative charges (due to Asp and Glu) may also hinder interaction with negative sites within the membrane (Figure 1a and 1c). Thus, Cyt c would have a lower propensity to interact with the membrane and its electrotransport less likely to modulate skin permselectivity.

With respect to the feasibility of delivering small proteins through the proposed transport pathways in the skin, analysis of the results from streaming potential measurements using excised human cadaver abdominal skin, using a capillary pore model, suggested the presence of nanopores with a Gaussian size distribution and a mean radius on the order of ~20 nm (38). The pore diameter would be sufficient to enable passage of a small globular protein such as Cyt c. More recently, scanning electrochemical microscopy (SECM) studies into the electroosmotic transport of acetaminophen across full-thickness human cadaver skin demonstrated that electroosmotic phenomena occurred in pores, tentatively identified as skin appendageal structures, much larger than nanopores (39). Conversion of the SECM tip current to a concentration followed by fitting to an appropriate mathematical model, enabled estimation of the pore radius (~35 μm); obviously, protein transport through these appendageal structures would be entirely feasible.

In contrast, earlier studies with HMS suggested non-appendageal pore radii of 2.7, 1.35 and 0.675 nm for negative, neutral and positive pores, respectively (40). Similarly, a hydrodynamic model developed using rat skin suggested that the pore diameter was ~3.6 nm (41). For these two animal models, the passage of Cyt c through these narrower, non-appendageal channels would probably be hindered – these observations may also partly explain the poly-L-lysine transport results (12, 35).

CONCLUSIONS

These results demonstrate the feasibility of delivering significant amounts of Cyt c, a small, highly charged protein, non-invasively across intact skin (~0.9 $mg.cm^{-2}$ over an 8 hour period). They also show that Cyt c electrotransport was governed by EM (~90%) and not EO. Furthermore, neither Cyt c permeation nor its accumulation in the skin caused EO inhibition at current densities lower than 0.5 $mA.cm^{-2}$ (indeed, its occurrence at this current density had negligible effect on transport kinetics). Thus, a macromolecule with molecular weight exceeding 12 kDa, possessing a suitable charge:MW ratio (and hence, electric mobility) *and* the appropriate three-dimensional structure can be delivered non-invasively by transdermal iontophoresis. Globular proteins with a compact tertiary structure may be better candidates than highly charged polypeptides with extended random coil structures since the latter may be more prone to interaction with the transport pathway (they may also be more susceptible to enzymatic hydrolysis). Future studies will build upon the findings with this model protein and apply the same principles to the non-invasive delivery of therapeutic proteins across the skin.

ACKNOWLEDGEMENTS

We would like to thank Prof. Leonardo Scapozza and Dr. Shaheen Ahmed for help with the molecular graphics representations of Cytochrome c. J. Cázares Delgadillo acknowledges financial support from CONACYT (Mexico).

ABBREVIATIONS

EM, electromigration
EO, electroosmosis
Cyt c, cytochrome c
ACE, acetaminophen
CZE, capillary zone electrophoresis

$J_{tot, Cyt\ c}$ total steady-state flux of Cyt c

$J_{EM, Cyt\ c}$ flux due to electromigration of Cyt c

$J_{EO, Cyt\ c}$ flux due to electroosmosis of Cyt c

V_w, convective solvent flow

REFERENCES

1. Y. B. Schuetz, P-A. Carrupt, A. Naik, R. H. Guy, and Y. N. Kalia. Structure-permeation relationships for the non-invasive transdermal delivery of cationic peptides by iontophoresis**.** Eur J Pharm Sci. 29:53-59 (2006).
2. R. R. Burnette. Iontophoresis. In J. Hadgraft and R. Guy (eds.), Transdermal Drug Delivery. Marcel Dekker, Inc., New York, 1989, pp. 247-288.
3. Y. N. Kalia, A. Naik, J. Garrison, and R. H. Guy. Iontophoretic drug delivery. Adv Drug Deliv Rev. 56:619-658 (2004).
4. M.C. Heit, P.L. Williams, F.L. Jayes, S.K. Chang, and J. E. Riviere. Transdermal iontophoretic peptide delivery: in vitro and in vivo studies with luteinizing hormone releasing hormone. J Pharm Sci. 82:240-243 (1993).
5. J. Raiman, M. Koljonen, K. Huikko, R. Kostiainen, and J. Hirvonen. Delivery and stability of LHRH and Nafarelin in human skin: the effect of constant/pulsed iontophoresis. Eur J Pharm Sci. 21:371-377 (2004).
6. P. Santi, N. M. Volpato, R. Bettini, P. L. Catellani, G. Massimo, and P. Colombo. Transdermal iontophoresis of salmon calcitonin can reproduce the hypocalcemic effect of intravenous administration. Farmaco 52:445-448 (1997).
7. A. Chaturvedula, D. P. Joshi, C. Anderson, R. L. Morris, W. L. Sembrowich, and A. K. Banga. In vivo iontophoretic delivery and pharmacokinetics of salmon calcitonin. Int J Pharm. 297:190-196 (2005).
8. S. Kumar, H. Char, S. Patel, D. Piemontese, A. W. Malick, K. Iqbal, E. Neugroschel, and Ch. R. Behl. Effect of iontophoresis on in vitro skin permeation of an analog of growth hormone releasing factor in the hairless guinea pig model. J Pharm Sci. 81:635-639 (1992).
9. Y. Suzuki, K. Iga, Sh. Yanai, Y. Matsumoto, M. Kawase, T. Fukuda, H. Adachi, N. Higo, and Y. Ogawa. Iontophoretic pulsatile transdermal delivery of human parathyroid hormone (1-34). J Pharm Pharmacol. 53:1227-1234 (2001).
10. L. Langkjaer, J. Brange, G. M Grodsky, and R. H Guy. Iontophoresis of monomeric insulin analogs in vitro: effects of insulin charge and skin pretreatment. J Control Release. 51:47-56 (1998).

11. O. Pillai and R. Panchagnula. Transdermal iontophoresis of insulin: V. Effect of terpenes. J Control Release. 88:287– 296 (2003).
12. N. G. Turner, L. Ferry, M. Price, C. Cullander, R. H. Guy. Iontophoresis of Poly-L-lysines: The role of molecular weight? Pharm Res. 14:1322-1331 (1997).
13. R. Haak and S. K. Gupta. Pulsatile drug delivery from electrotransport therapeutic systems. In R. Gurny, H. E. Junginger and N. A. Peppas (eds.), Pulsatile Drug Delivery – Current Applications and Future Trends, Wiss. Verl.-Ges., Stuttgart, 1993, pp. 99-112.
14. P. Green. Iontophoretic delivery of peptide drugs. J Control Release. 41:33-48 (1996).
15. M. B. Delgado-Charro and R. H. Guy. Iontophoresis of peptides. In: Bret Berner and S M. Dinh (eds.), Electronically controlled drug delivery, CRS Press, New York, 1998, Vol. 1, pp. 129-157.
16. R. H. Guy, Y. N. Kalia, M. B. Delgado-Charro, V. Merino, A. López, and D. Marro Iontophoresis: electrorepulsion and electroosmosis. J Control Release. 64:129-132 (2000).
17. N. Abla, A. Naik, R. H. Guy, and Y. N. Kalia. Effect of charge and molecular weight on transdermal peptide delivery by iontophoresis. Pharm Res. 22:2069-2078 (2005).
18. N. Abla, L.Geiser, M. Mirgaldi, A. Naik, J-L. Veuthey, R. H. Guy, and Y. N. Kalia Capillary zone electrophoresis for the estimation of transdermal iontophoretic mobility. J Pharm Sci. 94:2667-2675 (2005).
19. G. W. Bushnell, G. V. Louie, and G, D. Brayer High-resolution three-dimensional structure of horse heart cytochrome c. J Mol Biol. 214:585-595 (1990).
20. Y. B. Schuetz, A. Naik, R. H. Guy, E. Vuaridel, and Y. N. Kalia. Transdermal iontophoretic delivery of vapreotide acetate across porcine skin in vitro. Pharm Res. 22: 1305-1312 (2005).
21. M. J. Picklo, J. Zhang, V. Q. Nguyen, D. G. Graham, and T. J. Montine. High pressure liquid chromatography quantitation of Cytochrome c using 393 nm detection. Anal Biochem. 276: 166-170 (1999).
22. N. Abla, A. Naik, R. H. Guy, and Y. N. Kalia. Contributions of electromigration and electroosmosis to peptide iontophoresis across intact and impaired skin skin. J Control Release. 108:319-330 (2005).
23. J. E. De Muth. Basic Statistics and Pharmaceutical Statistical Applications. Marcel Dekker, New York, 1999.
24. D. T. W. Lau, J. W. Sharkey, L. Petryk, F. A. Mancuso, Z. Yu, and F. L. S. Tse. Effect of current magnitude and drug concentration on iontophoretic delivery of octreotide acetate (Sandostatin®) in the rabbit. Pharm Res. 11:1742-1746 (1994).

25. S. K. Gupta, M. Southam, G. Sathyan, and M. Klausner. Effect of current density on pharmacokinetics following continuous or intermittent input from a fentanyl electrotransport system. J Pharm Sci. 87:976–981 (1998).
26. P. Singh**,** S. Boniello, P. Liu, and S. Dinh. Transdermal iontophoretic delivery of methylphenidate HCl in vitro**.** Int J Pharm. 178:121-128 (1999).
27. Y. B. Schuetz, A. Naik, R. H. Guy, E. Vuaridel, and Y. N. Kalia. Transdermal iontophoretic delivery of triptorelin in vitro. J Pharm Sci. 94:2175-2182 (2005).
28. G. B. Kasting and J. C. Keister. Application of electrodiffusion theory for a homogeneous membrane to iontophoretic transport through skin. J Control Release. 8:195-210 (1989).
29. W. H. M. Craane-van Hinsberg, L. Bax, N. H. M. Flinterman, J. Verhoef, H. E. Junginger, and H. E. Bodde. Iontophoresis of a model peptide across human skin in vitro: effects of iontophoresis protocol, pH and ionic strength on peptide flux and skin impedance. Pharm Res. 11:1296 – 1300 (1994).
30. M. F. Lu, D. Lee, R. Carlson, G. S. Rao, H. W. Hui, L., Adjei, M. Herrin, D. Sundberg, and L. Hsu. The effects of formulation variables on iontophoretic transdermal delivery of leuprolide to humans. Drug Deliv Ind Pharm. 19:1557-1571 (1993).
31. Y. B. Schuetz, A. Naik , R. H. Guy, and Y. N. Kalia. Effect of amino acid sequence on transdermal iontophoretic peptide delivery. Eur J Pharm Sci. 26:429-437 (2005).
32. G. H. Barlow and E. Margoliash. Electrophoretic behaviour of mammalian-type cytochromes c. J Biol Chem. 241:1473-1477 (1966).
33. J. Hirvonen and R. H. Guy. Transdermal iontophoresis: modulation of electroosmosis by polypeptide. J Control Release. 50:283-289 (1998).
34. R. V. Rice, M. A. Stahmann, and R. A. Alberty. The interaction of lysine polypeptides and bovine plasma albumin. J Biol Chem. 209:105-15 (1954).
35. J. Hirvonen and R. H. Guy. Iontophoretic delivery across the skin: electroosmosis and its modulation by drug substances. Pharm Res. 14:1258-1263 (1997).
36. D. Marro, Y. N. Kalia, M. B. Delgado-Charro, and R. H. Guy. Contributions of electromigration and electroosmosis to iontophoretic drug delivery. Pharm Res. 18:1701-1708 (2001).
37. I. Ichinose, Y. Hashimoto, and T. Kunitake. Wrapping of bio-macromolecule (dextran, amylopectin and horse heart Cytochrome c) with ultrathin silicate layer. Chemistry Letters 33:656-657 (2004).
38. V. Aguilella, K. Kontturi, L. Murtomäki, and P. Ramirez. Estimation of the pore size and charge density in human cadaver skin. J Control Release. 32:249-257 (1994).

39. O. D. Uitto and H. S. White. Electroosmotic pore transport in human skin. Pharm Res. 20:646-652 (2003).
40. M. J. Pikal. Transport mechanisms in iontophoresis: I. A theoretical model for the effect of electroosmotic flow on flux enhancement in transdermal iontophoresis. Pharm Res. 7: 118-126 (1990).
41. S. B. Ruddy and B. W. Hadzija. Iontophoretic permeability of polyethylene glycols through hairless rat skin: application of hydrodynamic theory for hindered transport through liquid-filled pores. Drug Design Discovery 8:207-224 (1992).

Human growth hormone: new delivery systems and alternative routes of administration and their pharmacological relevance

J. Cázares-Delgadillo[1], A. Ganem-Rondero[2], Y. N. Kalia[1]

[1] School of Pharmaceutical Sciences, University of Geneva & University of Lausanne, 30 Quai Ernest Ansermet, 1211 Geneva, Switzerland.
[2] División de Estudios de Posgrado (Tecnología Farmacéutica), Facultad de Estudios Superiores Cuautitlán, Universidad Nacional Autónoma de México, Av. 1° de Mayo S/N Cuautitlán Izcalli, Estado de México 54704, Mexico.

Submitted to European Journal of Pharmaceutics and Biopharmaceutics

CONTENTS **Page**

ABSTRACT

The availability of recombinant human growth hormone (GH) has broadened its clinical applications. Approved indications for GH therapy include treatment of growth hormone deficiency (in children and in adults), Turner Syndrome, Prader-Willi Syndrome, chronic renal insufficiency and more recently, idiopathic short stature in children, AIDS-related wasting and fat accumulation associated with lipodystrophy in adults. Therapy with GH usually begins at a low dose and is gradually titrated to obtain optimal efficacy while minimizing side-effects. It is usually administered on a daily basis by subcutaneous injection; since this was considered to impact upon patient compliance, extended-release GH preparations were developed and new delivery platforms – e.g., autoinjectors and needle-free devices – were introduced in order to improve not only compliance and convenience but also dosing accuracy. In addition, alternative less invasive modes of administration such as the nasal, pulmonary and transdermal routes have been also been investigated. Here we provide an overview of the different technologies and routes of GH administration and discuss the principles, limitations and pharmacological profiles for each approach.

Key words: human growth hormone, therapeutics, delivery

1. GROWTH HORMONE: STRUCTURE, SECRETION AND FUNCTIONS

Human growth hormone (GH; somatotropin) is a single chain polypeptide comprising 191 amino acids; the tertiary structure contains four helices and two disulfide bridges (Figure 1).

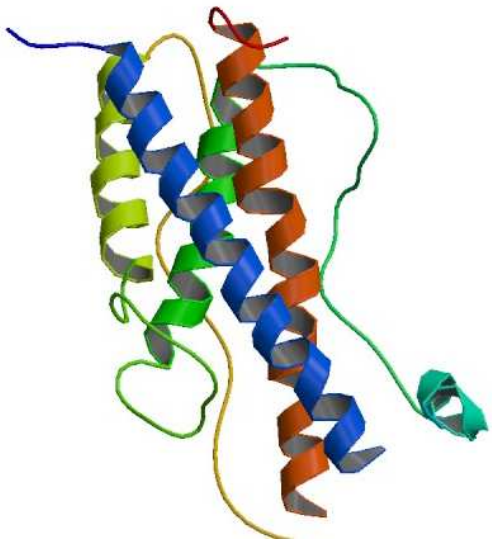

Figure 1. Three-dimensional structure of GH

It is synthesized, stored, and secreted by the somatotroph cells within the lateral section of the anterior pituitary, which typically contains 3 to 5 mg GH and secretes between 0.5 to 0.875 mg of protein per day. Although circulating levels of GH are low (GH has an average plasma half-life of 20 to 30 minutes), pulsatile release of GH – usually in 4 to 8 discrete bursts – occurs throughout the day and at night with a mean peak amplitude of ~4-6 µg/l [1]. GH release is sexually dimorphic with women having more daytime GH pulses than men but a relatively modest nocturnal surge (Figure 2) [2, 3]. Basal GH levels and the frequency and amplitude of GH secretion are low in infancy, increase during childhood and reach a peak during puberty (~10 µg/l) [4, 5]; secretion then gradually decreases and a progressive decline is observed after the third decade.

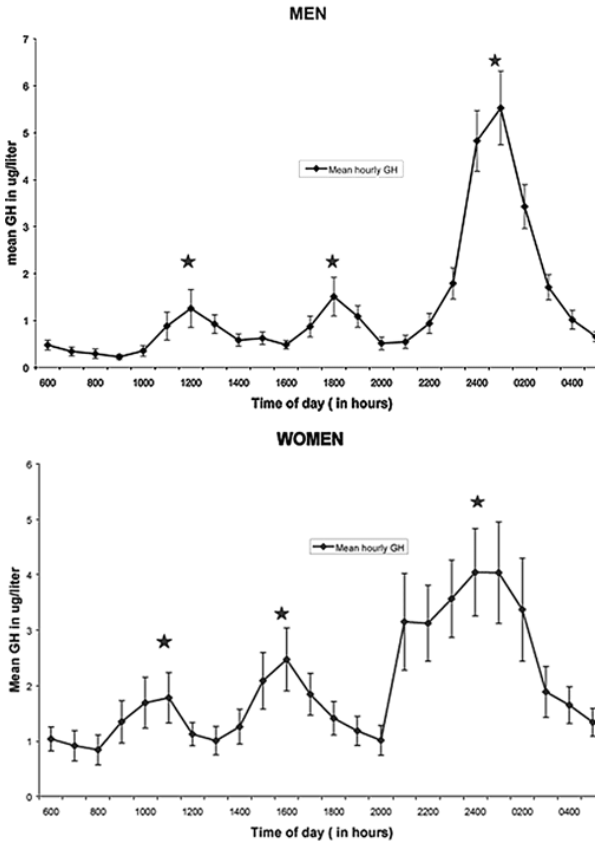

Figure 2. Circardian pattern of growth hormone. The 24 h plasma profiles were determined in 93 healthy, young (18–45 years old), non-obese (BMI < 26 kg/m^2) and regularly-fed men (*n*=67) and women (*n*=26). Data are shown as mean ± standard error (Mean ± S.E).

Reproduced by permission from Surya *et al.*, Complex rhythmicity of growth hormone secretion in humans, *Pituitary.* 9 (2006), pp.121–125. Copyright Springer Netherlands (2006).

The secretion profile is modulated through a complex neuroendocrine control system comprising two main hypothalamic regulators, GH-releasing hormone (GHRH; 44 amino acid peptide) and somatostatin (SS; cyclic tetradecapeptide), exerting stimulatory and inhibitory influences, respectively, on the somatotroph cell (Figure 3). Although the interplay between these peptides is the main determinant of GH release, other physiological stimulators and inhibitors can affect GH secretion. For example ghrelin, which is synthesized principally in the epithelial cells lining the fundus of the stomach, with smaller amounts produced in the placenta, kidney, pituitary and hypothalamus, can stimulate GH secretion by downregulating

somatostatin release [6]. Other physiological stimulators include sleep, hypoglycemia, exercise, dietary protein, short-term fasting and arginine [7]. GH secretion can be inhibited by hyperglycemia, chronic glucocorticoid use, estradiol, and circulating concentrations of insulin-like growth factor-1 (IGF-1) through negative feedback on the hypothalamus.

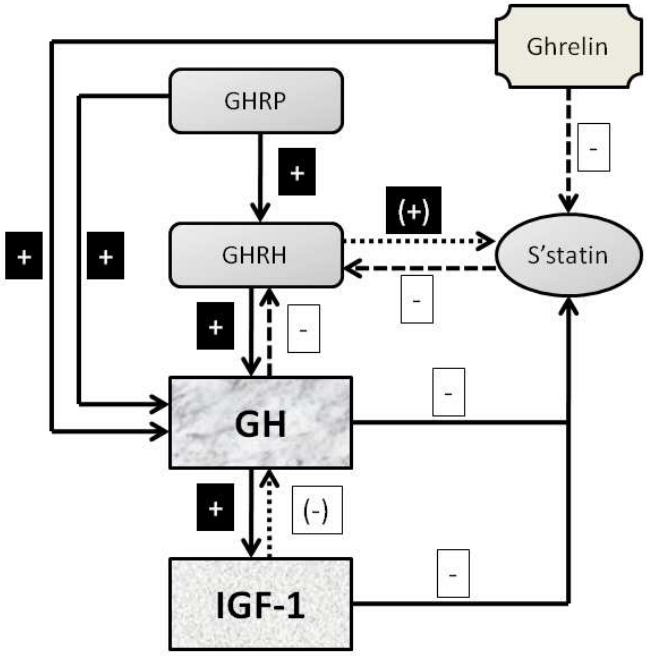

Figure 3. Physiology of GH secretion.

The effects of GH on growth and metabolism may be direct or mediated through other hormones. The most important of these is insulin-like growth factor-1 (IGF-1) – GH acts on the liver to increase synthesis and secretion of IGF-1, which in turn stimulates division and multiplication of chondrocytes and osteoblasts, which are the primary cells in the epiphyses of long bones. GH also increases amino acid uptake and protein synthesis in muscle and other tissues [8].

2. THERAPEUTIC USES AND INDICATIONS OF HUMAN GROWTH HORMONE

GH, extracted from human pituitary glands was first used to treat children suffering from growth hormone deficiency (GHD) in the 1950's. Pituitary-derived GH continued to be used until 1985 when Creutzfeldt-Jacob disease was diagnosed in four patients receiving GH treatment.

.

The availability of recombinant human GH (somatropin; from *E. coli* in 1985 and from murine cells in 1987) meant that biosynthetic GH quickly replaced pituitary-derived GH for therapeutic use. Although the initial indication was limited to the treatment of children with GHD, investigations into other therapeutic applications quickly followed (Table 1). GH deficiency may occur as an isolated hormonal deficiency or in combination with multiple pituitary hormone deficiency as a result of hypopituitarism, tumours in the central nervous system, cranial irradiation or other organic causes. Idiopathic growth hormone deficiency is the most common form, accounting for approximately 50–70% of cases. Growth failure is a prominent feature in children with chronic renal insufficiency and Turner syndrome; the causes being multifactorial, including reduced sensitivity to GH, rather than decreased GH levels [9]. Therefore, supraphysiological doses of GH are required for treatment in children with these conditions. In contrast, children with Prader-Willi syndrome are considered to have a hypothalamic disorder and thus GH therapy is intended to restore physiological levels of GH [10]. The FDA approved GH therapy for GHD in adults in 1996.

Treatment with GH may be considered at three distinct dose levels [11]. Replacement therapy for GH failure in both children and adults typically consists of 0.01–0.025 mg/kg/day. Supraphysiological dosages of GH are used to treat growth deficit not due to growth hormone deficiency, such as Turner's syndrome, chronic renal insufficiency, and idiopathic short stature; GH doses for these indications are regularly around 0.05 mg/kg/day. A third pharmacological dose level is used for metabolic indications such as short-bowel syndrome or AIDS-associated cachexia; for these indications, doses range from 0.1 to 0.2 mg/kg/day. The optimal dosing schedule remains open to question; for example, it has been shown that the efficacy of a thrice weekly injection regimen, was comparable to that observed in patients treated with daily GH therapy [12]. Nocturnal administration provides more physiological GH profiles than morning injections [13].

Side effects of GH therapy are rare, but may include headache, visual problems, nausea and vomiting, fluid retention (peripheral oedema), arthralgia, myalgia, paraesthesia, antibody formation, hypothyroidism and reactions at the injection site.

Table 1. Conditions that involve treatment with human growth hormone

Pathology	Description
GH failure in childhood	Disorder caused principally by mutations of specific genes e.g. GHRHR, GH1.
GH deficiency in adulthood	The most common cause is a pituitary adenoma or treatment of the adenoma with pituitary surgery or radiotherapy.

Turner syndrome	Chromosomal disorder caused by a partially or completely missing X chromosome. It is a condition that only affects females. It is characterized by: -short neck -low hairline at the back of the neck -low-set ears -hands and feet that are swollen or puffy at birth -soft nails that turn upward Most individuals with Turner syndrome lose ovarian function in early childhood and do not start puberty at a normal age. Some have problems with specific visual-spatial coordination tasks (such as mentally rotating objects in space) and may have trouble learning mathematics (geometry and arithmetic).
Chronic renal insufficiency	Slowly worsening loss of the ability of the kidneys to remove wastes, concentrate urine, and conserve electrolytes. Principal causes: - Diabetes and high blood pressure - Alport syndrome - Analgesic nephropathy - Glomerulonephritis of any type (one of the most common causes) - Kidney stones and infection - Obstructive uropathy - Polycystic kidney disease - Reflux nephropathy
Prader-Willi syndrome	Genetic disorder in which seven genes (or some subset thereof) on chromosome 15 are missing or unexpressed (chromosome 15q partial deletion) on the paternal chromosome. This condition is characterized in infancy by weak muscle tone (hypotonia), feeding difficulties, poor growth, and delayed development. In childhood affect individuals develop an insatiable appetite and chronic overeating (hyperphagia). People with this syndrome typically have intellectual impairment or learning disabilities and behavioral problems.
Short-bowel syndrome	Malabsorption disorder caused by the surgical removal of the small intestine, or more rarely due to the complete dysfunction of a large segment of bowel. It can be classified as acquired and congenital, the last is less common. Caused by surgery for: -Crohn's disease, an inflammatory disorder of the digestive tract -Volvulus, a spontaneous twisting of the small intestine that cuts off the blood supply and leads to tissue death -Tumors of the small intestine -Injury or trauma to the small intestine -Necrotizing enterocolitis (premature newborn) -Bypass surgery to treat obesity, a now commonly performed surgical procedure -Surgery to remove diseases or damaged portion
AIDS-associated weight loss or cachexia	Involuntary loss of weight, muscle atrophy, fatigue, weakness and significant loss of appetite.
Idiopathic short stature	Extreme short stature - unclear etiology.

3. CONVENTIONAL ADMINISTRATION OF HUMAN GROWTH HORMONE VIA INJECTION

GH is routinely administered by daily intramuscular (i.m.) or subcutaneous (s.c.) injection (Table 2) [14].

Table 2. Indications and usage of somatropin

Trade name		Indications and usage	Administration	Dosage
Accretropin™	Cangene Corporation	Growth failure in children	s.c.	0.18 to 0.3 mg/kg/wk divided into 6 or 7 injections
		Turner syndrome		0.36 mg/kg/wk divided into 6 or 7 injections
Genotropin®, Genotropin preservative free®	Pharmacia and Upjohn, Pfizer	Growth failure in children	s.c.	0.24 mg/kg/wk divided into 6 or 7 injections
		Replacement of endogenous GH in adults		start with up to 0.04 mg/kg/wk given as a daily injection, increasing the dose at 4- to 8-wk intervals according to patient requirements (max, 0.08 mg/kg/wk)
		Turner syndrome		0.33 mg/kg/wk divided into 6 or 7 injections
		Prader-Willi syndrome		0.24 mg/kg/wk divided into 6 or 7 injections
		Idiopathic growth stature		up to 0.47 mg/kg/wk divided into 6 or 7 injections
Humatrope®	Eli Lilly and Co	Growth failure in children	s.c., i.m.	0.18 mg/kg/wk (divided into equal doses given on 3 alternate days, 6 times/wk, or daily) to a max of 0.3 mg/kg
		Turner syndrome	s.c.	up to 0.375 mg/kg/wk divided into equal doses given either daily or on 3 alternate days.
		Replacement of endogenous GH in adults		start with up to 0.006 mg/kg/day, increasing the dose according to patient requirements (max, 0.0125 mg/kg/day
		Idiopathic short stature		0.37 mg/kg divided into equal doses given 6 to 7 times/wk
Norditropin®, Norditropin Nordiflex®	Novo Nordisk INC	Growth failure in children	s.c.	0.024 to 0.034 mg/kg 6 to 7 times/wk
		Replacement of endogenous GH in adults		start with up to 0.004 mg/kg daily. The dose may be increased to a max of 0.016 mg/kg daily after approximately 6 wk according to patient requirements
		Turner syndrome		up to 0.067 mg/kg daily
		Growth failure in children		up to 0.3 mg/kg weekly divided into daily injections; pubertal patients may receive up to 0.7 mg/kg weekly in

Nutropin®, Nutropin AQ®	Genentech INC		s.c.	divided daily doses
		Replacement of endogenous GH in adults		start with up to 0.006 mg/kg/day, increasing the dose according to patient requirements to a max of 0.025 mg/kg/day in patients younger than 35 yr of age and max of 0.0125 mg/kg daily in patients older than 35 yr of age
		Chronic renal insufficiency		up to 0.35 mg/kg weekly (divided into daily injections) continued up to time of renal transplantation
		Turner syndrome		up to 0.375 mg/kg/wk divided into equal doses 3 to 7 times/wk.
		Idiopathic growth stature		start with up to 0.3 mg/kg weekly divided into daily doses
Omnitrope®	Sandoz	Growth failure in children	s.c.	0.16 to 0.24 mg/kg weekly, divided into 6 or 7 daily doses
		Replacement of endogenous GH in adults		start with no more than 0.04 mg/kg weekly given as a daily injection, increasing the dose at 4- to 8-wk intervals according to individual patient requirements (max, 0.08 mg/kg/wk)
Serostim®, Serostim LQ®	Merck Serono INC	AIDS-associated weight loss or cachexia	s.c., i.m.	- more than 55 kg, 6 mg daily - 45 to 55 kg, 5 mg daily - 35 to 45 kg, 4 mg daily; less than 35 kg, 0.1 mg/kg
Saizen®	Merck Serono INC	Growth failure in children	s.c., i.m.	0.06 mg/kg 3 times/wk
		Replacement of endogenous GH in adults	s.c.	start with up to 0.005 mg/kg daily. Increase the dose to no more than 0.01 mg/kg daily after 4 wk according to individual patient requirements
Tev-tropin™	TEVA-Pharmaceuticals	Growth failure in children	s.c.	up to 0.1 mg/kg 3 times weekly
Valtropin®	Biopartners	Growth failure in children	s.c.	0.23 mg/kg of body weight/week (0.033 mg/kg/day)
		Replacement of endogenous GH in adults		0.33 mg/day (equivalent to 0.005 mg/kg/day in a 66 kg adult) (6 days/week)
		Turner syndrome		0.37 mg/kg of body weight/week (0.053 mg/kg/day)
				0.1 mg/kg daily (max, 8 mg/day), rotating the injection sites. Administration for more

Zorbtive®	Serono /Novartis	Short bowel syndrome	s.c.	than 4 wk has not been adequately studied. Treat moderate fluid retention and arthralgia symptomatically, or reduce the dose by 50%. Discontinue treatment for up to 5 days for severe toxicities. Upon resolution of symptoms, resume treatment at 50% of the original dose. Permanently discontinue treatment if severe toxicity persists or does not disappear in 5 days

s.c.- subcutaneous ; i.m.-intramuscular

The pharmacokinetic/pharmacodynamic (PK/PD) parameters of approved formulations are expected to be similar; PK parameters including the median (range) maximum concentration (C_{max}), the area under the curve (*AUC*), the median (range) terminal half-life ($t_{½}$) and clearance (*CL/F*) as well as bioavailability (*BA*) after administration of different short-acting formulations to healthy adults are shown in Table 3.

Table 3. Pharmacokinetic parameters of short-acting GH formulations following administration to healthy adults.

Formulation	**Sex/dose /route of administration**	***AUC* (µg/h/l)**	**Maximal concentration (C_{max}; µg/l)**	**Terminal half-life ($t_{1/2}$; h)**	***CL/F* (ml/h/kg)**	***BA* (%)**
Nutropin®	Males 0.1 mg/kg s.c.	643 (C.V. 12.0)	67.2 (C.V. 29.0)	2.1 (C.V. 20.0)	158 (C.V. 12.0)	
Nutropin AQ®	Males 0.1 mg/kg s.c.	677 (C.V. 13.0)	71 (C.V. 17.0)	2.3 (C.V. 18.0)	150 (C.V. 13.0)	81
Humatrope®	Males and females 0.1 mg/kg s.c.	495 (S.D. 11.0)	53.2 (S.D. 25.9)	4.9 (S.D. 2.7)	215 (S.D. 47.0)	75
	Males and females 0.1 mg/kg i.m.	585 (S.D. 90.0)	63.3 (S.D. 18.2)	3.8 (S.D. 1.4)	175 (S.D. 28.8)	63
Accretropin®	Males and females 4 mg s.c.	255.3 (S.D. 43.0)	29.4 (S.D. 8.3)	3.6 (S.D. 1.3)		70
Genotropin®	Males and females 0.03 mg/kg s.c.		23.0 (S.D. 9.4)	3.0		80

C.V.- Coefficient of variation (%); S.D.- Standard deviation

Data.com data sources include Micromedex™ [Updated 8 April 2009], Cerner Multum™ [Updated 21 April 2009], Wolters Kluwer™ [Updated 17 April 2009], and others. Copyright Drugs.com (2000-2009). Rxlist.com data sources include. Copyright by RxList Inc (2009).

Comparison of the pharmacokinetics following i.m. and s.c. administration of GH (Humatrope®; 0.1 mg/kg in men and women) suggested that although C_{max} and *AUC* were higher following i.m. injection, the half-life and bioavailability were greater after s.c. administration [15]. Serum GH levels achieved after s.c. injection of Nutropin AQ® at the same dose (0.1 mg/kg) in male volunteers appeared to show a higher peak and shorter half-life than those obtained with Humatrope®**;** perhaps pointing to the effect of formulation. In addition to the differences between absorption following i.m. and s.c. administration, studies have also tried to relate GH pharmacokinetics/pharmacodynamics to age, gender and body composition [16].

Following administration of an i.v. bolus (200 µg), younger subjects showed higher peak GH levels and *AUC* – the volume of distribution and clearance were higher in the older group [16].

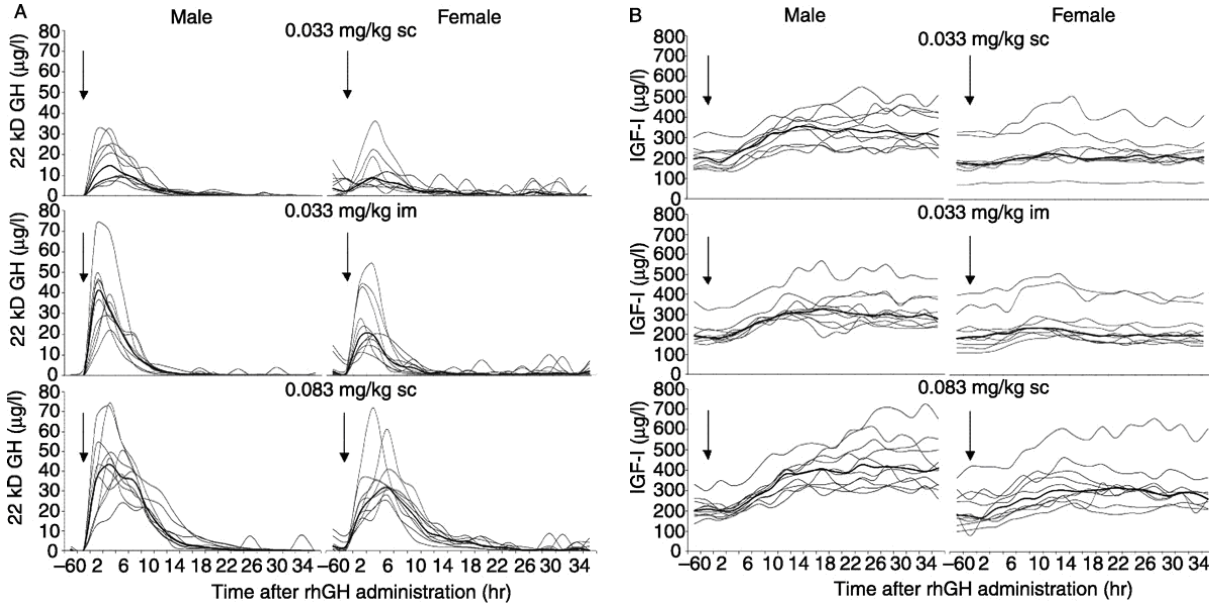

Figure 4. Plasma GH concentration and IGF-1 generation following 0.033 or 0.083 mg/kg s.c. or 0.033 mg/kg i.m. administration of hGH to healthy adult males and females. Individual responses=light lines; median response=black line.

Reproduced by permission from Keller *et al.*, Pharmacokinetics and pharmacodynamics of GH: dependence on route and dosage of administration. *Eur. J. Endocrinol.* 156 (2007), pp. 647-653. Copyright Society of Endocrinology (2007).

A more recent report compared pharmacokinetics / pharmacodynamics following i.m. and s.c. administration in a group of young healthy adults performing regular physical training (Figure 4). The bioavailability of GH was again principally influenced by the route of

administration with higher C_{max} and *AUC* of GH after i.m. injection while PD parameters were mainly determined by gender [17].

Replacement GH therapy is well accepted by endocrinologists and patients; however, the need for daily injections still limits its use and this has driven the development of long-acting formulations that provide a sustained release of GH – even though endogenous GH is released in discrete pulses. The formulations tested in experimental animals or in humans include GH microspheres, GH macrolide microparticles, crystalline GH, hyaluronate-conjugated GH and pegylated GH [18-23].

Studies in children using micronized zinc-stabilized GH encapsulated in poly (D,L-lactic-co-glycolic acid) biodegradable microspheres (Nutropin® depot) showed that after administration of either 0.75 mg/kg twice a month or 1.5 mg/kg once a month, GH levels were significantly increased as compared to controls [24]. The compound was clearly effective, but the principal disadvantage was that its use frequently resulted in the formation of subcutaneous nodules (60% of injections) [24]. The depot formulation was also studied in adults using a single dose of either 0.25 mg/kg or 0.5mg/kg [25]; the results showed a substantial increase in GH concentration reaching a peak 24 h after injection. The efficacy and adverse effects were evaluated in a separate multi-dose study in which the formulation was administered every 14 days and was compared with daily somatropin injection (Nutropin AQ®) in GH-deficient subjects [26]. The results confirmed that the long-lasting GH preparation could provide effective hormone replacement therapy, maintaining normal adult serum IGF-1 levels without evidence of increased side effects. Recent preclinical studies using a GH-containing PLGA microsphere formulation (DA-3003) demonstrated that GH concentration was sustained for 14 and 28 days in rats and monkeys, respectively after a single administration of the new formulation [27]. The plasma concentration of IGF-1 was also increased and remained elevated for approximately 28 days in monkeys.

Although encapsulation with biodegradable polymers is very attractive, the manufacturing processes are still complicated and expensive [20]. The withdrawal of Nutropin® depot from the market was due in part to the cost of manufacturing. Moreover, since the encapsulation approaches are principally based on diffusion control and polymer degradation for slower drug release, particle sizes tend to be large (~50 µm) and as a result larger gauge needles were required for GH administration – a problem in terms of patient compliance. For example, Nutropin® depot required delivery through a specially designed 21-gauge needle. In terms of patient compliance and for market approval, administration of the drug through finer needles (29-31 gauge) is much preferred.

Another approach for sustained GH delivery was based on crystallization and complexation with polyelectrolytes; a monomolecular layer of positively charged poly (arginine) applied to

GH crystals to form polyelectrical coated crystals [19]. The PK/PD studies were determined in hypophysectomized rats and monkeys. The results suggested that crystals allowed *in vivo* release over several days. The efficacy of the crystalline formulation injected subcutaneously once a week appeared to be equivalent to seven daily soluble injections in the standard weight gain assay in rats and by measurement of serum IFG-I factor in monkeys. The suspension also facilitated easy administration through a 30-gauge needle. Bidlingmaier *et al*. analyzed the effect of hyaluronate-conjugated GH (LB03002) incorporated into microparticles versus daily recombinant GH in adults with GH deficiency [21]. The observed maximal serum GH concentration was approximately doubled after LB03002 compared with daily GH. The mean maximal serum IGF-1 concentration was 34-41% greater with LB03002 than with daily GH and AUC was 7-fold greater; however, normalized to GH dose, AUC for IGF-1 was comparable. Another study investigated a novel formulation of recombinant GH developed as a once-a-week injection using sodium hyaluronate (HA). Microparticles were subsequently produced by spray drying technology. A single administration of the optimized formulation (1:1 GH:HA) to cynomolgus monkeys and beagle dogs for 6 days apparently induced increases in serum IGF-1 levels. The bioavailability of both formulations was equivalent to that of daily GH injection.

PEGylated GH is formulated by covalent attachment of polyethylene glycol (PEG) to GH (PEG-GH). This increases the hydrodynamic size and hence prolongs its circulatory time by reducing renal clearance. Studies have compared the pharmacokinetics of PEG-GH to those of somatropin in healthy volunteers and adults suffering from GHD [22, 28, 29]. In the first part of a Phase I study, healthy male volunteers (aged 25-55 years) received a single subcutaneous dose of human GH (3.6 mg, ~50 µg/kg). They were then divided into seven groups and received 3, 10, 30, 60, 100, 300 or 500 µg/kg PEGylated GH (PHA-794428) or placebo. The results showed that PHA-794428 had a prolonged elimination half-life (>20 h) and that at equivalent subcutaneous doses (50 µg/kg), PEGylation resulted in a 10 to 20-fold increase in AUC; the renal clearance of PHA-794428 was significantly lower than that of somatropin (0.1 and 9.6 l/h, respectively). It was proposed that in addition to the effect of PEGylation on glomerular filtration, it also impacted on a second receptor-mediated clearance mechanism by reducing the affinity of the conjugate for the receptor. A sustained pharmacological response was also observed as IGF-1 levels remained elevated for up to 1 week and was confirmed by increased levels of other biomarkers. PHA-794428 was well-tolerated at doses up to 300 µg/kg – most side effects were related to fluid retention.

PHA-794428 was administered to seven patients with GHD in an open-label crossover study (with washout) at doses of 20 and 60 µg/kg; the half life was 43.3 h and IGF-1 was increased (max. conc. of 153.3 and 286.5 ng/ml at the 20 and 60 µg/kg doses, respectively. The drug was reported to be well-tolerated and there did not appear to be any production of

PHA-794428 antibodies [28]. Somewhat disappointingly, a recent report from a multicentre Phase II study using PHA-794428 in GHD patients described the incidence of lipoatrophy at the injection site, which was suggested as being due to the lipolytic action of GH on subcutaneous adipose tissue [30]. Its increased prevalence in female patients might have been due to larger amounts adipose in women, although a gender-specific response was not ruled out.

Other PEGylated GH analogues have shown efficacy in animal models. Cox *et al.* described a PEGylated GH threonine-3 analogue with a longer circulating half-life than GH following s.c. administration in rats; it was also reported to be more potent than GH at stimulating weight gain and bone growth in GH deficient rats [31]. Pasut *et al*. recently described a new PEGylating agent, PEG-βAla-NHCO [32]; the pharmacokinetic profile of the GH conjugate was investigated in rats and monkeys and the potency evaluated in hypophysectomized rats. Conjugation led to an increase in residence time in both animal models; GH half-life increased from 0.8 to 8.3 h in rats and from 3.1 to 20.8 h in monkeys. A single subcutaneous injection of GHPEG-βAla (1 × 240 μg/rat, protein equiv) was found to be similar to the same total amount of unconjugated GH given daily over a period of six days (6×40 μg/rat).

4. NEW DELIVERY DEVICES

Compliance issues with some patients, especially children, may ultimately lead to a discontinuation of treatment because of pain and other adverse effects due to the injection procedure. In order to address this, novel administration delivery devices such as pre-filled syringes, manual injector pens, auto-injectors, injectors with hidden needles and needle-free devices have been introduced in an attempt to increase dosing accuracy and adjustability, ease of use, convenience and compliance [33, 34]. Needle-based auto-injectors are devices that incorporate a pre-filled syringe or cartridge fitted with a needle (Figure 5). Needle-free injectors administer the drug (without a needle) by high pressure, expelling it through a fine nozzle, and can be as effective as a conventional injection [35]. Injectors are available for single and multiple doses and are suitable for a wide range of primary containers including pre-filled glass and plastic syringes and pre-filled cartridges.

A number of reports have addressed the efficacy and safety of injection devices in GH therapies; for example, the physiological responses to a needle-free injector (Medi-Jector®, Medi-Ject Corporation, MN, USA) and a multiple dose injection pen with 28G needles (Disetronic AG, Buegder, Switzerland) have been compared [36]. Use of the needle-free device (Medi-Jector®) showed fewer adverse physiological responses.

Figure 5. GH pen injectors (NordiPen® and NordiPenmate®: permanent hidden needle) (Novo Nordisk Pharma SA, Danemark.).
Reproduced by permission from Novonordisk.com -Copyright NovoNordisk Pharma S.A. (2009).

Agerso *et al.* [35] compared the administration of a new GH formulation (Zomacton®; target dose of 1.67 mg GH) by conventional syringe and with a new needle-free device (ZomaJet® 2 Vision). The results demonstrated that administration with the ZomaJet® 2 Vision GH was bioequivalent based on AUC values; GH absorption appeared to be faster than after injection resulting in higher C_{max} values. Serum concentrations of IGF-1 and free fatty acids served as pharmacodynamic markers and confirmed bioequivalence of the needle-free device.

In another study, Dörr *et al.* determined GH pharmacokinetics after administration of Genotropin® with Genotropin® ZipTip, a needle-free device, and a fine gauge needle in children [37]. The needle-free injector was shown to be bioequivalent and more than 20% of the patients preferred to continue using it after the study. Interestingly, statistical analysis suggested that the fine gauge needle device (Genotropin® Pen) produced less bleeding, bruising, pain or soreness. More recently, Brearley *et al.* evaluated the relative bioavailability of GH (Saizen®) administered by the cool.click™ 2 needle-free device and a standard needle and syringe [38]. Figure 7 shows the GH serum profiles following s.c. administration of 2.92 mg of GH to healthy volunteers by either the cool.click™ 2 device or by needle injection throughout the 25 hour monitoring period. Statistical assessment of the

rate and extent of absorption of GH suggested that administration by cool.click™ 2 was bioequivalent to standard needle injection and demonstrated similar tolerability.

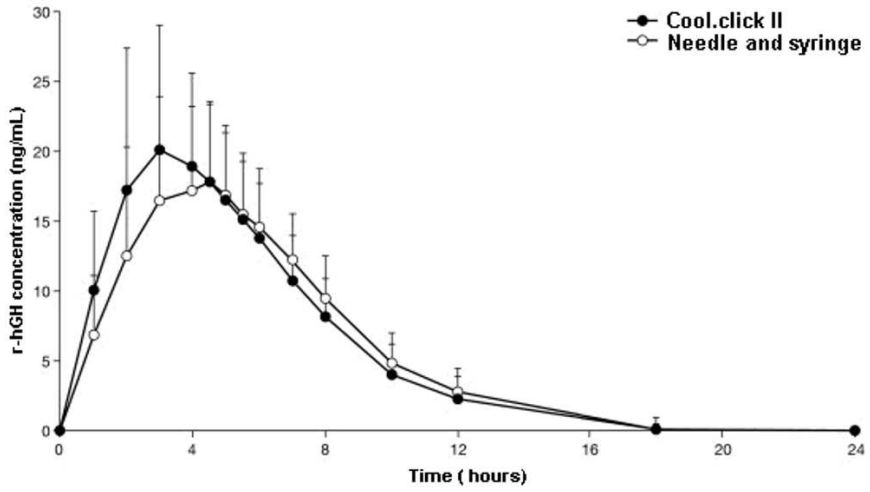

Figure 6. Mean GH serum concentration vs. time profiles following subcutaneous administration of rhGH (Dose 2.92 mg/subject) (Mean ± S.D.).
Reproduced by permission from Brearley *et al*,. Pharmacokinetics of recombinant human growth hormone administered by cool.click 2, a new needle-free device, compared with subcutaneous administration using a conventional syringe and needle, *BMC Clin. Pharmacol.* 7 (2007), 10. Copyright BioMed Central Ltd. (2007).

Dedicated GH delivery devices that are currently on the market include cool.click™ (Figure 7), Serojet® and Zomajet® 2 Vision. Cool.click™ is a modified version of Bioject's Vitajet™ 3 needle-free injection system incorporating dosage features to accurately deliver different doses of Saizen®. It received FDA market clearance for delivering s.c. injections of Saizen® in June 2000. The SeroJet® system (EMD Serono, USA) is a needle-free injection for delivering Serostim®, recombinant GH for treatment of HIV-associated wasting in adults. Zomajet® 2 Vision (Antares Pharma, Switzerland) was licensed to Ferring Pharmaceuticals for delivery of Zomacton®, GH for treatment of GH deficiency in children and Turner Syndrome. This needle-free system was launched in Europe in 2003 and is a customized version of the Medi-Jector Vision® device.

Although needle-free injectors are recognized for their propensity to cause bruising, these devices can be superior to needle injection in terms of comfort and compliance. The advantage of this technology, compared to conventional syringe injection, is the absence of a needle which may be of benefit to children.

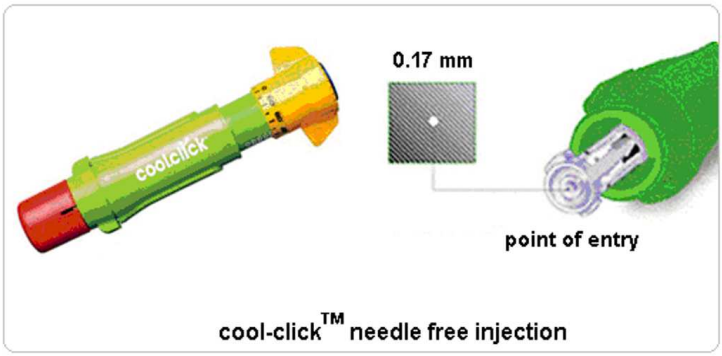

Figure 7. Cool.click™ needle free injection designed for the delivery of hGH (Merck Serono SA, Switzerland).
Reproduced by permission from Justgrowth.com. Copyright Merck Serono S.A.–Geneva (2008).

5. ALTERNATIVE ADMINISTRATION ROUTES FOR THE DELIVERY OF HUMAN GROWTH HORMONE

The efforts to improve GH therapy and increase compliance have also led to the investigation of less invasive administration routes.

5.1 Intranasal delivery

The nasal route has been investigated as a non-invasive means of delivering therapeutic macromolecules due to its vascularized and permeable mucosal surfaces, no first-pass metabolism, rapid kinetics and the ease of administration [39]. However, in the absence of a promoting agent, intranasal administration of high molecular weight molecules generally results in low bioavailability; they must overcome a diffusional barrier, which is comprised of the mucus gel layer covering mucosal membranes and an enzymatic barrier (the major obstacle for these compounds), due to secreted and membrane bound peptidases, in order to reach the systemic circulation [40]. Membrane transport is also limited by the rapid clearance of the administered formulation from the nasal cavity due to the mucociliary clearance mechanism, which decreases local residence time at the site of absorption [41]. The effectiveness of absorption promoters agents such as i) surfactants – laureth-9, bile salts, fatty acids, phospholipids, cyclodextrins, ii) enzymatic inhibitors and iii) multifunctional polymers in enhancing the nasal absorption of polar drugs has been evaluated [42, 43]. These enhancers function by different mechanisms that change the permeability of the epithelial cell layer by modifying the phospholipid bilayer. The mechanisms include reduction in mucus viscosity, enzyme inhibition and enhancement of membrane fluidity.

Sodium tauro-24, 25-dihydrofusidate (STDHF) was shown to promote the nasal absorption of GH in rat, rabbit and sheep [44]. After intranasal delivery of GH formulations containing STDHF, significant plasma GH levels were achieved (more markedly for sheep), closely mimicking the endogenous secretory pattern of GH release. Hedin *et al.* evaluated the efficacy of STDHF-based GH solutions administered to humans with GH deficiency [45] – the bioavailability was considerably lower (1.6–3.0 %) relative to that obtained by s.c. injection. Fisher and co-workers studied the intranasal delivery of GH formulated with l-α-phosphatidylcholine (LPC) in rats, rabbits and sheep [46]. The bioavailability attained with the surfactant was 17.5%, 72.8% and 16%, respectively; this corresponded to 7.6, 52 and 80-fold improvements in the bioavailability achieved in the absence of LPC.

The potential of using bioadhesive microspheres as a nasal delivery system for recombinant GH has also been assessed in sheep [47]. GH was administered as an aqueous solution and as lyophilized powders containing the microsphere system alone or in combination with LPC. Although GH absorption from the nasal solution was very poor when administered, both the microsphere system alone and in combination with the biological surfactant improved uptake. Relative to the s.c. injection, the estimated bioavailabilities of the nasal formulations were 2.7 and 14.4%. However, damage to cell membranes was also observed; this was most likely due to the surfactant (LPC).

Other absorption enhancers such as didecanoyl-L-alpha-phosphatidylcholine (DDPC) and alpha-cyclodextrin have also been evaluated [48]; when tested in rabbits GH bioavailability was estimated to be 20%. It was suggested that GH was delivered via the transcellular pathway through damaged ciliated cells. The pharmacokinetics of different doses of GH in GH deficient patients following intranasal administration using DDPC resulted in bioavailabilities of 3.8 to 8.9 %, with respect to the applied dose [49].

More recently, a new polycarbophil-cysteine (PCP-Cys)/glutathione (GSH) gel was evaluated across nasal mucosa for the delivery of GH *in vitro* and *in vivo* [50]. The permeation of GH from the gel formulation across excised bovine nasal mucosa was improved 3-fold in the presence of PCP-Cys/GSH. The nasal administration of the PCP-Cys/GSH gel to rats resulted in a significantly increased and prolonged GH plasma concentration compared to the unmodified PC gel and physiological saline solution. Microparticulate systems containing PCP-Cys/GSH have also been evaluated for the delivery of GH *in vitro* and *in vivo* using the same animal models [51]; PCP-Cys/GSH/GH and PCP/GH microparticles exhibited similar sustained drug release profiles. The intranasal administration of GH microparticles formulated with the thiomer resulted in a bioavailability of 8.11% which represented a 3-fold improvement compared to that of PCP/GH microparticles.

Chitosan has also been investigated as an excipient for improving intranasal absorption of GH; a powder blend (Formulation A) and granules (Formulation B) were evaluated in sheep

[52]. Figure 8 shows the serum concentration profiles after intranasal administration (Formulation A, 20 ± 1 mg; Formulation B, 19 ± 1 mg) and s.c. injection (1.7 mg); this corresponded to normalized GH doses of 0.3 and 0.03 mg/kg, respectively. The results for the two intranasal formulations were comparable. However, despite the 10-fold excess in dose, the relative bioavailabilities of Formulations A and B – as compared to s.c. injection – were only 14 and 15%, respectively. Moreover, nasal administration required the insertion of 5mm siliconised tracheal tube 6–7 cm into the nasal cavity and the contents emitted using a one-way bellows. Anatomical differences prevented the use of more advanced delivery systems designed for human use.

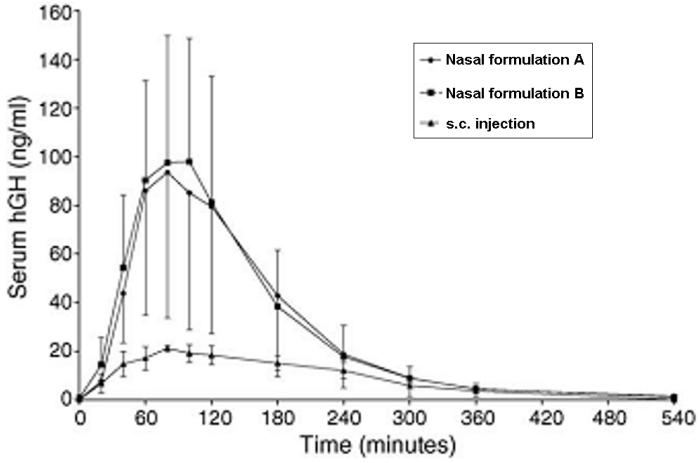

Figure 8. Plasma GH concentration profile following intranasal and subcutaneous administration of GH (Mean ± S.D. n=6).

Reproduced by permission from Cheng *et al.*, Intranasal delivery of recombinant human growth hormone (somatropin) in sheep using chitosan-based powder formulations, *Eur. J. Pharm*. *Sci*. 26 (2005), pp. 9-15. Copyright Elsevier B.V. (2005).

Nevertheless, these seemingly aggressive conditions may have contributed to the results. Given that the daily GH dose for in adults with GH deficiency is 6–12 μg/kg (by s.c. injection), this implies that for a 70 kg adult, the total amount of GH administered daily is ~0.4–0.8 mg [52]. Although nasal delivery has the advantage that it enables pulsatile administration which better mimics endogeneous GH secretion, the dosing requirements pose a considerable challenge.

In summary, surfactant materials and bile salts have been shown to enhance GH bioavailability. However, the enhancing effect is usually correlated to the damage caused to the nasal membrane; although for other enhancers such as cyclodextrins, chitosan and selected phospholipids (e.g., LCP), the absorption enhancing effect is reported to outweigh irritation to the mucosa [45, 46, 48]. The possibility of delivering therapeutic amounts of GH

by the intranasal route will depend on the quantities that can be dosed in a patient-friendly system and the potential nasal and systemic toxicity of the selected enhancer material.

5.2 Pulmonary delivery

Delivery into the respiratory tract is an interesting alternative for non-invasive administration of peptides and proteins for both local and systemic disorders that require fast onset and sharp pharmacokinetics; it also avoids the GI tract and the hepatic first pass effect. The lungs contain ~300 million alveoli, providing a total surface area of absorption of ~70-140 m^2, each wrapped in a fine mesh of capillaries which allows passage of 5 l of blood per minute. The thickness of the alveolar epithelium (0.1 – 0.2 mm) permits rapid drug absorption. Pulmonary application of proteins and peptides by aerosols is principally influenced by physiological factors such as the breathing pattern, structure and function of the physiological pulmonary defense mechanisms (e.g., physiological absorbance barrier, alveolar macrophages, proteases/peptidases) and specific properties of the biopharmaceuticals (e.g., molecular weight, lipophilicity, solubility in water and lipids) [53-56]. Tight junctions in alveolar type I cells (which occupy 96% of the alveolar epithelium) have a molecular weight cutoff of 0.6 nm while the value in endothelial junctions can range between 4 and 6 nm. It has also been shown that pulmonary alveolar macrophages form the first line of host defense by employing short-lived peroxidases, inflammatory and immunomodulatory mediators [57, 58]. Moreover, the protective mucus blanket which coats the airway epithelium and the thin lining fluid (called surfactant) that covers the alveolar epithelium also limit peptide and protein absorption from the lungs [58, 59].

Another important parameter that influences the pulmonary delivery of aerosol drugs, including proteins and peptides is the particle properties of the aerosol. The aerosol must be in a size range suitable for delivery to the lungs and the aerodynamic diameter should be optimized (1-3 μm) for deposition in the alveolar region of the lung [60]. Generally, particles with diameter <1 μm are exhaled and larger particles (>3 μm) are deposited preferentially in the tracheobronchial airways and do not reach the alveolar region.

Following intratracheal instillation of GH in rats, female rats showed higher bioavailability than males; there was also a tendency to saturation as the instilled dose was increased [61]. Colthorpe *et al.* compared the pulmonary deposition and pharmacokinetics of recombinant GH administered in the form of an aerosol and instillation in rabbits [62]. The results showed that the peripheral: central deposition ratio tended to be greater for the aerosol than for the instillate. The bioavailable fraction for aerosolized GH was greater than that for instilled GH (45% vs. 16%); this was probably due to mucociliary clearance, as previously suggested for insulin [63]. A dry powder aerosol formulated with lactose and dipalmitoylphosphatidylcholine was assessed for systemic delivery of GH in rats; the powder

prepared by spray drying presented a particle diameter of 4.4 µm. The bioavailabilities following intratracheal insufflation of the dry powder and intratracheal spray-instillation of the GH solution were reported to be 23% and 8%, respectively [64]. More recently, Wolff demonstrated the delivery of GH in humans following inhalation of large porous GH powder particles; the estimated bioavailability was 5-10% [65].

Dry powder GH aerosol containing 100 µg protein and different amounts of dimethyl-β-cyclodextrin (DM- β-CD) to protect against aggregation were tested in rats [66]. The formulations were administered by insufflation through a polyethylene tube inserted into the trachea following incision between the fifth and sixth tracheal rings. Absolute bioavailabilities of 25.4%, 76.5% and 64.0% were observed from formulations containing GH:DM-β-CD at molar ratios of 10, 100 and 1000, respectively.

5.3 Transdermal delivery

Transdermal delivery offers several advantages over conventional routes. However, passive diffusion of macromolecules through the lipid-rich stratum corneum is restricted by their size, physicochemical properties and susceptibility to metabolism by skin enzymes [67]. A number of chemical and physical means to enhance transdermal delivery of peptide and protein therapeutics have been explored.

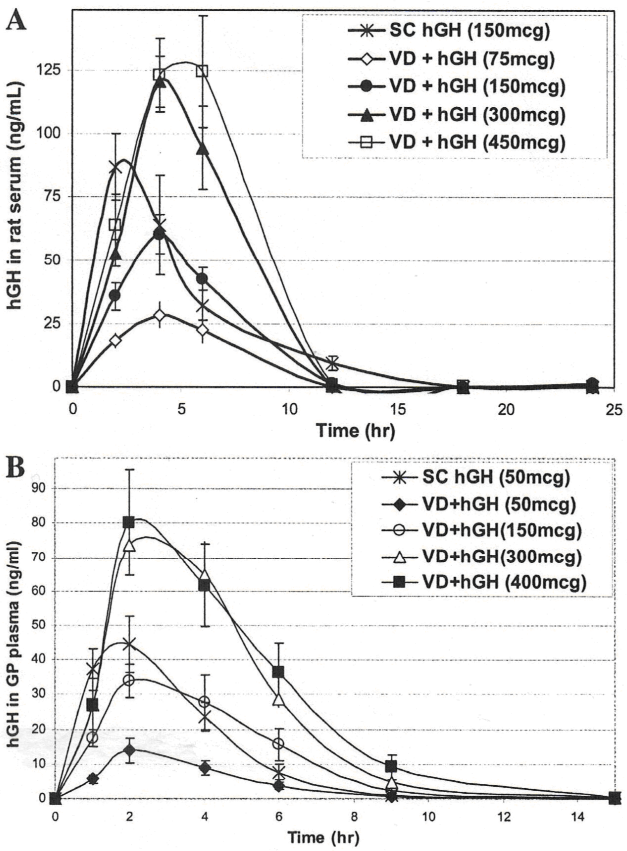

Figure 9. Plasma GH levels after s.c. and transdermal administration of GH. Increasing doses of GH were applied transdermally using ViaDerm device (treated area = 1.4cm^2). A) plasma concentration in rats; B) plasma concentration in guinea pigs (Mean ± S.D.; n=5-6).

Reproduced by permission from Levin G. *et al.*, Transdermal delivery of human growth hormone through RF-Microchannels, *Pharm. Res.* 22 (2005), pp. 550-555. Copyright Springer Science+Business Media, Inc. (2005).

Radio-frequency induced stratum corneum ablation was used to enhance GH transport in rats and guinea pigs [68]. The ViaDerm system (TransPharma Medical Ltd) generates an electrical current at high frequency (100–500 kHz) whose passage through resistive elements in contact with the skin creates an array of small microchannels in the epidermis by microablating skin cells (Figure 9). In the GH study, the device was applied twice on each skin area resulting in a microchannel density of 200 microchannels/cm^2. Dry printed patches with increasing GH content (rat: 75-450 □g; guinea pig: 50-400 µg) were then applied for up to 24 h; s.c. injection (100 µg in guinea pigs and 150 µg in rats) was used as the reference. For both animal models, plasma GH levels after stratum corneum ablation showed a dose-dependent increase up to a loading of 300 µg; for rats, at identical doses (150 µg), relative bioavailability was reported as ~75%. For guinea pigs, the corresponding value was ~32% (at a dose of 50%). Elevated levels of IGF-1 observed after delivery in hypophysectomized rats confirmed that the GH was bioactive. The Viaderm-GH system using a 5 cm^2 dry patch is reported to be in Phase 1b human clinical trials.

6. CONCLUDING REMARKS

The growing number of therapeutic applications of GH and the drive to provide alternatives to conventional “needle and syringe” delivery has led to the investigation of different technologies and routes of administration. The development of jet-injectors has provided a “needle-free” alternative to patients and although they have demonstrated bioequivalence, patients frequently prefer to continue using “needle-based” systems [37], in part due to the problems of local bruising at the application site. However, advances in the technology may reduce these effects in the future. Sustained release GH formulations have been developed but their complex manufacturing process (aseptic processing and scaling-up) as well as the regulatory concern regarding safety mean that none are commercially available. Studies into non- or minimally-invasive delivery using alternative administration routes, e.g., intranasal or pulmonary have shown that it is technically feasible. However, relative bioavailability is poor and the use of penetration enhancers is limited by the risk of damage to sensitive mucous membranes. Pulmonary delivery systems have demonstrated efficacy in animal models; however, the large drug doses needed for achieving high peak serum concentrations may induce local tissue reactions or systemic side-effects. Finally, stratum corneum ablation technologies have proved to be as effective as s.c. administration with minor adverse effects and initial clinical results appear promising; however, the dosing requirements for GH mean that significant quantities of the protein need to be administered and this is a considerable challenge. Furthermore, the practicality of the devices needs to be evaluated on a long-term basis as they are required for treatment of chronic disorders.

REFERENCES

1. S. Surya, K. Symons, E. Rothman, A. L. Barkan, Complex rhythmicity of growth hormone secretion in humans, Pituitary. 9 (2006) 121 - 125.
2. C. A. Jaffe, B. Ocampo-Lim, W. Guo, K. Krueger, I. Sugahara, R. DeMott-Friberg, M. Bermann, A. L. Barkan, Regulatory mechanisms of growth hormone secretion are sexually dimorphic, J. Clin. Invest. 102 (1998) 153 - 164.
3. S. K. Jessup, E. V. Dimaraki, K. V. Symons, A. L. Barkan, Sexual dimorphism of growth hormone (GH) regulation in humans: endogenous GH-releasing hormone maintains basal GH in women but not in men, J. Clin. Endocrinol. Metab. 88 (2003) 4776 - 4780.
4. L. M. Carlsson, S. Rosberg, R. V. Vitangcol, W. L. Wong, K. Albertsson-Wikland, Analysis of 24-hour plasma profiles of growth hormone (GH)-binding protein, GH/GH-binding protein-complex, and GH in healthy children, J. Clin. Endocrinol. Metab. 77 (1993) 356 - 361.
5. Z. Zadik, S. A. Chalew, A. Kowarski, The definition of a spontaneous growth hormone (GH) peak: studies in normally growing and GH-deficient children, J. Clin. Endocrinol. Metab. 74 (1992) 801 - 805.
6. P. Zizzari, M. T. Bluet-Pajot, Ghrelin, from GH secretagogue to orexigenic peptide, Metabolismes, Hormones, Diabetes et Nutrition. 8 (2004) 58 - 65.
7. J. Alba-Roth, O. A. Muller, J. Schopohl, K. von Werder, Arginine stimulates growth hormone secretion by suppressing endogenous somatostatin secretion, J. Clin. Endocrinol. Metab. 67 (1988) 1186 - 1189.
8. T. E. Oggle, A. Costoff, Endocrinology, Medical College of Georgia, Georgia, US, 2007.
9. A. Mehta, P. C. Hindmarsh, The use of somatropin (recombinant growth hormone) in children of short stature, Paediatr. Drugs. 4 (2002) 37 – 47.
10. P. D. Lee, Effects of growth hormone treatment in children with Prade-Willi syndrome, Growth. Horm. IGFRes. 10 (2000) S75 - S79.
11. K. Van Loon, Safety of high doses of recombinant human growth hormone, Horm. Res. 49 (1998) 78 - 81.
12. G. Amato, G. Mazziotti, C. Di Somma, E. Lalli, G. De Felice, M. Conte, M. Rotondi, M. Pietrosante, G. Lombardi, A. Bellastella, C. Carella, A. Colao, Recombinant growth hormone (GH) therapy in GH-deficient adults: a long-term controlled study on daily versus thrice weekly injections, J. Clin. Endocrinol. Metab. 85 (2000) 3720 - 3725.

13. A. A. Toogood, R. M. Nass, S. S. Pezzoli, P. A. O'Neill, M. O. Thorner, S. M. Shalet, Preservation of growth hormone pulsatility despite pituitary pathology, surgery, and irradiation, J. Clin. Endocrinol. Metab. 82 (1997) 2215 - 2221.
14. F. a. D. Administration. Approved drug products with therapeutic equivalence evaluations, FDA 2009.
15. E. L. a. Company. Humatrope somatropin (rDNA origin) for injection, 2009.
16. N. Vahl, N. Moller, T. Lauritzen, J. S. Christiansen, J. O. Jorgensen, Metabolic effects and pharmacokinetics of a growth hormone pulse in healthy adults: relation to age, sex, and body composition, J. Clin. Endocrinol. Metab. 82 (1997) 3612 - 3618.
17. A. Keller, Z. Wu, J. Kratzsch, E. Keller, W. F. Blum, A. Kniess, R. Preiss, J. Teichert, C. J. Strasburger, M. Bidlingmaier, Pharmacokinetics and pharmacodynamics of GH: dependence on route and dosage of administration, Eur. J. Endocrinol. 156 (2007) 647 - 653.
18. B. L. Silverman, S. L. Blethen, E. O. Reiter, K. M. Attie, R. B. Neuwirth, K. M. Ford, A long-acting human growth hormone (Nutropin Depot): efficacy and safety following two years of treatment in children with growth hormone deficiency, J. Pediatr. Endocrinol. Metab. 15 (Suppl. 2) (2002) 715 - 722.
19. C. Govardhan, N. Khalaf, C. W. Jung, B. Simeone, A. Higbie, S. Qu, L. Chemmalil, S. Pechenov, S. K. Basu, A. L. Margolin, Novel long-acting crystal formulation of human growth hormone, Pharm. Res. 22 (2005) 1461 - 1470.
20. P. Herbert, K. Murphy, O. Johnson, N. Dong, W. Jaworowicz, M. A. Tracy, J. L. Cleland, S. D. Putney, A large-scale process to produce microencapsulated proteins, Pharm. Res. 15 (1998) 357 - 361.
21. M. Bidlingmaier, J. Kim, C. Savoy, M. J. Kim, N. Ebrecht, S. de la Motte, C. J. Strasburger, Comparative pharmacokinetics and pharmacodynamics of a new sustained-release growth hormone (GH), LB03002, versus daily GH in adults with GH deficiency, J. Clin. Endocrinol. Metab. 91 (2006) 2926 - 2930.
22. P. E. Harris, E. Didier, C. Kantaridis, A. Boonen, G. Weissgerber, First in human study of pegylated recombinant human growth hormone, Horm. Res. 65 (suppl. 4) (2006) 30.
23. R. Webster, R. Xie, E. Didier, R. Finn, J. Finnessy, A. Edgington, D. Walker, PEGylation of somatropin (recombinant human growth hormone): impact on its clearance in humans, Xenobiotica. 38 (2008) 1340 - 1351.
24. E. O. Reiter, K. M. Attie, T. Moshang, Jr., B. L. Silverman, S. F. Kemp, R. B. Neuwirth, K. M. Ford, P. Saenger, A multicenter study of the efficacy and safety of sustained release GH in the treatment of naive pediatric patients with GH deficiency, J. Clin. Endocrinol. Metab. 86 (2001) 4700 - 4706.

25. D. M. Cook, B. M. Biller, M. L. Vance, A. R. Hoffman, L. S. Phillips, K. M. Ford, D. P. Benziger, A. Illeperuma, S. L. Blethen, K. M. Attie, L. N. Dao, J. D. Reimann, P. J. Fielder, The pharmacokinetic and pharmacodynamic characteristics of a long-acting growth hormone (GH) preparation (nutropin depot) in GH-deficient adults, J. Clin. Endocrinol. Metab. 87 (2002) 4508 - 4514.

26. A. R. Hoffman, B. M. Biller, D. Cook, J. Baptista, B. L. Silverman, L. Dao, K. M. Attie, P. Fielder, T. Maneatis, B. Lippe, Efficacy of a long-acting growth hormone (GH) preparation in patients with adult GH deficiency, J. Clin. Endocrinol. Metab. 90 (2005) 6431 - 6440.

27. H. H. Kwak, W. S. Shim, M. K. Choi, M. K. Son, Y. J. Kim, H. C. Yang, T. H. Kim, G. I. Lee, B. M. Kim, S. H. Kang, C. K. Shim, Development of a sustained-release recombinant human growth hormone formulation, J. Control. Release. 137 (2009) 160 - 165.

28. R. Abs, E. Didier, A. Boonen, C. Kantaridis, G. Weissgerber, P. E. Harris, The pharmacokinetics, pharmacodynamics and safety of pegylated recombinant human growth hormone after single subcutaneous injections in adult male patients with growth hormone deficiency, Horm. Res. 65 (Suppl. 4) (2006) 148.

29. R. Xie, E. Didier, P. E. Harris, P. A. Milligan, M. O. Karlsson, Population pharmacokinetic/ pharmacodynamic analysis for pegylated recombinant human growth hormone (PHA- 794428) in healthy male volunteers, *88th Annual Meeting of the Endocrine Society Program and Abstracts*, Boston, MA, 2006.

30. P. Touraine, G. A. D'Souza, I. Kourides, R. Abs, P. Barclay, R. Xie, A. Pico, E. Torres-Vela, B. Ekman, Lipoatrophy in GH deficient patients treated with a long-acting pegylated GH, Eur. J. Endocrinol. 161 (2009) 533 - 540.

31. G. N. Cox, M. S. Rosendahl, E. A. Chlipala, D. J. Smith, S. J. Carlson, D. H. Doherty, A long-acting, mono-PEGylated human growth hormone analog is a potent stimulator of weight gain and bone growth in hypophysectomized rats, Endocrinology. 148 (2007) 1590 - 1597.

32. G. Pasut, A. Mero, F. Caboi, S. Scaramuzza, L. Sollai, F. M. Veronese, A new PEG-beta-alanine active derivative for releasable protein conjugation, Bioconjug. Chem. 19 (2008) 2427 - 2431.

33. E. Fidotti, A history of growth hormone injection devices, J. Pediatr. Endocrinol. Metab. 14 (2001) 497 - 501.

34. H. Dumas, P. Panayiotopoulos, D. Parker, V. Pongpairochana, Understanding and meeting the needs of those using growth hormone injection devices, BMC Endocr. Disord. 6 (2006) 5.

35. H. Agerso, J. Moller-Pedersen, S. Cappi, P. Thomann, B. Jesussek, T. Senderovitz, Pharmacokinetics and pharmacodynamics of a new formulation of recombinant human growth hormone administered by ZomaJet 2 Vision, a new needle-free device, compared to subcutaneous administration using a conventional syringe, J. Clin. Pharmacol. 42 (2002) 1262 - 1268.
36. G. H. Verrips, R. A. Hirasing, M. Fekkes, T. Vogels, S. P. Verloove-Vanhorick, H. A. Delemarre-Van de Waal, Psychological responses to the needle-free Medi-Jector or the multidose Disetronic injection pen in human growth hormone therapy, Acta. Paediatr. 87 (1998) 154 - 158.
37. H. G. Dorr, S. Zabransky, E. Keller, B. J. Otten, C. J. Partsch, L. Nyman, B. K. Gillespie, N. R. Lester, A. M. Wilson, C. Hyren, M. A. van Kuijck, P. Schuld, S. L. Schoenfeld, Are needle-free injections a useful alternative for growth hormone therapy in children? Safety and pharmacokinetics of growth hormone delivered by a new needle-free injection device compared to a fine gauge needle, J. Pediatr. Endocrinol. Metab. 16 (2003) 383 - 392.
38. C. Brearley, A. Priestley, J. Leighton-Scott, M. Christen, Pharmacokinetics of recombinant human growth hormone administered by cool.click 2, a new needle-free device, compared with subcutaneous administration using a conventional syringe and needle, BMC Clin. Pharmacol. 7 (2007) 10.
39. L. Illum, Nasal drug delivery-possibilities, problems and solutions, J. Control. Release. 87 (2003) 187 - 198.
40. L. Jorgensen, E. Beckgaard, Intranasal permeation of thyrotropin-releasing hormone: in vitro study of permeation and enzymatic degradation, Int. J. Pharm. 107 (1994) 231 - 237.
41. A. S. Harris, I. M. Nilsson, Z. G. Wagner, U. Alkner, Intranasal administration of peptides: nasal deposition, biological response, and absorption of desmopressin, J. Pharm. Sci. 75 (1986) 1085 - 1088.
42. L. Illum, Bioadhesive formulations for nasal peptide delivery, Marcel Dekker, New York, 1998.
43. M. I. Ugwoke, N. Verbeke, R. Kinget, The biopharmaceutical aspects of nasal mucoadhesive drug delivery, J. Pharm. Pharmacol. 53 (2001) 3 - 21.
44. P. A. Baldwin, C. K. Klingbeil, C. J. Grimm, J. P. Longenecker, The effect of sodium tauro-24,25-dihydrofusidate on the nasal absorption of human growth hormone in three animal models, Pharm. Res. 7 (1990) 547 - 552.
45. L. Hedin, B. Olsson, M. Diczfalusy, C. Flyg, A. S. Petersson, S. Rosberg, K. Albertsson-Wikland, Intranasal administration of human growth hormone (hGH) in

combination with a membrane permeation enhancer in patients with GH deficiency: a pharmacokinetic study, J. Clin. Endocrinol. Metab. 76 (1993) 962 - 967.

46. A. N. Fisher, N. F.Farraj, D. T. O'Hagan, I. Jabbal-Gill, B. R. Johansen, S. S. Davis, L. Illum, Effect of L-α-lysophosphatidylcholine on the nasal absorption of human growth hormone in three animal species, Int. J. Pharm. 74 (1991) 147 - 156.
47. L. Illum, N. F. Farraj, S. S. Davis, B. R. Johansen, D. T. O'Hagan, Investigation of the nasal absorption of biosynthetic human growth hormone in sheep-use of a bioadhesive microsphere delivery system, Int. J. Pharm. 63 (1990) 207 - 211.
48. C. Agerholm, L. Bastholm, P. B. Johansen, M. H. Nielsen, F. Elling, Epithelial transport and bioavailability of intranasally administered human growth hormone formulated with the absorption enhancers didecanoyl-L-alpha-phosphatidylcholine and alpha-cyclodextrin in rabbits, J. Pharm. Sci. 83 (1994) 1706 - 1711.
49. T. Laursen, B. Grandjean, J. O. Jorgensen, J. S. Christiansen, Bioavailability and bioactivity of three different doses of nasal growth hormone (GH) administered to GH-deficient patients: comparison with intravenous and subcutaneous administration, Eur. J. Endocrinol. 135 (1996) 309 - 315.
50. V. M. Leitner, D. Guggi, A. Bernkop-Schnürch, Thiomers in noninvasive polypeptide delivery: In vitro and in vivo characterization of a polycarbophil-cysteine/glutathione gel formulation for human growth hormone, J. Pharm. Sci. 93 (2004) 1682 - 1691.
51. V. M. Leitner, D. Guggi, A. H. Krauland, A. Bernkop-Schnurch, Nasal delivery of human growth hormone: in vitro and in vivo evaluation of a thiomer/glutathione microparticulate delivery system, J. Control. Release. 100 (2004) 87 - 95.
52. Y. H. Cheng, A. M. Dyer, I. Jabbal-Gill, M. Hinchcliffe, R. Nankervis, A. Smith, P. Watts, Intranasal delivery of recombinant human growth hormone (somatropin) in sheep using chitosan-based powder formulations, Eur. J. Pharm. Sci. 26 (2005) 9 - 15.
53. R. U. Agu, M. I. Ugwoke, M. Armand, R. Kinget, N. Verbeke, The lung as a route for systemic delivery of therapeutic proteins and peptides, Respir. Res. 2 (2001) 198 - 209.
54. J. S. Patton, P. R. Byron, Inhaling medicines: delivering drugs to the body through the lungs, Nat. Rev. Drug. Discov. 6 (2007) 67 - 74.
55. R. K. Wolff, Safety of inhaled proteins for therapeutic use, J. Aerosol. Med. 11 (1998) 197 - 219.
56. C. Lombry, D. A. Edwards, V. Preat, R. Vanbever, Alveolar macrophages are a primary barrier to pulmonary absorption of macromolecules, Am. J. Physiol. Lung. Cell. Mol. Physiol. 286 (2004) L1002 - 1008.

57. R. W. Niven, Delivery of biotherapeutics by inhalation aerosol, Crit. Rev. Ther. Drug. Carrier. Syst. 12 (1995) 151 - 231.
58. X. H. Zhou, Overcoming enzymatic and absorption barriers to non-parenterally administered protein and peptide drugs, J. Control. Release. 29 (1994) 239 - 252.
59. Z. Shen, Q. Zhang, S. Wei, T. Nagai, Proteolytic enzymes as a limitation for pulmonary absorption of insulin: in vitro and in vivo investigations, Int. J. Pharm. 192 (1999) 115 - 121.
60. H. Chrystyn, Is total particle dose more important than particle distribution?, Respir. Med. 91 (Suppl. A) (1997) 17 - 19.
61. H. G. Folkesson, L. Hedin, B. R. Westrom, Lung to blood passage of human growth hormone after intratracheal instillation: stimulation of growth in hypophysectomized rats, J. Endocrinol. 134 (1992) 197 - 203.
62. P. Colthorpe, S. J. Farr, I. J. Smith, D. Wyatt, G. Taylor, The influence of regional deposition on the pharmacokinetics of pulmonary-delivered human growth hormone in rabbits, Pharm. Res. 12 (1995) 356 - 359.
63. P. Colthorpe, S. J. Farr, G. Taylor, I. J. Smith, D. Wyatt, The pharmacokinetics of pulmonary-delivered insulin: a comparison of intratracheal and aerosol administration to the rabbit, Pharm. Res. 9 (1992) 764 - 768.
64. C. Bosquillon, V. Préat, R. Vanbever, Pulmonary delivery of growth hormone using dry powders and visualization of its local fate in rats, J. Control. Release. 96 (2004) 233 - 244.
65. R. K. Wolff. Personal Communication, The International Society for Aerosols in Medicine Congress, 2003.
66. M. Jalalipour, A. R. Najafabadi, K. Gilani, H. Esmaily, H. Tajerzadeh, Effect of dimethyl-beta-cyclodextrin concentrations on the pulmonary delivery of recombinant human growth hormone dry powder in rats, J. Pharm. Sci. 97 (2008) 5176 - 5185.
67. T. Tanner, R. Marks, Delivering drugs by the transdermal route: review and comment, Skin. Res. Technol. 14 (2008) 249 - 260.
68. G. Levin, A. Gershonowitz, H. Sacks, M. Stern, A. Sherman, S. Rudaev, I. Zivin, M. Phillip, Transdermal delivery of human growth hormone through RF-microchannels, Pharm. Res. 22 (2005) 550 - 555.

ACKNOWLEDGEMENTS

J. Cázares-Delgadillo wishes to acknowledge financial support from CONACYT (Mexico).

LISTE DE PUBLICATIONS

ARTICLES SCIENTIFIQUES

- J. Cázares-Delgadillo, A. Naik, A. Ganem-Rondero, D. Quintanar-Guerrero and Y. N. Kalia. Transdermal delivery of Cytochrome c – a 12.4 kDa protein – across intact skin by constant current iontophoresis. Pharm Res. 2007; 24(7): 1360-1369.
- J. Cázares-Delgadillo, A. Ganem-Rondero, D. Quintanar-Guerrero, A. C. López Castellano, V. Merino, Y. N. Kalia. Using transdermal iontophoresis to increase granisetron delivery across skin in vitro and in vivo: effect of experimental conditions and a comparison with other enhancement strategies. Eur. J. Pharm. Sci. 2010; *39 (5): 387-393.*
- J. Cázares-Delgadillo, C. Balaguer-Fernández, A. Calatayud-Pascual, A. Ganem-Rondero, D. Quintanar-Guerrero, A. C. López Castellano, V. Merino, Y. N. Kalia. Comparing metoclopramide electrotransport kinetics in vitro and in vivo: relative contributions of electromigration and electroosmosis and the effect of drug transport on skin permselectivity. Submitted to Pharmaceutical Research.
- J. Cázares-Delgadillo, C. Balaguer-Fernández, A. Calatayud-Pascual, A. Ganem-Rondero, D. Quintanar-Guerrero, A. C. López Castellano, V. Merino, Y. N. Kalia. Transdermal iontophoresis of dexamethasone sodium phosphate *in vitro* and *in vivo*: Effect of experimental parameters and skin type on drug stability and transport kinetics. Eur. J. Pharm. Biopharm., *in press*
- J. Cázares-Delgadillo, A. Ganem-Rondero, D. Quintanar-Guerrero, A. C. López Castellano, V. Merino, Y. N. Kalia. New therapeutic approaches to treat chemotherapy induced emesis: simultaneous co-iontophoresis of granisetron, metoclopramide and dexmethasone sodium phosphate in vitro and in vivo. Submitted to Journal of Controlled Release.

REVUE SCIENTIFIQUE

- J. Cázares-Delgadillo, A. Ganem-Rondero, Y. N. Kalia. Human growth hormone: new delivery systems, alternative routes of administration and their pharmacological relevance. Submitted to European Journal of Pharmaceutics and Biopharmaceutics.

SYMPOSIUMS

- J. Cázares -Delgadillo, S. Kumar, A. Naik, A. Ganem-Rondero, D. Quintanar-Guerrero, Y. N. Kalia. Iontophoretic delivery of a 13 kDa protein across intact skin. 33rd Annual Meeting and Exposition of the Controlled Release Society. Vienna, Jul 22nd -26th, 2006.
- J. Cázares-Delgadillo, A. Ganem-Rondero, D. Quintanar-Guerrero, Y. N. Kalia. Transdermal iontophoretic delivery of doxylamine succinate. Pharmaceutical Sciences World Congress. Amsterdam, Apr 22nd -Apr 25th, 2007.
- J. Cázares-Delgadillo, I. Ben Aziza, A. Ganem-Rondero, D. Quintanar-Guerrero, Y. N. Kalia. Electrotransport kinetics of metoclopramide across porcine skin *in vitro*. 34th Annual Meeting and Exposition of the Controlled Release Society. Long Beach, Jul 7th – Jul 11th, 2007.
- J. Cázares-Delgadillo, A. Ganem-Rondero, D. Quintanar-Guerrero, Y. N. Kalia. Transdermal iontophoretic delivery of granisetron across porcine skin in vitro. 34th Annual Meeting and Exposition of the Controlled Release Society. Long Beach, Jul 7th – Jul 11th, 2007.
- A. Romand, J. Cázares-Delgadillo, Y. G. Bachhav, Y. N. Kalia. Optimizing iontophoretic delivery kinetics of diclofenac *in vitro*. 6th World Meeting on Pharmaceutics, Biopharmaceutics and Pharmaceutical Technology. Barcelona, Apr 7th- Apr 10th, 2008.
- J. Cázares-Delgadillo, A. Ganem-Rondero, D. Quintanar-Guerrero, Y. N. Kalia. Co iontophoresis of granisetron and metoclopramide for chemotherapy induced nausea and vomiting. 6th World Meeting on Pharmaceutics, Biopharmaceutics and Pharmaceutical Technology. Barcelona, Apr 7th - Apr 10th, 2008.
- J. Cázares-Delgadillo, A. Ganem-Rondero, D. Quintanar-Guerrero, Y. N. Kalia. Co-iontophoresis of dexamethasone sodium phosphate, granisetron and metoclopramide for treating chemotherapy induced nausea and vomiting. 35th Annual Meeting and Exposition of the Controlled Release Society. New York, Jul 12th – Jul 16th, 2008.
- J. Cázares-Delgadillo, A. Ganem-Rondero, D. Quintanar-Guerrero, Y. N. Kalia. Iontophoretic delivery of dexamethasone sodium phosphate across porcine skin *in vitro*. 35th Annual Meeting and Exposition of the Controlled Release Society. New York, Jul 12th – Jul 16th, 2008.
- J. Cázares-Delgadillo, C. Balaguer-Fernández, A. Calatayud-Pascual, A. Ganem-Rondero, D. Quintanar-Guerrero, V. Merino, A. C. López Castellano, Y. N. Kalia. Non-invasive transdermal iontophoretic delivery of granisetron *in vivo*. 36th Annual Meeting

and Exposition of the Controlled Release Society. Bella Center, Copenhagen, Jul 18th – Jul 22nd, 2009.

- J. Cázares-Delgadillo, C. Balaguer-Fernández, A. Calatayud-Pascual, A. Ganem-Rondero, D. Quintanar-Guerrero, V. Merino, A. C. López Castellano, Y. N. Kalia. Co-iontophoresis of granisetron, metoclopramide and dexamethasone *in vivo*. 36th Annual Meeting and Exposition of the Controlled Release Society. Bella Center, Copenhagen, Jul 18th – Jul 22nd, 2009.